

**Cytochrome *c* Nitrite Reductase:
Further Investigations of the Multiheme Enzyme by
X-Ray Crystallography, Site-Directed Mutagenesis,
and EPR Spectroscopy**

Dissertation submitted to
Fachbereich Biologie, Universität Konstanz, Germany
for the degree of
Doctor of Natural Sciences

presented by

Dipl.-Chem. Marc Rudolf

Konstanz, August 2004

Examiner: Prof. Dr. P.M.H. Kroneck
Coexaminer: Prof. Dr. O. Einsle

Phantasie ist wichtiger als Wissen, denn Wissen ist begrenzt.

Albert Einstein

für Sonja und Luca

Table of Contents

Zusammenfassung	IV
Summary	VII
1 Introduction	1
1.1 The Biogeochemical Nitrogen Cycle.....	1
1.2 Nitrate Reductases	5
1.3 Nitrite Reductases	7
1.3.1 Dissimilatory Cytochrome <i>c</i> Nitrite Reductase.....	8
1.3.2 Assimilatory Siroheme Nitrite Reductase	10
1.3.3 Cytochrome <i>cd</i> ₁ Nitrite Reductase	12
1.3.4 Copper-Containing Nitrite Reductase	13
1.4 Scope of the Study	15
2 Materials and Methods	17
2.1 Chemicals	17
2.2 Organisms and Cultivation	18
2.2.1 Cultivation of <i>Wolinella succinogenes</i> Wild-Type	18
2.2.2 Cultivation of <i>Wolinella succinogenes</i> Variants	20
2.2.3 Cultivation of <i>Pseudomonas stutzeri</i>	20
2.2.4 Cultivation of <i>Thiobacillus denitrificans</i>	20
2.3 Preparation of Cellular Components.....	20
2.3.1 Preparation of Cell Fractions	20
2.3.2 Solubilization of the Membrane Fraction.....	21
2.4 Purification Protocols	21
2.4.1 Cytochrome <i>c</i> Nitrite Reductase from the Soluble Fraction	21
2.4.2 Cytochrome <i>c</i> Nitrite Reductase from the Membrane Fraction	22
2.4.3 Purification of Cytochrome <i>cd</i> ₁ Nitrite Reductase from <i>Pseudomonas stutzeri</i>	22
2.4.1 Purification of Cytochrome <i>cd</i> ₁ Nitrite Reductase from <i>Thiobacillus denitrificans</i>	22
2.5 Analytical Methods.....	23
2.5.1 Protein.....	23
2.5.2 Ammonia	23
2.5.3 Iron, Calcium, Molybdenum.....	23
2.5.4 Polyacrylamide Gel Electrophoresis	23
2.6 Cytochrome <i>c</i> Nitrite Reductase Activity	24
2.7 Removal of Dioxide.....	24
2.8 Protein Crystallography	25
2.8.1 Protein Crystallization	25
2.8.1.1 Crystallization of Membranous NrfA Nitrite Reductase	25
2.8.1.2 Crystallization of Membranous NrfHA Nitrite Reductase	26
2.8.1.3 Crystallization of Cytochrome <i>cd</i> ₁ Nitrite Reductase from <i>P. stutzeri</i>	26
2.8.1.4 Crystallization of Cytochrome <i>cd</i> ₁ Nitrite Reductase from <i>T. denitrificans</i>	27
2.8.2 Substrate Complexes of NrfA Nitrite Reductase	27
2.8.3 Cryocrystallography.....	27

2.8.3.1 NrfA Nitrite Reductase.....	28
2.8.3.2 NrfHA Nitrite Reductase.....	28
2.8.3.3 Cytochrome <i>cd</i> ₁ Nitrite Reductase from <i>P. stutzeri</i>	28
2.8.3.4 Cytochrome <i>cd</i> ₁ Nitrite Reductase from <i>T. denitrificans</i>	28
2.8.4 Measurement of Datasets.....	28
2.8.5 Data Processing.....	28
2.8.6 Molecular Replacement Using Experimental Phases.....	29
2.8.7 Interpretation of Electron Density Maps.....	29
2.8.8 Model Building and Refinement.....	29
2.8.9 Graphical Representations.....	29
2.9 Reduction of Nitrite Reductase.....	29
2.10 Ultraviolet / Visible Spectroscopy.....	30
2.10.1 Spectrophotometric Titrations.....	30
2.11 Magnetic Measurements.....	30
2.12 Electron Paramagnetic Resonance Spectroscopy.....	33
2.12.1 Theoretical Background.....	33
2.12.2 EPR Spectra of Multiheme Enzymes.....	35
2.12.3 Multifrequency EPR Spectroscopy.....	38
2.12.3.1 Perpendicular Mode X-Band EPR Spectroscopy.....	38
2.12.3.2 Parallel Mode X-Band EPR Spectroscopy.....	38
2.12.3.3 Q-Band EPR Spectroscopy.....	39
2.12.3.4 S-Band EPR Spectroscopy.....	39
3 Results.....	41
3.1 Cytochrome <i>c</i> Nitrite Reductase and Variants from <i>Wolinella succinogenes</i>	41
3.1.1 Cultivation of <i>W. succinogenes</i>	41
3.1.2 Purification of ccNir from <i>W. succinogenes</i>	42
3.1.2.1 Purification of ccNirWT.....	42
3.1.2.2 Purification of ccNirK134H.....	43
3.1.2.3 Purification of ccNirQ276E.....	44
3.1.2.4 Purification of ccNirY218F.....	45
3.1.2.5 Purification of ccNirStopI.....	46
3.1.3 Metal Content.....	47
3.1.4 UV-Vis Spectra.....	48
3.1.5 Reaction of ccNir with Hydroxylamine and Derivatives.....	51
3.1.6 Multifrequency EPR Spectroscopy.....	53
3.1.6.1 EPR Spectra of ccNirWT.....	54
3.1.6.2 EPR Spectra of ccNirK134H.....	56
3.1.6.3 EPR Spectra of ccNirQ276E.....	57
3.1.6.4 EPR Spectra of ccNirY218F.....	59
3.1.6.5 EPR Spectra of ccNirStopI.....	60
3.1.6.6 Comparison of the EPR Parameters for ccNir and Variants.....	61
3.1.6.7 Power Saturation Studies.....	62
3.1.6.8 Influence of Yttrium(III) on the EPR Spectra of ccNirQ276E (NrfA _S).....	64
3.1.6.9 Simulation of the X-Band EPR Spectrum of ccNirQ276E (NrfA _S).....	65
3.1.7 Magnetic Susceptibility.....	67
3.1.8 Probing the Active Site of ccNir by X-ray Crystallography – 3D Structures of ccNir Variants.....	68
3.1.8.1 ccNirK134H.....	68
3.1.8.2 ccNirQ276E.....	71
3.1.8.3 ccNirY218F.....	72
3.1.8.4 Crystal Structure of ccNirY218F N-Methylhydroxylamine Complex.....	73
3.1.9 Crystallization of ccNirQ276E (NrfHA).....	75
3.2 Cytochrome <i>cd</i> ₁ Nitrite Reductase.....	77
3.2.1 Crystallization of <i>cd</i> ₁ Nir from <i>Pseudomonas stutzeri</i> and <i>Thiobacillus denitrificans</i>	77

4 Discussion	79
4.1 Crystal Structure of Cytochrome <i>c</i> Nitrite Reductase	79
4.1.1 Assembly of the Wild-Type Protein	79
4.1.2 Comparison of the Crystal Structures of ccNir Variants	82
4.1.3 Substrate Binding Motifs	86
4.2 Spectroscopic Properties of Cytochrome <i>c</i> Nitrite Reductase	87
4.2.1 UV-Vis Spectroscopy	87
4.2.2 EPR Spectroscopy	88
4.2.2.1 Microwave Frequency Independent Resonances	89
4.2.2.2 Microwave Frequency Dependent Resonances	91
4.2.2.3 Comparison of the EPR Spectra from Multiheme Enzymes	92
4.3 Mechanism and Reactivity of Cytochrome <i>c</i> Nitrite Reductase	96
4.3.1 Substrate Binding and Reactivity	97
4.3.2 Reactivity Towards NO	100
4.3.3 Hydroxylamine as Reaction Intermediate	101
4.3.4 Binding of Ammonium	102
 5 References	 103
 6 Appendix	 119
6.1 Abbreviations	119
6.2 Amino Acids	120
6.3 Curriculum Vitae	121
6.4 Publications	122
6.5 Conference Abstracts	123
 7 Acknowledgment	 125

Zusammenfassung

1. Cytochrom *c* Nitritreduktasen katalysieren die Sechs-Elektronen Reduktion von Nitrit zu Ammoniak. Dieser Teil des respiratorischen Stoffwechselweges der Nitrat-Ammonifikation stellt einen wichtigen Schritt im biologischen Stickstoffkreislauf dar.

Die Cytochrom *c* Nitritreduktasen (ccNir) aus *Wolinella succinogenes* Wildtyp, K134H-, Q276E-, Y218F- und StopI-Variante wurden sowohl aus der löslichen als auch aus der Membranfraktion zur Homogenität gereinigt. Aus der Membranfraktion wurden sie als Monomer (NrfA) und als Komplex NrfHA mit einem Tetrahäm *c*-Typ Cytochrom (NrfH) isoliert.

Für die Aktivitäten ergaben sich im Vergleich zum Wildtyp für die K134H-Variante ein Wert von 35 %, für die Q276E-Variante 60 % und für die Y218F-Variante 3 %. Die StopI-Variante war inaktiv. Mittels ICP-MS wurde der Gehalt an Eisen, Calcium und Molybdän bestimmt. Die Q276E-Variante zeigte vergleichbare Werte wie der Wildtyp, die StopI-Variante ergab vier Eisen pro Monomer NrfA, was den Verlust des aktiven Zentrums (Häm 1) bestätigt (Pisa *et al.*, 2002). Der Molybdängehalt von ca. 2-4 % pro Monomer NrfA lässt auf Verunreinigungen mit Nitratreduktase schließen.

Die spektroskopische Untersuchung der Reaktion von ccNir mit Hydroxylamin, N- bzw. O-substituierten Derivaten und Hydrazin zeigte, dass ausgehend vom oxidierten (wie isoliert, alle Fe Atome im Fe(III)-Zustand) Enzym maximal 16 % der ccNir reduziert wurde. Das photochemisch reduzierte Enzym (alle Fe Atome im Fe(II)-Zustand) ergab eine spontane Reoxidation mit einer Ausbeute von ca. 90 %. Demzufolge bindet das Hydroxylamin und die N- bzw. O-substituierten Derivate an das Eisenatom von Häm 1 (Einsle *et al.*, 2002b) in oxidiertem ccNir und reduziert es nicht. Hydrazin bildet eine Ausnahme und reduziert ccNir vollständig.

Die X-Band EPR Spektren von ccNir Wildtyp und der untersuchten Varianten zeigen Resonanzen bei $g = 2,98$ bis $g = 1,46$, was auf zwei separate Fe(III) low-spin Häme mit nahezu parallelen Imidazolflächen (Häm 2 und 3 in der Struktur; Einsle *et al.*, 2000) hinweist.

Die Signale bei $g = 2,5$; $2,15$; $1,8$ und $1,48$ in den Spektren der Q276E- und Y218F-Variante sind mikrowellenfrequenzabhängig, was auf ein spingekoppeltes Paar von zwei $S = 1/2$ Zuständen hindeutet. Die Resonanzen zwischen $g = 3,5$ bis $g = 3,16$ werden Fe(III) low-spin Hämen mit nahezu senkrechten Imidazolflächen (Häm 4 und 5 in der Struktur; Einsle *et al.*, 2000) zugeordnet. Diese Signale fehlen nur in der StopI-Mutante. Resonanzen bei $g = 6$, welche auf ein Fe(III) high-spin Häm hinweisen, wurden lediglich in den Spektren vom Wildtyp und der K134H-Variante beobachtet. Weiterhin wurden die Signale bei $g = 9,8$ und $g = 3,8$, welche auf ein $S = 5/2 \leftrightarrow 1/2$ gekoppeltes Paar hinweisen, nur in den Spektren des Wildtyps und der K134H-Variante beobachtet. Jedoch wurde bei der K134H-Variante trotz der Gegenwart des high-spin Signals bei $g = 6$ und den Signalen bei $g = 9,8$ und $g = 3,8$ im „Perpendicular Mode“, die einer $S = 5/2 \leftrightarrow 1/2$ Kopplung zugeordnet werden können, kein Signal bei $g = 9,8$ im „Parallel Mode“ gefunden.

Magnetische Suszeptibilitätsmessungen mittels SQUID-Magnetometer (Variation des Magnetfeldes und der Temperatur) von ccNir Wildtyp unterstützen die Annahme einer antiferromagnetischen Kopplung der einzelnen Häm-Zentren.

Die Kristallisation und die räumlichen Strukturen der ccNir K134H-, Q276E- und Y218F-Variante wurden zusammen mit Prof. A. Messerschmidt vom Max-Planck-Institut für Biochemie in Martinsried durchgeführt. Die Gesamtstruktur von NrfA mit Dimerenbildung und α -Helices als überwiegendes Strukturmotiv sowie die Anordnung der fünf Häme wurde durch die Punktmutationen nicht verändert. In der K134H-Variante wurde das für ccNir hoch konservierte Lysin als proximaler Ligand durch Histidin als proximaler Ligand ausgetauscht. Bedingt durch die relative Starrheit der Aminosäureseitenkette und das „Aufliegen“ des aktiven Zentrums (Häm 1) auf Häm 3 ergibt sich ein ungewöhnlich langer Fe-N Bindungsabstand von $2,43 \text{ \AA}$ zum His 134. Außerdem wird das distale Wasser durch Acetat ausgetauscht, das auch einen verlängerten Bindungsabstand zwischen dem Carboxylsauerstoff und dem Eisen von $2,37 \text{ \AA}$ hat. In der Q276E-Variante wurde das Glutamin der Calciumbindestelle durch Glutamat ausgetauscht, dessen zwei Sauerstoffatome zweizählig koordinieren. In dieser Struktur wird ein achtfach koordiniertes Y(III) Ion anstelle des siebenfach koordinierten Ca(II) Ions gefunden. Weiterhin ändert sich das Oberflächenpotential des aktiven Zentrums. In der Y218F-Variante wurde das Tyrosin nahe dem Eisen des aktiven Zentrums durch ein Phenylalanin ausgetauscht. Durch das Fehlen der Hydroxylgruppe kann keine Wasserstoffbrückenbindung zum distalen Liganden aufgebaut werden. Außerdem ist eine Protonenübertragung auf das Substrat nicht mehr möglich, weshalb die Aktivität signifikant sinkt.

In der Struktur des N-Methylhydroxylaminkomplexes der Y218F-Variante ergab sich eine Sauerstoffbindung zum Eisen des aktiven Zentrums (Häm 1) im Vergleich zur Stickstoffbindung beim Hydroxylaminkomplex (Einsle *et al.*, 2002b). Dies steht im Einklang mit DFT-Rechnungen, die von PD Dr. F. Neese vom Max-Planck-Institut für Bioanorganische Chemie in Mülheim/Ruhr durchgeführt wurden. Bei Hydroxylamin wird eine Stickstoffbindung und bei N-Methylhydroxylamin eine Sauerstoffbindung vorhergesagt.

Erste Kristalle des Membran-assoziierten Nitritreduktasekomplexes (NrfHA) aus der Q276E-Variante wurden erhalten. Die Strukturanalyse ist noch in Arbeit.

2. Die Cytochrom *cd*₁ Nitritreduktasen aus den Denitrifizierern *Pseudomonas stutzeri* und *Thiobacillus denitrificans* katalysieren die Ein-Elektron Reduktion von Nitrit zu Stickstoffmonoxid. Die Kristalle der Enzyme wurden in Zusammenarbeit mit Prof. A. Messerschmidt analysiert und streuten bis zu einer Auflösung von 3,0 bzw. 3,5 Å.

Summary

1. Cytochrome *c* nitrite reductases catalyze the six-electron reduction of nitrite to ammonia. This part of the respiratory pathway of nitrate ammonification is a key step in the biological nitrogen cycle.

Cytochrome *c* nitrite reductases from *Wolinella succinogenes* wild-type, K134H-, Q276E-, Y218F-, and StopI-variant were purified to homogeneity both from the soluble and the membrane fraction. From the membrane fraction they were isolated as a monomer (NrfA) and as a complex NrfHA with a tetraheme *c*-type cytochrome (NrfH).

Compared to wild-type the activities were for the K134H-variant 35 %, for the Q276E-variant 60 % and for the Y218F-variant 3 %. The StopI-variant was inactive. The metal content (Fe, Ca, Mo) was determined with ICP-MS. The Q276E-variant showed values similar to wild-type, the StopI-variant had four Fe atoms per monomer NrfA which confirmed the deletion of the active site (heme 1) (Pisa *et al.*, 2002). The molybdenum content was 2-4 % per monomer NrfA which can be linked to an impurity with nitrate reductase.

The spectroscopic investigation of the reaction of ccNir with hydroxylamine, its N- and O-substituted derivatives and hydrazine showed, starting from the oxidized (as isolated, all Fe atoms in Fe(III) state) enzyme, that at most 16 % of ccNir became reduced. The photochemically reduced enzyme (all Fe atoms in Fe(II) state) was reoxidized spontaneously with a yield of about 90 %. Therefore, hydroxylamine and its N- and O-substituted derivatives bind to the iron atom of heme 1 (Einsle *et al.*, 2002b) in oxidized ccNir but do not reduce it. As an exception, hydrazine is able to reduce ccNir.

The X-Band EPR spectra of ccNir wild-type and the investigated variants showed resonances at $g = 2.98$ to $g = 1.46$ which can be assigned to two separate Fe(III) low-spin hemes with nearly parallel imidazole planes (heme 2 and 3 in the structure; Einsle *et al.*, 2000). The signals at $g = 2.5$, 2.15, 1.8, and 1.48 in the spectra of the Q276E- and the Y218F-variant are microwave frequency dependent, indicating a spin-coupled pair of two $S = 1/2$ states. The resonances at $g = 3.5$ to $g = 3.16$ can be assigned to Fe(III) low-spin hemes with

nearly perpendicular imidazole planes (hemes 4 and 5 in the structure; Einsle *et al.*, 2000). These signals are only missing in the StopI-variant. Resonances at $g = 6$, which most likely originate from a Fe(III) high-spin heme, were only observed in the spectra of the wild-type enzyme and the K134H-variant. Additionally, signals at $g = 9.8$ and $g = 3.8$, which can be assigned to a $S = 5/2 \leftrightarrow 1/2$ spin-coupled pair, were only observed in the spectra of ccNirWT and ccNirK134H. However, despite of the presence of the high-spin signal at $g = 6$ and the signals at $g = 9.8$ and $g = 3.8$ in the “perpendicular mode” spectra, which can be assigned to a $S = 5/2 \leftrightarrow 1/2$ spin-coupled pair, no signal at $g = 9.8$ in the “parallel mode” was observed in the spectra of ccNirK134H.

Measurements of the magnetic susceptibility with a SQUID-magnetometer (variation of magnetic field and temperature) of ccNirWT support the presence of antiferromagnetically coupling between the heme centers.

Crystallization and structure determination of ccNir K134H-, Q276E-, and Y218F-variant were carried out in collaboration with Prof. A. Messerschmidt at the Max-Planck-Institute of Biochemistry in Martinsried. The overall structure of ccNir with the dimeric architecture and α -helices as the predominant structural motif as well as the arrangement of the five hemes were not changed during site-directed mutagenesis. In the K134H-variant the unusual lysine, which is highly conserved in ccNir as the proximal ligand, was replaced by histidine, which is the typical proximal ligand in *c*-type cytochromes. Because of the relative inflexibility of the amino acid side chain and the “stacking” of the active site (heme 1) to heme 3, an unusually long bond distance of 2.43 Å to His 134 is formed. Furthermore, the distal water is replaced by acetate, which has also an elongated bond distance between the carboxyl-oxygen and the active site iron of 2.37 Å. In the Q276E-variant glutamine of the calcium-binding site was exchanged against glutamate. Because of the two oxygens in glutamate it acts as a bidentate ligand. In the structure, an eightfold coordinated Y(III) ion was found instead of a sevenfold coordinated Ca(II) ion. Additionally, the electrostatic surface potential of the active site cavity is changed. In the Y218F-variant the tyrosine close to the active site iron was replaced by phenylalanine. Because there is no hydroxyl-group in phenylalanine, the hydrogen bond to the distal ligand cannot be assembled. Moreover, a proton transfer to the substrate is impossible, thus the activity decreases significantly.

In the structure of the N-methylhydroxylamine complex of the Y218F-variant, the ligand N-methylhydroxylamine coordinates through oxygen to the Fe atom of heme 1, compared to nitrogen in the complex with hydroxylamine (Einsle *et al.*, 2002b). This finding is supported by DFT-calculations carried out by PD Dr. F. Neese at the Max-Planck-Institute

of Bioinorganic Chemistry in Mülheim/Ruhr. In the hydroxylamine complex a nitrogen binding and in the N-methylhydroxylamine complex a oxygen binding are predicted.

First crystals of the membrane-associated nitrite reductase complex (NrfHA) of the Q276E-variant were obtained. The structure determination is still in progress.

2. Cytochrome *cd*₁ nitrite reductases from denitrifying *Pseudomonas stutzeri* and *Thiobacillus denitrificans* catalyze the one-electron reduction of nitrite to nitric oxide. Preliminary investigations on the crystals of the enzymes were done in collaboration with Prof. A. Messerschmidt. The crystals diffracted to a resolution of 3.0 and 3.5 Å, respectively.

1 Introduction

1.1 The Biogeochemical Nitrogen Cycle

The biological nitrogen cycle has received considerable attention over the past decades because of its global importance (Figure 1.1) (Sprenst, 1987; Kroneck, 1990; Kroneck *et al.*, 1992; Kroneck and Abt, 2002; Rudolf and Kroneck, 2005). The amount of nitrogen, in comparison to hydrogen, carbon, and oxygen, is only minor in living organisms (roughly 3 % in humans). The three basic elements hydrogen, carbon and oxygen are readily bioavailable in form of water and carbon dioxide for plants which are the key players in our food chain (Smil, 1997). Dinitrogen, though the major constituent of the atmosphere, has to be converted first to ammonia by a complex process called nitrogen fixation. Nitrate reduction plays a key role and has important agricultural, environmental and public health implications. Assimilatory nitrate reduction, performed by bacteria, fungi, algae, and higher plants, is one of the most fundamental biological processes.

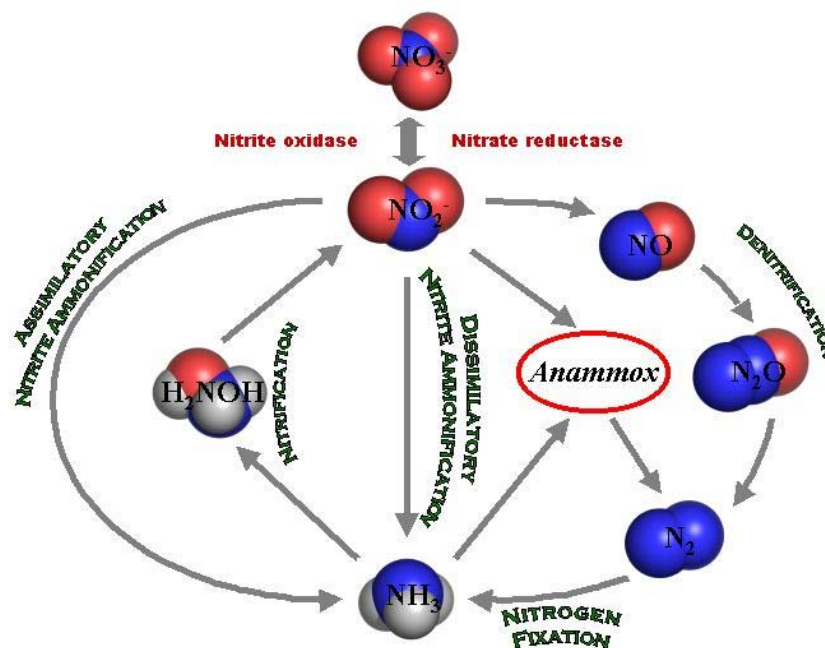


Figure 1.1: The biogeochemical nitrogen cycle.

The tremendous use of fertilizers in agricultural activities led to a significant nitrate accumulation in groundwater, and consumption of drinking water with high levels of nitrate had been associated with severe diseases due to formation of highly toxic N-nitroso compounds.

Nitrogen is a basic element for life because it is a component of essential biomolecules, such as amino acids, proteins and nucleic acids. Nitrogen exists in the biosphere in several oxidation states, ranging from N(+5), as in nitrate, to N(-3) as in ammonia. Interconversions of these nitrogen species constitute the global biogeochemical nitrogen cycle which is sustained by biological processes, with bacteria playing a predominant role (Conrad, 1996; Zumft, 1997; Lin and Stewart, 1998; Moreno-Vivián, 1999; Richardson and Watmough, 1999; Brune *et al.*, 2000; Ye and Thomas, 2001; Richardson, 2001; Anbar and Knoll, 2002; Simon, 2002; Morel and Price, 2003). Although multicellular organisms such as fungi, algae, higher plants, and humans have made a significant mark on the geochemistry of the earth, averaged over geological time, it is clear that the most important geochemical agents by far have been unicellular microorganisms, e.g. *Bacteria*, *Archaea*, and single-celled *Eucarya* (Newman and Banfield, 2002). Microbes have altered the chemistry of the atmosphere via oxygenic photosynthesis, nitrogen fixation, and carbon sequestration. Most remarkably, they perform these many chemical reactions in every nook and cranny from the near surface to the depths, including even the most extreme environments (Reysenbach and Shock, 2002).

Inorganic nitrogen is converted to a biologically useful form by dinitrogen fixation ($\text{N}_2 \rightarrow \text{NH}_3$) or nitrate assimilation ($\text{NO}_3^- \rightarrow \text{NH}_3$) and the incorporation of ammonia into organic molecules. Inorganic nitrogen compounds are recycled from the environment by nitrification ($\text{NH}_3 \rightarrow \text{NO}_3^-$), the oxidative conversion of ammonia to nitrate, denitrification ($\text{NO}_3^- \rightarrow \text{N}_2$) whereby nitrate is successively transformed to nitrite, nitrogen monoxide (NO), dinitrogen monoxide, and dinitrogen, and nitrate-ammonification ($\text{NO}_3^- \rightarrow \text{NH}_3$), with nitrite as intermediate (Figure 1.1). Nitrate plays a key role in the biogeochemical nitrogen cycle which is contributed to by both prokaryotic and eukaryotic organisms. It is a source of nitrogen for assimilation, whereby the key enzymatic reaction is the reduction of nitrate to nitrite. Nitrite is further reduced to ammonium, which can be further assimilated into organic nitrogen. The same series of reactions, though often catalyzed by distinct enzymes, can also occur as part of a nitrate respiration process in some enteric and sulfate-reducing bacteria, whereby nitrate serves as a terminal electron acceptor during anaerobic metabolism (Richardson, 2001).

In denitrification, NO_3^- is reduced via NO_2^- to the gaseous products NO , N_2O , and N_2 . The biological process comprises several steps including the formation of the N-N bond in N_2O and the cleavage of the N-O bond in N_2O . The biology and microbial ecology of the denitrification pathway has been reviewed (Zumft, 1997; Ferguson, 1998; Ye and Thomas, 2001; Richardson, 2000; Moura and Moura, 2001). Denitrifying bacteria utilize the positive redox potentials of nitrate ($E^\circ(\text{NO}_3^-/\text{NO}_2^-) = +0.43 \text{ V}$), nitrite ($E^\circ(\text{NO}_2^-/\text{NO}) = +0.35 \text{ V}$), nitric oxide ($E^\circ(\text{NO}/\text{N}_2\text{O}) = +1.175 \text{ V}$), and nitrous oxide ($E^\circ(\text{N}_2\text{O}/\text{N}_2) = +1.355 \text{ V}$) (Thauer *et al.*, 1977) for energy conservation by chemiosmotic coupling of ATP synthesis and electron transport. Nitrogen oxides produced by denitrification are also linked with the greenhouse effect and the depletion of stratospheric ozone. Dinitrogen monoxide (N_2O , *laughing gas*) is recognized as a greenhouse gas with a tropospheric concentration of $\approx 300 \text{ ppb}$ by volume (Kim and Craig, 1993). The terminal oxidoreductases of denitrifying bacteria obtain the reducing equivalents via quinones (Zumft, 1997). Recently, a novel species of the *Ectothiorhodospira* clade was isolated that grew anaerobically with As(III) as the electron donor (Oremland and Stolz, 2003).

It was thought for a long time that in the ocean denitrification was the only mechanism of N_2 production. However, most recently it was shown by two independent groups that large scale conversion of fixed inorganic nitrogen (nitrate, nitrite, ammonium) to N_2 can occur through another important route, the so-called Anammox process (Equation 1.1) (Devol, 2003).



In this context, a new autotrophic member of the order *Planctomycetales* was isolated earlier and identified which possessed the Anammox pathway (Strous *et al.*, 1999). The process of Anammox has to be considered to be one of the most innovative technological advances in removal of ammonia nitrogen from wastewater.

Ammonium oxidation has been observed in many bacterial species, it is oxidized by two pathways. First, ammonia is oxidized aerobically to hydroxylamine, which is then oxidized to nitrite in a four-electron step. Second, ammonia and nitrite are converted anaerobically to dinitrogen gas by the Anammox process. Nitrifying bacteria connect the oxidized and reduced sides of the nitrogen cycle by nitrification, the conversion of ammonium to nitrogen oxyanions (Kroneck *et al.*, 1992; Hooper *et al.*, 1996; Kroneck and Abt, 2002).

The most important microorganisms involved in the transformation of ammonia to nitrite, and nitrite to nitrate, are the lithoautotrophic ammonia- and nitrite-oxidizing bacteria placed in the family *Nitrobacteraceae* (Kroneck and Abt, 2002). The obligate aerobic lithotrophic bacterium *Nitrosomonas europaea* derives energy from the oxidation of ammonia to nitrite. Hereby, ammonia is oxidized to hydroxylamine by ammonia monooxygenase which is converted to nitrite by hydroxylamine oxidoreductase (Equations 1.2, 1.3) (Hooper *et al.*, 1991; Whittaker *et al.*, 2000).



Two of the four electrons generated from hydroxylamine oxidation are used to support the oxidation of additional ammonia molecules, while the other two electrons enter the electron transfer chain and are used for CO₂ reduction and ATP biosynthesis (Frijlink, 1992; Ensign, 1993). The three-dimensional structure (resolution 2.8 Å) of the hydroxylamine oxidoreductase from *N. europaea* revealed a homotrimeric unit, with each monomer carrying a complex array of eight heme centers including the so-called P₄₆₀ catalytic center (Igarashi, 1997). Surprisingly, this enzyme revealed structural homologies to other multiheme *c*-type cytochromes, amongst them the pentaheme cytochrome *c* Nir (NrfA) from *S. deleyianum* and *W. succinogenes* (Einsle *et al.*, 1999; Einsle *et al.*, 2000). These homologies mainly concern the arrangement of heme groups but not the surrounding protein. The five hemes of the cytochrome *c* Nir aligned to hemes 4 to 8 of hydroxylamine oxidoreductase with a root-mean-square deviation of 2.00 Å (Einsle *et al.*, 2000). However, while a protoporphyrin IX heme with a novel lysine coordination forms the active site of nitrite reductase, the hydroxylamine oxidoreductase features the P₄₆₀-type heme with a covalent link to a tyrosine residue. The iron atom of heme P₄₆₀ appears to be five-coordinated, with a histidine as an axial protein ligand. The sixth position of the heme iron is not occupied and hydroxylamine can bind to this position (Igarashi, 1997).

The close coupling of nitrification and denitrification has been demonstrated by measuring the overall dinitrogen flux from microcosms in a helium/dioxygen atmosphere (Arth, 1998). Within the microenvironment of the rice rhizosphere, the activities of nitrifiers and of denitrifiers depended on the presence of dioxygen and ammonium. Carbon and nitrogen cycles are clearly interrelated. Methane monooxygenases and ammonia

monooxygenases are relatively unspecific, and may also oxidize ammonium or methane, respectively (Brune *et al.*, 2000).

1.2 Nitrate Reductases

Nitrate is a major source of inorganic nitrogen for plants, fungi, and many species of bacteria. Animals cannot assimilate nitrate. Assimilation involves three pathway-specific steps: uptake followed by reduction to nitrite, and further reduction to ammonia which is then metabolized into central pathways.

Next to its role as a nutrient, nitrate is an important oxidant for the conservation of metabolic energy, i.e. nitrate respiration, and the dissipation of excess reducing power for redox balancing, nitrate dissimilation (Richardson *et al.*, 2001; Kroneck and Abt, 2002). All eukaryotic and bacterial nitrate reductases are molybdenum-dependent enzymes and possess a unique cofactor, the so-called molybdopterin (Figure 1.2) (Kisker *et al.*, 1999). Nitrate-reducing archaea are also known and putative molybdopterin-binding enzymes can be identified in the genome sequence of *Archaeoglobus fulgidus* which suggests the presence of molybdopterin-dependent enzymes, such as nitrate reductase, DMSO reductase, or polysulfide reductase (Richardson, 2000). Four types of nitrate reductases catalyze the two-electron reduction of nitrate to nitrite (Equation 1.4).



These are the eukaryotic assimilatory nitrate reductases and three distinct bacterial enzymes, comprising the cytoplasmic assimilatory (Nas), the membrane-bound (Nar), and the periplasmic dissimilatory (Nap) (Figure 1.2) nitrate reductases (Moreno-Vivián, 1999).

Nitrite oxidoreductase, a membrane-bound enzyme from nitrifying bacteria also exhibits nitrate reductase activity. This enzyme shows high sequence similarity to the membrane-bound Nar, and catalyzes the nitrite oxidation to nitrate, to allow chemoautotrophic growth (Sundermeyer-Klinger, 1984). Many bacteria have more than one of the four types of nitrate reductases (Zumft, 1997). The functional, biochemical and structural properties of prokaryotic and eukaryotic nitrate reductases have been recently reviewed (Kroneck *et al.*, 1992; Campbell, 2001; Kroneck and Abt, 2002). Protein sequence data have been used to determine phylogenetic relationships and to examine similarities in structure and function of nitrate reductases. Three distinct clades of nitrate reductase evolved: the eukaryotic assimilatory enzyme (Euk-Nas), the membrane-associated prokaryotic enzyme

(Nar), and a clade that included both the periplasmatic (Nap) and prokaryotic assimilatory enzyme (Pro-Nas) (Stolz and Basu, 2002).

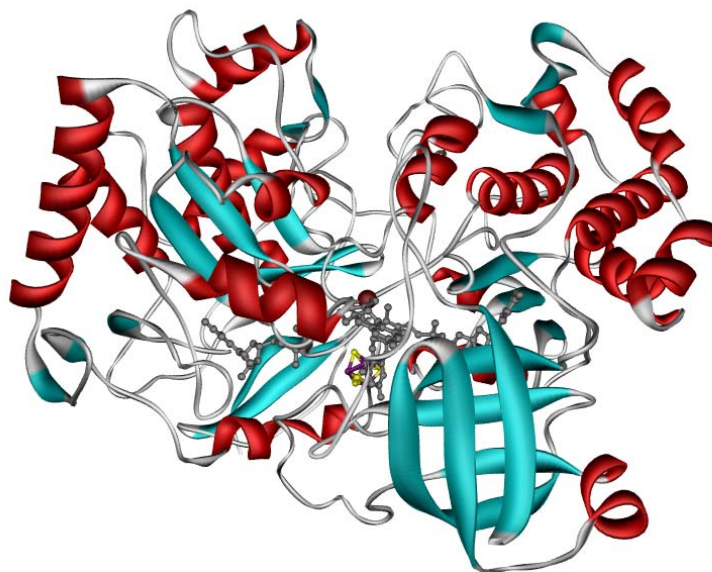


Figure 1.2: Schematic representation of the nitrate reductase from *Desulfovibrio desulfuricans* ATCC 27774. PDB code: 2NAP.

E. coli, when grown anaerobically with nitrate as respiratory oxidant, develops a respiratory chain terminated by the membrane-bound quinol-nitrate oxidoreductase, NarGHI (Jormakka *et al.*, 2002). The heterotrimeric NarGHI is composed of a Moco-containing Mo-bisMGD catalytic subunit, an FeS-cluster containing electron transfer subunit and a heme-containing membrane anchor subunit. The catalytic and electron transfer subunits form a membrane-extrinsic catalytic dimer anchored to the membrane. These redox-active groups are supposed to define an electron transfer chain linking a periplasmatically oriented site of quinol oxidation to a cytoplasmatically oriented site of nitrate reduction. In the respiratory chain composed of formate dehydrogenase N (FdnGHI) and NarGHI, electron transfer from formate to nitrate is coupled to the generation of a proton-motive force across the cytoplasmic membrane by a redox loop mechanism (Jormakka *et al.*, 2002). Meanwhile, high resolution X-ray structure of both FdnGHI and NarGHI have been reported which allow insights into the respiratory electron transfer pathway and proton-motive force generation (Jormakka *et al.*, 2002; Jormakka *et al.*, 2003; Bertero *et al.*, 2003).

Most recently, NarGHI has been studied by protein film voltammetry, with the enzyme adsorbed on a rotating disk pyrolytic graphite edge electrode. Nitrate binding might be influenced by the redox state of either the molybdenum site, or of the pterin moiety (Elliot *et al.*, 2004). At the same time, the structure of the catalytic and electron-transfer subunits (NarGH) of the integral membrane protein nitrate reductase has been determined revealing the

molecular architecture of the molybdenum enzyme which included a previously undetected FeS cluster (Jormakka *et al.*, 2004). In this structure, an aspartate was detected as a ligand to the Mo center for the first time.

A first model for the organization of respiratory nitrate-ammonification and direction of proton exchange associated with electron transfer from formate to nitrate in *E. coli* had been described earlier (Schumacher *et al.*, 1997). The reduction of nitrate to nitrite by the oxidation of formate is linked to the generation of a proton electrochemical potential. Whether the overall architecture of the nitrate reductase complex from *E. coli* also holds for other nitrite-ammonifying bacteria, has to be investigated. *S. deleyianum* and *D. desulfuricans* (Figure 1.2) also showed a membrane-associated or soluble nitrate reductase catalyzing the respiratory reduction of nitrate to nitrite (Costa *et al.*, 1990; Schumacher, 1993; Pereira *et al.*, 2000). A cytochrome *c*-dependent nitrate reductase was also isolated from *Geobacter metallireducens* (Naik *et al.*, 1993). Obviously, nitrate uptake and nitrite extrusion into the bulk phase is dispensable for periplasmic nitrate reductases. In addition, a periplasmic location of nitrate reductases will prevent the interaction of potentially toxic compounds such as nitrite or NO with cytoplasmic proteins.

1.3 Nitrite Reductases

Nitrite reducing enzymes can be divided in two classes: those involved in denitrification which reduce nitrite to nitric oxide, and the assimilatory and dissimilatory enzymes which reduce nitrite directly to ammonia (Berks *et al.*, 1995; Averill, 1996).

In bacterial denitrification, two classes of dissimilatory nitrite reductases are known, either a cytochrome *cd₁*, or a copper enzyme carrying the type-1 and a type-2 Cu center (Adman *et al.*, 1995; Murphy *et al.*, 1997; Williams *et al.*, 1997; Dodd *et al.*, 1997; Richardson and Watmough, 1999; Gray *et al.*, 2000).

In nitrite-ammonifying bacteria, especially in enterobacteria, there may exist two independently regulated dissimilatory ways of nitrite reduction to ammonia with two different physiological functions (Cole, 1996). A cytoplasmic siroheme-dependent nitrite reductase activity (NADH : nitrite oxidoreductase) (Jackson *et al.*, 1981; Harborne *et al.*, 1992) confers on *E. coli* the advantage of regenerating NAD⁺ during anaerobic growth to maintain glycolysis (Cole and Brown, 1980). Besides the supply of ammonia for biosynthesis, this nitrite reductase leads to the detoxification of intracellularly accumulated nitrite. The other nitrite reductase is a periplasmic cytochrome *c* that was isolated from *E. coli* (Fujita, 1966;

Cole, 1968). A membrane-bound formate-nitrite oxidoreductase complex with a respiratory function was first described for *E. coli* (Schumacher *et al.*, 1997).

1.3.1 Dissimilatory Cytochrome *c* Nitrite Reductase

The reduction of nitrite to ammonia was described for bacteria with a fermentative rather than a respiratory metabolism (Cole, 1996). However, growth of various bacteria by oxidation of non-fermentable substrates such as formate linked to the reduction of nitrite to ammonia, demonstrated that nitrite-ammonification may also function as respiratory energy conserving process (Schumacher *et al.*, 1997). The enzymology and bioenergetics of respiratory nitrite ammonification have been recently reviewed (Simon, 2002). In respiratory nitrite ammonification, nitrite is reduced to ammonia without the release of intermediate products, such as NO or N₂O, in a six-electron step by a cytochrome *c* nitrite reductase, the so-called NrfA protein (Figure 1.3; Equation 1.5) (Einsle *et al.*, 1999; Einsle *et al.*, 2000; Dias *et al.*, 2000; Almeida *et al.*, 2003).



This process can be regarded as a shortcircuit that bypasses denitrification and nitrogen fixation (Figure 1.1). Dihydrogen and formate are the predominant electron donors (Simon, 2002) but sulfide can also serve as electron donor, thus connecting the biogeochemical cycles of nitrogen and sulfur (Eisenmann *et al.*, 1995). Organisms capable of nitrite ammonification usually catalyze nitrate to nitrite reduction in dissimilatory metabolism (Simon, 2002). Note that the majority of sulfate-reducing *Desulfovibrio* species use nitrite but not nitrate (Mitchell *et al.*, 1986). In the sulfur- and sulfate-reducing species of the δ - and ϵ -proteobacteria, dissimilatory nitrite reduction to ammonia is the predominant metabolism during anaerobic growth on formate or dihydrogen. In γ -proteobacteria like *E. coli* however, the observed expression levels of nitrite reductase were considerably lower. The presence of a highly active nitrite reduction system might serve an important purpose, namely the disposal of toxic nitrite anion.

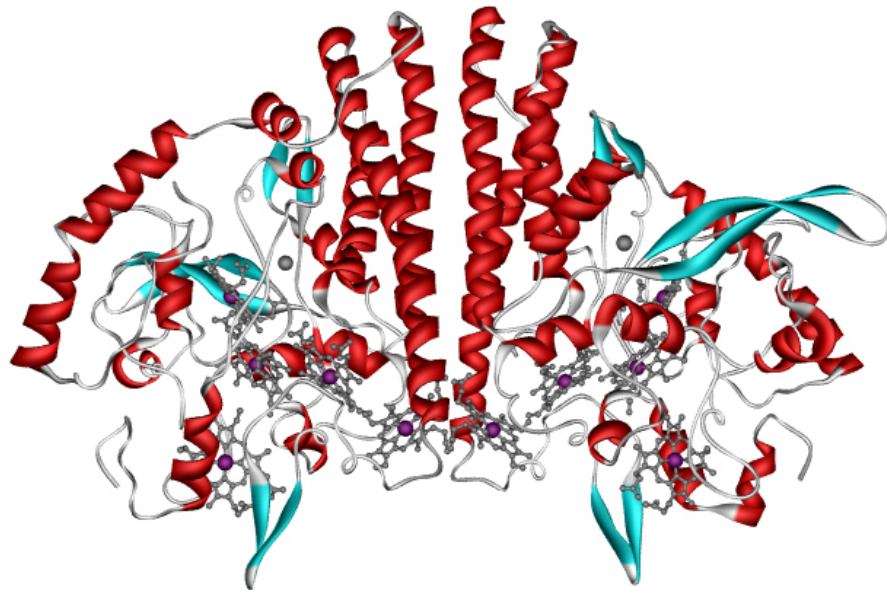


Figure 1.3: Schematic representation of the cytochrome *c* nitrite reductase from *Sulfurospirillum deleyianum*. PDB code: 1QDB.

A first model of the respiratory chain for the transformation of nitrite was proposed for nitrite-ammonifying bacteria, such as *Sulfurospirillum deleyianum* (Figure 1.3) and *Wolinella succinogenes* (Schumacher *et al.*, 1997). A periplasmically oriented membrane-bound formate dehydrogenase, or a hydrogenase, was included in the model. Most likely, the primary dehydrogenases functioning in the reduction of nitrate to nitrite, and nitrite to ammonia, are identical entities (Berks *et al.*, 1995). The complete electron transport chain from formate to nitrite was recently characterized for *W. succinogenes* by reconstituting the coupled electron transfer chain into liposomes (Simon *et al.*, 2000). A model of the electron transport chain of *W. succinogenes* has been developed showing the three major enzyme complexes involved in electron transfer from formate (or dihydrogen) to nitrite (Simon, 2002).

The enzyme from *E. coli* was the first cytochrome *c* Nir which had been completely sequenced (Darwin *et al.*, 1993; Hussain *et al.*, 1994). It is a heterooligomeric complex encoded by the *nrfABCDEFG* operon, with *nrfA* encoding for the periplasmic nitrite-reactive cytochrome *c* (M_r 51 kDa). Later on, sequences of cytochrome *c* Nir from other microorganisms including *S. deleyianum* and *W. succinogenes* became available in the GenBankTM/EBI sequence database, and high-resolution structures of cytochrome *c* Nir (soluble part, NrfA) of *S. deleyianum* (Figure 1.3), *W. succinogenes*, *D. desulfuricans* and *E. coli* were reported (Simon, 2002).

The functional nitrite reductase system of *W. succinogenes* and *S. deleyianum* was shown to be a complex of the soluble part NrfA and a membrane-anchored tetraheme *c*-type

cytochrome NrfH, which acts as a quinol oxidase to receive electrons from the membraneous quinone pool (Simon *et al.*, 2000). The current working hypothesis thus implies that the NrfA dimer is associated with the peripheral membrane protein NrfH as depicted in the model. Preliminary crystal data for the membrane associated complex were presented recently (Einsle *et al.*, 2002a).

Based on the observation of reaction intermediates in the crystal structure and on quantum chemical calculations Einsle *et al.* (2002b) propose an outline of the first detailed reaction mechanism of the cytochrome *c* nitrite reductase from *W. succinogenes*. Nitrite reduction starts with a heterolytic cleavage of the weak N-O bond, which is facilitated by a pronounced backbonding interaction between nitrite and the reduced active site iron. The protons comes from a highly conserved histidine and tyrosine. Elimination of one of both amino acids results in a significant reduced activity. Subsequently, two rapid one-electron reductions lead to a $\{\text{FeNO}\}^8$ form and, by protonation, to a HNO adduct. A further two-electron two-proton step leads to hydroxylamine. The iron in the hydroxylamine complex is in the ferric state (Rudolf *et al.*, 2002), which is unusual comparing to synthetic iron-hydroxylamine complexes where the iron is mainly in the ferrous state. Finally, it readily loses water to give the product, ammonia. This presumably dissociates from the Fe(III) form of the active site, whose re-reduction closes the reaction cycle.

1.3.2 Assimilatory Siroheme Nitrite Reductase

A cytoplasmic siroheme nitrite reductase has been described for *E. coli* (Zarowny and Sanwal, 1963). Assimilatory nitrite reductases reduce nitrite directly to ammonia, which is utilized for biosynthetic purpose, with no detectable intermediates. Siroheme nitrite reductases and sulfite reductases show a relationship in the sense that they have the capability of catalyzing the analogous six-electron reduction of nitrite to ammonia and from sulfite to sulfide, respectively. The X-ray structure of assimilatory sulfite reductase from *E. coli* (Figure 1.4), which shows sequence homologies to assimilatory nitrite reductase, has been solved to a resolution of 1.6 Å (Crane *et al.*, 1995).

Siroheme nitrite reductases and related sulfite reductases are the only known class of enzymes that couple a metalloporphyrin to an iron-sulfur cluster in a catalytically redox center. The siroheme (tetrahydroporphyrin of the isobacteriochlorin class) and the [4Fe-4S] cluster are bridged by a cysteine thiolate. The remaining distal axial coordination position of the siroheme is available for substrate binding. Sulfite and nitrite bind the siroheme iron through sulfur and nitrogen, respectively (Crane *et al.*, 1997a). Sulfite and nitrite both form

low-spin ($S = 1/2$) complexes with the ferric siroheme. Spectroscopic studies indicate that the siroheme and iron-sulfur cluster are closely associated and electronically influenced by each other in all oxidation states of the enzyme. In the oxidized state, the ferric siroheme is high-spin ($S = 5/2$) and the $[4\text{Fe-4S}]^{2+}$ cluster is diamagnetic (Crane *et al.*, 1997b).

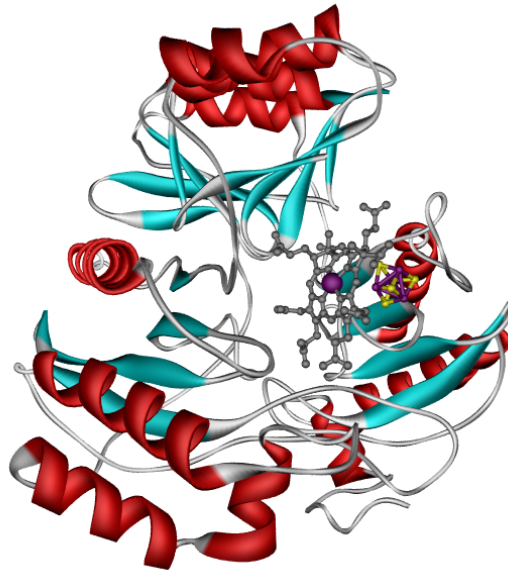


Figure 1.4: Schematic representation of the assimilatory sulfite reductase from *Escherichia coli*. PDB code: 1AOP.

Bacterial siroheme nitrite reductase, which is located in the cytoplasm, uses NADH as electron donor (Jackson *et al.*, 1981). Electrons are transferred via a further flavin-containing subunit to the iron-sulfur cluster and then to the heme iron. In contrast, cyanobacterial proteins directly interact with ferredoxins.

The crystal structure of the *E. coli* sulfite reductase hemoprotein revealed a completely different type of protein fold and cofactor composition (Figure 1.4), but the reaction also takes place by binding nitrite or sulfite to a tetrapyrrole-ligated iron (Crane *et al.*, 1995). It has been suggested that siroheme is a more ancient form of tetrapyrrole cofactor than the protoporphyrin-IX-derived hemes due to its higher stability towards a reducing environment as it existed prior to the oxidation of the atmosphere as a consequence of photosynthesis. Cytochrome *c* nitrite reductase is the only *c*-type cytochrome that has been shown to perform six-electron reductions from sulfite to sulfide and from nitrite to ammonia, both with a considerably higher activity than the siroheme proteins. This appears reasonable in the light of dissimilatory nitrite ammonification being an energy metabolism which will experience an evolutionary pressure towards higher energy yield and faster kinetics. The assimilatory pathway of the siroheme proteins is older and essential for the organisms - meaning resistant

to evolutionary changes which are often unfavourable for the individual - and does not require high performance enzymes.

1.3.3 Cytochrome *cd*₁ Nitrite Reductase

Cytochrome *cd*₁ nitrite reductase is a bifunctional multiheme enzyme catalyzing the one-electron reduction of nitrite to NO and the four-electron reduction of dioxygen to water. The enzyme has been purified from several sources as a homodimer (60 kDa/subunit), each subunit containing one heme *c* and one heme *d*₁ (Figure 1.5), and is located in the bacterial periplasm. A high resolution structure has been presented for the enzyme from *Paracoccus pantotrophus* (Figure 1.5) (Fülöp *et al.*, 1995) and the enzyme from *Pseudomonas aeruginosa* (Nurizzo *et al.*, 1997). In both enzymes, heme *c* is covalently linked to the N-terminal α -helical domain and heme *d*₁ is bound non-covalently to the C-terminal β -propeller domain. Heme *c* from the *P. pantotrophus* enzyme has a bis-histidine coordination, whereas the iron in heme *d*₁ is coordinated to Tyr 25 and His 200. Mutation of Tyr 25 by Serine does not result in decreased activity of reduction of any substrate (Gordon *et al.*, 2003). Instead, unlike the wild-type enzyme, the Y25S mutant is active as a reductase towards nitrite, oxygen and hydroxylamine without a reductive activation step. Heme *c* in the *P. aeruginosa* enzyme is more like the classical cytochrome *c* fold because it has His 51 and Met 88 as heme ligands. The *d*₁-heme domains are almost identical in both structures. Intramolecular electron transfer between the heme *c* as the electron uptake site and heme *d*₁ as the nitrite reduction site is an essential step in the catalytic cycle and has been studied by several groups using different methods (Parr *et al.*, 1977; Blatt and Pecht, 1979; Schichman and Gray, 1981; Silvestrini *et al.*, 1990; Kobayashi *et al.*, 1997). The rate constant of the *P. pantotrophus* enzyme (Kobayashi *et al.*, 1997) with $1.4 \times 10^3 \text{ s}^{-1}$ is 1000 times higher than the rate of the *P. aeruginosa* enzyme with 1 s^{-1} (Parr *et al.*, 1977; Schichman and Gray, 1981; Silvestrini *et al.*, 1990). Recently, the electron transfer rate of the enzyme from *Pseudomonas stutzeri* has been detected with a rate of 23 s^{-1} (Farver *et al.*, 2002).

Catalysis commences with the binding of nitrite, through its nitrogen atom, to the reduced *d*₁ heme (Fülöp *et al.*, 1995; Nurizzo *et al.*, 1997). This relatively rare example of an anion binding to a Fe(II) heme is followed by transfer of one electron and two protons to nitrite, with the result that water is released and a nitrosyl species is generated at the *d*₁ heme. The protons are provided by two highly conserved histidine residues on the distal side of the *d*₁ heme. The product of reduction and dehydration of nitrite can be regarded as *d*₁-Fe²⁺-NO⁺ or *d*₁-Fe³⁺-NO, which are isoelectronic (Williams *et al.*, 1995). It is expected that the *d*₁-Fe³⁺-

NO species should be unstable and dissociate to give NO and Fe(III) d_1 heme. Most recently, kinetics and thermodynamics of the internal electron transfer process in the enzyme from *P. stutzeri* were found to be dominated by pronounced interactions between the c and the d_1 hemes (Farver *et al.*, 2003). The interactions are expressed both in significant changes in the internal electron transfer rates between these sites and in marked cooperativity in their electron affinity.

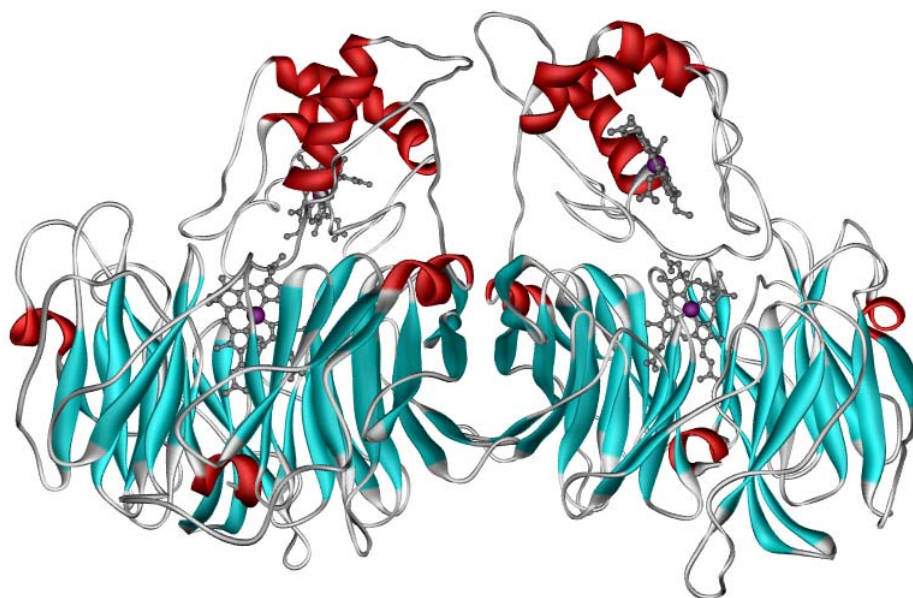
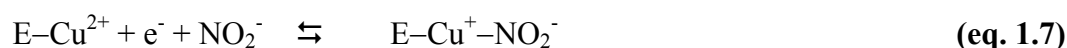


Figure 1.5: Schematic representation of the cytochrome cd_1 nitrite reductase from *Paracoccus pantotrophus*. PDB code: 1QKS.

1.3.4 Copper-Containing Nitrite Reductase

The Cu-dependent nitrite reductase, which transforms nitrite to nitric oxide in denitrifying bacteria, contains both the type-1 and the type-2 Cu center but lacks the binuclear type-3 site (Suzuki *et al.*, 2000). Yet, its arrangement of Cu atoms within the protein indicates a strong structural relationship with the 'classical' blue multi-copper oxidases (Murphy *et al.*, 1997). It catalyzes the single-electron reduction of NO_2^- to NO and water (Equations 1.6-1.8).



Nitrite reductase is a homotrimer in its native state. Depending on the origin the chain length of the respective subunits vary between 340 and 379 amino acid residues. The trimer contains three type-1 and three type-2 Cu centers. The type-1 Cu centers are localized within

the subunits, whereas the type-2 Cu centers are coordinated by residues from two different subunits. The physiological electron-donor of nitrite reductase is the type-1 Cu protein pseudoazurin, which transfers a single electron to the type-1 Cu center of nitrite reductase, from where it is transferred to the type-2 Cu (Murphy *et al.*, 2002). The type-2 Cu is the binding-site for nitrite and where it is reduced to NO. The subunits of nitrite reductase from *Alcaligenes faecalis* contain two domains. Each domain consists of a β -barrel structure, similar to that in the small blue proteins. The type-1 Cu is embedded in one of these β -barrels and is coordinated by ligands His 95 (domain 1), Cys 136, His 145 and Met 150 (domain 2).



Figure 1.6: Schematic representation of the copper containing nitrite reductase from *Achromobacter cycloclastes*. PDB code: 1AS6.

The type-2 copper center is coordinated by a water molecule and three histidines, it is situated at the interface of two subunits. The water molecule is displaced from the type-2 Cu ion upon nitrite binding. Although both Cu ions are coordinated by neighboring residues, they are located approximately 12.5 Å apart, which prevents a direct electron-transfer. Most proteins with type-1 Cu are blue, the nitrite reductases from *Achromobacter cycloclastes* (Figure 1.6), *Alcaligenes faecalis* and *Pseudomonas aureofaciens*, however, are green. The geometric distortion primarily responsible for the electronic structure changes in ‘green’ nitrite reductase, relative to the blue type-1 Cu protein plastocyanin, was determined to involve a coupled angular movement of the Cys and Met residues toward a more flattened tetrahedral (towards square planar) structure (LaCroix *et al.*, 1996).

A new class of copper-containing nitrite reductases constitutes the major anaerobically induced outer membrane protein from pathogenic *Neisseria gonorrhoeae*. The crystal

structure of the soluble domain of this protein revealed a type-1 Cu with unusual visible absorption spectra, and a bidentate mode of nitrite binding to the type-2 Cu center (Boulanger and Murphy, 2002). In this organism, the expression of nitrite reductase appears to enhance the resistance against human sera (Cardinale and Clark, 2000).

1.4 Scope of the Study

The complex spectroscopic and biochemical properties as well as the 3-dimensional structure of the multiheme enzyme cytochrome *c* nitrite reductase isolated from several different bacteria have been extensively investigated, and a preliminary reaction mechanism was established for the enzyme from *W. succinogenes* (Einsle *et al.*, 2000; Stach *et al.*, 2000; Einsle *et al.*, 2002b). Nevertheless, the influence of highly conserved amino acids near the active site on the activity, the spectroscopic properties, the mechanism and the arrangement and stabilization of the active site cavity are still unclear and leave a number of questions.

In the present study, continuative functional aspects of wild-type ccNir from *W. succinogenes* and functional and structural aspects of variants of ccNir from *W. succinogenes* were investigated.

Firstly, the variant proteins were purified and their activities were compared to that of the wild-type. Furthermore, the variants were characterized by biochemical and spectroscopic (UV-Vis and EPR) techniques. In addition to spectroscopic studies, several forms of ccNir were investigated by SQUID susceptometry to get insights into the magnetic interactions between the heme centers. Furthermore, the X-ray structures of the variant proteins were solved.

Secondly, interactions of the enzyme with the potential reaction intermediate hydroxylamine were studied. Note that hydroxylamine had been also shown to act as a substrate (Stach *et al.*, 2000). The binding mode of hydroxylamine and derivatives was investigated using UV-Vis spectroscopy, and the X-ray structure with bound substrate was solved.

To solve the high-resolution X-ray structure of the NrfHA complex, the initial step was the investigation of diffracting crystals of the NrfHA complex from the Q276E-variant.

In addition, the investigation of the X-ray structures of cytochrome *cd*₁ nitrite reductase from *Pseudomonas stutzeri* and *Thiobacillus denitrificans* was started.

2 Materials and Methods

2.1 Chemicals

If not specified elsewhere, chemicals were of p.a. quality and obtained from Merck, Darmstadt. Additional chemicals in p.a. quality from other manufacturers:

Buffers:

Roth, Karlsruhe: TRIS (tris-(hydroxymethyl)-aminomethane), HEPES (N-[2-hydroxyethyl]piperazine-N'-[ethane sulfonic acid]). *Fluka, Neu-Ulm:* dipotassium hydrogen phosphate, potassium dihydrogen phosphate.

Chromatographic resins:

Whatman, Maidstone, UK: DE 52. *Calbiochem, Frankfurt:* hydroxylapatite (high resolution). *Merck, Darmstadt:* hydroxylapatite 15 μm . *Pierce Chemical Company, Illinois, USA:* Extracti-Gel D (detergent removing gel).

Detergents:

Fluka, Neu-Ulm: SDS (sodium dodecylsulfate). *Sigma, Deisenhofen:* Triton X-100 (t-octylphenoxypolyethoxyethanol), Triton X-114 (octylphenoxypolyethoxyethanol).

Dyes:

Serva, Heidelberg: Coomassie-brilliant blue G-250, bromphenol blue (sodium salt), methyl viologen.

Enzymes:

Fluka, Neu-Ulm: Dnase I (deoxyribonuclease I). *Serva, Heidelberg:* BSA (bovine serum albumin).

Gas:

Messer Griesheim, Krefeld: Argon 5.0, Helium 4.6. *Sauerstoffwerk Friedrichshafen*: N₂ 5.0, N₂/CO₂ (8:2, v/v), N₂/H₂ (95:5, v/v).

Microbiology:

Riedel-de Haën, Seelze: L-cysteine·HCl, sodium fumarate, sodium acetate. *Fluka, Neu-Ulm*: calcium chloride dihydrate, potassium dihydrogen phosphate, magnesium chloride hexahydrate, sodium hydrogen carbonate, sodium carbonate.

Protein standards:

BioRad, München: low molecular mass standards (PAGE).

Reagents:

Sigma, Deisenhofen: BCA (bicinchoninic acid), O-methylhydroxylamine hydrochloride. *Merck, Darmstadt*: hydroxylamine hydrochloride. *Fluka, Neu-Ulm*: N-methylhydroxylamine hydrochloride, N-tert-butyhydroxylamine hydrochloride, O-tert-butyhydroxylamine hydrochloride, hydroxylamine-O-sulfonic acid, hydrazine monohydrate, D(-)-2,3-butandiol.

5-deaza-10-methyl-3-sulfopropyl-isoalloxazine potassium salt (“5-deazaflavin”) was synthesized by Klaus Sulger, Konstanz (Blankenhorn, 1976). Titanium(III) citrate was synthesized by Dietmar Abt, Konstanz according to Zehnder and Wuhrmann (1976).

Crystal screen solutions were obtained from Hampton Research Corporation (Laguna Niguel, USA) and Jena Bioscience GmbH (Jena, Germany).

2.2 Organisms and Cultivation

2.2.1 Cultivation of *Wolinella succinogenes* Wild-Type

Cells of *W. succinogenes* were grown in batch cultures (0.1, 1, 20 or 50 l) at 30-35°C in a basic mineral medium (Table 2.1) with sodium formate as electron donor, sodium nitrate or sodium fumarate as electron acceptor, sodium acetate or sodium succinate as carbon source and L-cysteine as sulfur source and reductant.

The medium was autoclaved at 121°C and cooled under a N₂/CO₂ atmosphere (8:2, v/v). Trace elements (2 ml/l, Table 2.2) as well as substrates (Table 2.3) were added as sterile

solutions. The pH was adjusted to 7.2 with 1 M Na₂CO₃ or 1 M HCl. The medium was inoculated with 10 % of its volume from a stock culture and grown to early stationary phase.

Compound	Concentration	
	[mM]	[g/l]
KH ₂ PO ₄	10.0	1.4
MgSO ₄ ·7H ₂ O	1.5	0.4
CaCl ₂ ·2H ₂ O	0.7	0.1
NH ₄ Cl	2.5	0.13

Table 2.1: Basic mineral medium for the growth of *W. succinogenes*.

Growth was monitored by measuring the optical density at 578 nm. If necessary, the pH was adjusted to 7.2 with 1 M HCl or 1 M formic acid. The cell cultures were routinely tested for purity by microscopic inspection.

Compound	Concentration	
	[mM]	[mg/l]
FeCl ₂ ·4H ₂ O	5.0	994
ZnCl ₂	0.5	68
MnCl ₂ ·2H ₂ O	0.5	99
H ₃ BO ₃	0.1	6
CoCl ₂ ·6H ₂ O	0.5	119
CuCl ₂ ·2H ₂ O	0.01	2
NiCl ₂ ·6H ₂ O	0.1	24
Na ₂ MoO ₄ ·2H ₂ O	0.15	36

Table 2.2: Trace element solution SL 10 (Widdel, 1986). The salts were dissolved in 7 ml of 25 % HCl, the volume was adjusted to 1 l. The solution was autoclaved for 15 min at 121°C.

Cell cultures were concentrated to 1 l with the Pellicon filtration system (cutoff 100 kDa, Millipore Corporation, Eschborn). The concentrated suspension was centrifuged for 20 min at 10000 x g (4°C). The pellet was washed with 10 mM sodium phosphate buffer, pH 7.5, and centrifuged again. The cells were suspended in a small volume of buffer, frozen in liquid N₂, and stored at -70°C.

	100 ml and 1 l cultures		5 l and 50 l cultures	
	Concentration		Concentration	
	[mM]	[g/l]	[mM]	[g/l]
Na formate	20	1.4	40	2.7
Na fumarate	20	3.2	–	–
NaNO ₃	–	–	20	1.7
Na acetate	5	0.7	–	–
Succinic acid	–	–	10	1.2
NaHCO ₃	25	2.1	25	2.1
Na ₂ CO ₃	5	0.5	5	0.5
Na glutamate	0.2	0.04	0.2	0.04
L-cysteine·HCl	0.57	0.1	0.57	0.1

Table 2.3: Cultivation of *W. succinogenes*. Additional ingredients of the basic mineral medium (Table 2.1).

2.2.2 Cultivation of *Wolinella succinogenes* Variants

Mutation and cultivation of cells of *W. succinogenes* were kindly carried out by Jörg Simon and René Pisa, Frankfurt (Pisa, 2004).

2.2.3 Cultivation of *Pseudomonas stutzeri*

Cultivation of cells of *P. stutzeri* was kindly carried out by Ulrike Honisch, Karlsruhe (Coyle *et al.*, 1985).

2.2.4 Cultivation of *Thiobacillus denitrificans*

Cultivation of cells of *T. denitrificans* was kindly carried out by Klaus Sulger, Konstanz (Hole, 1996).

2.3 Preparation of Cellular Components

2.3.1 Preparation of Cell Fractions

Cells were suspended in 10 mM potassium phosphate buffer, pH 7.1, containing a few crystals of deoxyribonuclease I and MgCl₂·6H₂O. Cells were broken by two passages in a

French press (138 MPa, Aminco, Urbana, USA). The lysate was centrifuged at 8000 x g for 15 min (4°C) and the supernatant was referred to as crude extract. The crude extract was centrifuged for 1 h at 100000 x g at 4°C (Optima LE-80K, Beckman, München) giving the soluble fraction as supernatant. The soluble fraction contained both periplasmic and cytoplasmic proteins. The red-brownish pellet was referred to as membrane fraction.

2.3.2 Solubilization of the Membrane Fraction

The membrane fraction obtained after French press treatment of the cells was solubilized with 10 mM potassium phosphate buffer, pH 7.1, containing 1 % Triton X-100 (w/v, final concentration). The ratio protein:detergent was 1:1.25 (w/w). After stirring for 45 min at room temperature the suspension was centrifuged for 1 h at 100000 x g (4°C), giving the solubilized membrane fraction as supernatant.

2.4 Purification Protocols

All purification steps were performed at 4°C in the presence of dioxygen. Columns were connected to a Pharmacia FPLC system (pump P-500, gradient controller GP-250; Pharmacia Biotech, Freiburg). Detection was carried out at 280 and 405 nm (Uvicord SII; Pharmacia Biotech, Freiburg).

2.4.1 Cytochrome c Nitrite Reductase from the Soluble Fraction

The pH of the soluble fraction was adjusted to 7.1 by addition of 10 mM KH_2PO_4 . The solution was loaded onto a DE 52 column (Whatman) equilibrated with 10 mM potassium phosphate buffer, pH 7.1. The column was washed with buffer and nitrite reductase was eluted. Nitrite reductase did not bind to the DE 52 column. The eluate from the DE 52 column was loaded onto a hydroxylapatite column (1.3 x 11 cm, high resolution; Calbiochem) equilibrated with 10 mM potassium phosphate buffer, pH 7.1. A linear potassium phosphate gradient (50-300 mM) led to the elution of nitrite reductase at about 140 mM. Fractions containing nitrite reductase (judged by SDS-PAGE) were combined and concentrated by ultrafiltration (cutoff 30 kDa; Amicon, Witten) or by MicroSep or MacroSep concentrators (cutoff 30 kDa; Pall Gelman Sciences, Roßdorf). In a final purification step, the concentrated fractions were loaded onto a HiLoad 26/60 Superdex 200 gel filtration column (2.6 x 60 cm; Pharmacia Biotech, Freiburg) equilibrated with 50 mM HEPES/NaOH buffer, pH 7.5.

2.4.2 Cytochrome c Nitrite Reductase from the Membrane Fraction

The nitrite reductase from the membrane fraction was purified according to the purification protocol developed for the nitrite reductase from the soluble fraction. However, all buffers contained 0.05 % Triton X-100 (w/v).

The extract was loaded onto a DE 52 column (Whatman) equilibrated with 10 mM potassium phosphate buffer, 0.05 % Triton X-100 (w/v), pH 7.1. The column was washed with buffer and nitrite reductase was eluted. Nitrite reductase passed straight through the DE 52 column. The eluate from the DE 52 column was loaded onto a hydroxylapatite column (1.3 x 11 cm, high resolution; Calbiochem) equilibrated with 10 mM potassium phosphate buffer, 0.05 % Triton X-100 (w/v), pH 7.1. A linear potassium phosphate gradient (50-300 mM) led to the elution of nitrite reductase at \approx 140 mM. Fractions containing nitrite reductase (judged by SDS-PAGE) were combined and concentrated by ultrafiltration (cutoff 30 kDa; Amicon, Witten) or by MicroSep or MacroSep concentrators (cutoff 30 kDa; Pall Gelman Sciences, Roßdorf). In a final purification step, the concentrated fractions were loaded onto a HiLoad 26/60 Superdex 200 gel filtration column (2.6 x 60 cm; Pharmacia Biotech, Freiburg) equilibrated with 50 mM HEPES/NaOH buffer, 0.05 % Triton X-100 (w/v), pH 7.5.

2.4.3 Purification of Cytochrome *cd*₁ Nitrite Reductase from

Pseudomonas stutzeri

Purification of cytochrome *cd*₁ NiR from *P. stutzeri* was kindly carried out by Ulrike Honisch, Karlsruhe (Coyle *et al.*, 1985).

2.4.1 Purification of Cytochrome *cd*₁ Nitrite Reductase from *Thiobacillus denitrificans*

Purification of cytochrome *cd*₁ NiR from *T. denitrificans* was kindly carried out by Klaus Sulger, Konstanz (Hole, 1996).

2.5 Analytical Methods

2.5.1 Protein

Protein was determined using bicinchoninic acid (BCA) (Smith *et al.*, 1985). Bovine serum albumin (BSA) served as standard. The concentration of BSA in the stock solution was photometrically determined with $\epsilon_{279\text{nm}} = 0.667 \text{ (mg/ml)}^{-1}\text{cm}^{-1}$ (Foster and Stermann, 1956). 100 μl of unknown or standard protein (5-20 μg) were mixed with 1 ml of a solution containing 50 : 1 (v/v) BCA and $\text{CuSO}_4 \cdot 5\text{H}_2\text{O}$ (4 %, w/v). The reaction mixture was incubated for 20 min at 60°C. The calibration curve was recorded on a Hewlett Packard diode array spectrophotometer (Hewlett Packard, Waldbronn) and the absorbance was monitored at 562 nm.

2.5.2 Ammonia

The quantitative determination of ammonia was carried out by the indophenol reaction (Boltz and Taras, 1978). $(\text{NH}_4)_2\text{SO}_4$ was dried at 80°C for 24 h and cooled down in a desiccator before using as standard (calibration curve with 5-25 μM $(\text{NH}_4)_2\text{SO}_4$). The sample (100 μl) was added to 4.9 ml deionized water. 1 ml of phenol reagent (3 g phenol, 3 mg sodium nitroprusside in 100 ml deionized water) and 1 ml of a solution containing 2 g NaOH and 0.5 ml NaOCl (13 % Cl_2) in 100 ml were added. This reaction mixture was incubated for 1 h at room temperature in the dark and the absorption at 636 nm was measured on a Hewlett Packard diode array spectrophotometer (Hewlett Packard, Waldbronn).

2.5.3 Iron, Calcium, Molybdenum

Inductively coupled plasma mass spectrometry (ICP-MS) was performed by Spurenanalytisches Laboratorium Dr. Baumann (Maxhütte-Haidhof). The concentration of iron, calcium and molybdenum was determined by ICP-MS from samples containing *W. succinogenes* nitrite reductase.

2.5.4 Polyacrylamide Gel Electrophoresis

SDS-PAGE was carried out with the Mighty Small System (SE 250, 100 x 80 x 0.75 mm; Hoefer Scientific Instruments, San Francisco, USA) according to Lämmli (1970). 12.5 % polyacrylamide gels were used.

The molecular mass of the subunits was estimated using low molecular mass markers (BioRad Laboratories, München). Gels were stained with Coomassie (Zehr *et al.*, 1989) or silver (Heukeshoven and Dernick, 1985).

2.6 Cytochrome c Nitrite Reductase Activity

Nitrite reductase activity was determined by measuring the formation of ammonia. Methyl viologen reduced with $\text{Na}_2\text{S}_2\text{O}_4$ served as electron donor for the enzyme catalyzed reduction of nitrite to ammonia. Finally, ammonia was quantified colorimetrically. All steps were performed in the presence of dioxygen. Activity was calculated as $\mu\text{mol NO}_2^-$ reduced to ammonia per min ($1 \text{ U} = 1 \mu\text{mol NO}_2^- \text{ min}^{-1}$).

The standard reaction mixture contained sodium nitrite (final concentration 10 mM), methyl viologen (final concentration 0.5 mM) and nitrite reductase (0.5-0.7 μg of pure enzyme) in 0.95 ml 75 mM potassium phosphate buffer, pH 7.0. The assay was incubated at 37°C for 5 min. The reaction was started by addition of 50 μl 0.25 M $\text{Na}_2\text{S}_2\text{O}_4$ -solution (freshly prepared) and terminated with 200 μl 1 M H_2SO_4 after 5 min incubation at 37°C. Control experiments without enzyme were carried out. The assays were performed in double or triplicate. An aliquot (100 μl) of the reaction mixture was analyzed for ammonia using the indophenol method (Chapter 2.5.2).

Activity measurements with membranous nitrite reductase were performed in the presence of 0.05 % Triton X-100 (w/v).

2.7 Removal of Dioxygen

Experiments were carried out in an anaerobic chamber (Coy Laboratory Products, Grass Lake, USA; 95 % N_2 , 5 % H_2) equipped with a palladium catalyst (type K-0242, 0.5 % Pd/ Al_2O_3 ; ChemPur, Karlsruhe). All glass and plasticware was stored in the chamber for at least 24 h prior to use. Dioxygen from buffers was removed as described by Beinert *et al.* (1978). Argon was purified via passage through a glass/copper system filled with BASF catalyst type R3-11. For anaerobic conditions the sample was evacuated and flushed with argon at least eight to ten times. All buffers were stored 24 to 48 h in the anaerobic chamber in order to equilibrate with the atmosphere.

2.8 Protein Crystallography

A detailed description of the techniques used for protein crystallography can be found in relevant textbooks (Blundell and Johnson, 1994; Drenth, 1994; Massa, 1994; McRee, 1993).

2.8.1 Protein Crystallization

Protein crystals were grown by the method of vapor diffusion, where the protein solution was mixed with a precipitant solution and equilibrated against a higher concentrated precipitant reservoir in a closed environment. Under regular conditions, using non-volatile precipitants such as polyethylene glycol or salts, equilibrium is reached by diffusion of water from the protein drop to the reservoir, thus slowly increasing the concentration of all components in the drop (McPherson, 1982).

2.8.1.1 Crystallization of Membranous NrfA Nitrite Reductase

Before crystallization of membranous NrfA, the detergent Triton X-100 (0.05 %, w/v) was removed by Extracti-Gel D (Pierce Chemical Company, Illinois, USA).

The protein was stored at concentrations as high as 35 mg/ml and was diluted to 10-20 mg/ml immediately prior to crystallization.

Crystals of nitrite reductase were grown as described (Einsle *et al.*, 2000) by the sitting drop vapor diffusion method using Chryschen MVD/24 plates (Charles Supper Company, Natick, USA). Buffers of low ionic strength were used for crystallization experiments, most commonly 5 mM HEPES/NaOH buffer, pH 7.0. Buffer exchange was carried out on NAP gravity flow columns (Pharmacia Biotech, Freiburg). Each drop was prepared by mixing 2 μ l of the protein solution with the same amount of the crystallization solution in the well of the crystallization device, and was equilibrated by vapor diffusion against 500 μ l of the solution in the reservoir of Chryschen MVD/24 plates. The reservoir and the protein solution in the well were sealed with transparent tape.

Crystal platelets of *W. succinogens* nitrite reductase (NrfA_M) grew within two to three days from 12-14 % PEG 4000, 200 mM (NH₄)₂SO₄, and 100 mM sodium acetate, pH 5.7. With the addition of 15 mM YCl₃·6H₂O the plates were improved into reproducible, large single crystals.

2.8.1.2 Crystallization of Membranous NrfHA Nitrite Reductase

Before crystallization of membranous NrfHA Triton X-100 (0.05 %, w/v) had to be exchanged against Triton X-114 (0.5 %, w/v) by removing the present detergent with Extracti-Gel D (Pierce Chemical Company, Illinois, USA) and then adding the same buffer with desired detergent.

The protein was stored at concentrations as high as 35 mg/ml and was diluted to 10-20 mg/ml immediately prior to crystallization experiments.

Crystals of nitrite reductase were grown as described (Einsle *et al.*, 2002a) by the sitting drop vapor diffusion method using Chryschen MVD/24 plates (Charles Supper Company, Natick, USA). Buffers of low ionic strength were used for crystallization experiments, most commonly 10 mM HEPES/NaOH buffer, pH 7.5. Buffer exchange was carried out on NAP gravity flow columns (Pharmacia Biotech, Freiburg). Each drop was prepared by mixing 2 μ l of the protein solution with the same amount of the crystallization solution in the well of the crystallization device, and was equilibrated by vapor diffusion against 500 μ l of the solution in the reservoir of Chryschen MVD/24 plates. The reservoir and the protein solution in the well were sealed with transparent tape.

Single crystals of *W. succinogens* nitrite reductase (NrfHA) grew within seven to ten days from 4-4.5 % PEG 300, 1.9-2.0 M $(\text{NH}_4)_2\text{SO}_4$, and 100 mM HEPES/NaOH buffer, pH 7.0.

2.8.1.3 Crystallization of Cytochrome *cd*₁ Nitrite Reductase from *P. stutzeri*

Crystals of nitrite reductase were grown by the sitting drop vapor diffusion method using Chryschen MVD/24 plates (Charles Supper Company, Natick, USA). Buffers of low ionic strength were used for crystallization experiments, most commonly 5 mM TRIS/HCl buffer, pH 7.5. Buffer exchange was carried out on NAP gravity flow columns (Pharmacia Biotech, Freiburg). Each drop was prepared by mixing 2 μ l of the protein solution with the same amount of the crystallization solution in the well of the crystallization device, and was equilibrated by vapor diffusion against 500 μ l of the solution in the reservoir of Chryschen MVD/24 plates. The reservoir and the protein solution in the well were sealed with transparent tape.

Single crystals of *P. stutzeri* nitrite reductase grew within three to four days from 15 % PEG 4000, 100 mM CaCl_2 , 2.5% 2-propanol and 100 mM HEPES/NaOH, pH 8.5.

2.8.1.4 Crystallization of Cytochrome *cd*₁ Nitrite Reductase from *T. denitrificans*

Before crystallization of membranous cytochrome *cd*₁ nitrite reductase from *T. denitrificans*, the detergent Triton X-100 (0.05 %, w/v) was removed by Extracti-Gel D (Pierce Chemical Company, Illinois, USA).

The protein was stored at concentrations as high as 35 mg/ml and was diluted to 10-20 mg/ml immediately prior to crystallization experiments.

Crystals of nitrite reductase were grown by the sitting drop vapor diffusion method using Chryschen MVD/24 plates (Charles Supper Company, Natick, USA). Buffers of low ionic strength were used for crystallization experiments, most commonly 5 mM potassium phosphate buffer, pH 6.6. Buffer exchange was carried out on NAP gravity flow columns (Pharmacia Biotech, Freiburg). Each drop was prepared by mixing 2 µl of the protein solution with the same amount of the crystallization solution in the well of the crystallization device, and was equilibrated by vapor diffusion against 500 µl of the solution in the reservoir of Chryschen MVD/24 plates. The reservoir and the protein solution in the well were sealed with transparent tape.

Single crystals of *T. denitrificans* nitrite reductase grew within four to five days from 12 % PEG 4000, 100 mM (NH₄)₂SO₄, and 50 mM sodium acetate, pH 4.3.

2.8.2 Substrate Complexes of NrfA Nitrite Reductase

In order to examine the binding of different substrates, intermediates and products to the active site of NrfA nitrite reductase, crystals were transferred into a harvesting buffer containing the respective compound. After incubation for a sufficient time to allow for binding, the crystals were flash frozen and measured.

2.8.3 Cryocrystallography

A problem commonly observed in protein crystallography is the damage of crystals in the X-ray beam. This damage mainly results from water radicals formed during radiation by the X-ray photons, which in turn react with the protein molecules, destroying the order of the crystal lattice. To minimize crystal degradation, crystals were cooled to 100 K with a nitrogen stream cooling system (Oxford Instruments), reducing the mobility of solvent radicals significantly. The addition of cryoprotectant was necessary to flash-freeze protein crystals for data collection.

2.8.3.1 NrfA Nitrite Reductase

Crystals of NrfA nitrite reductase were frozen as previously described (Einsle *et al.*, 2000): all measurements were achieved under flash-freezing conditions after soaking the crystals in a cryoprotectant solution containing 12 % PEG 4000, 0.2 M $(\text{NH}_4)_2\text{SO}_4$, 0.1 M sodium acetate pH 5.7 and 15 % D(-)-2,3-butandiol.

2.8.3.2 NrfHA Nitrite Reductase

Crystals of NrfHA nitrite reductase were frozen as previously described (Einsle *et al.*, 2002a): all measurements were achieved under flash-freezing conditions after soaking the crystals in a cryoprotectant solution containing 4.5 % PEG 300, 2.4 M Li_2SO_4 , 0.1 M HEPES/NaOH buffer, pH 7.0.

2.8.3.3 Cytochrome *cd*₁ Nitrite Reductase from *P. stutzeri*

Cytochrome *cd*₁ nitrite reductase crystals were frozen with D(-)-2,3-butandiol as cryoprotectant. Crystals were transferred from the mother liquor into a buffer containing 100 mM HEPES/NaOH pH 8.5, 15 % PEG 4000, 0.1 M CaCl_2 , 2.5 % 2-propanole, 15 % D(-)-2,3-butandiol and incubated for 1-2 minutes. The crystals were then flash-frozen and measured or stored in $\text{N}_2(\text{l})$ for further use.

2.8.3.4 Cytochrome *cd*₁ Nitrite Reductase from *T. denitrificans*

Cytochrome *cd*₁ nitrite reductase crystals were frozen with D(-)-2,3-butandiol as cryoprotectant. Crystals were transferred from the mother liquor into a buffer containing 50 mM sodium acetate pH 4.3, 12 % PEG 4000, 0.1 M $(\text{NH}_4)_2\text{SO}_4$, 15 % D(-)-2,3-butandiol and incubated for 1-2 minutes. The crystals were then flash-frozen and measured or stored in $\text{N}_2(\text{l})$ for further use.

2.8.4 Measurement of Datasets

Data collection was performed using Cu K_α radiation at 1.5418 Å.

2.8.5 Data Processing

The computational work was done on a Unix PC workstation equipped with stereo display capabilities.

The data sets were indexed, integrated and reduced using the program MOSFLM (Leslie, 1991). For all further steps of structure solution, data sets were converted with XSCALE, XDSCONV (Kabsch, 1993); F2MTZ, TRUNCATE and MTZ2VARIOUS (Collaborative Computational Project No. 4, 1994) from intensities to structure factor amplitudes and to suitable file formats.

2.8.6 Molecular Replacement Using Experimental Phases

The model of the dissimilatory nitrite reductase from *W. succinogenes* (PDB ID 1FS7) was used by MOLREP (Collaborative Computational Project No. 4 1994).

2.8.7 Interpretation of Electron Density Maps

The electron density maps were calculated from measured amplitudes and density modified phases with the program FFT (Collaborative Computational Project No. 4 1994). O (Jones *et al.*, 1998) was used to visually inspect the electron density maps.

2.8.8 Model Building and Refinement

Atomic protein models were built into the density modified electron density map with the program O (Jones *et al.*, 1998). Later $2f_o - f_c$ and $f_o - f_c$ Fourier synthesis with the phase information from the existing model was used.

Protein structures were refined with individual temperature factors using CNS (Brünger *et al.*, 1998). The refinement was controlled by the separation of a set of reflections, which were only used for the calculation of quality indices (Brünger, 1992; Brünger, 1993).

2.8.9 Graphical Representations

Illustrations of structures were prepared using DEEP-VIEW (Guex and Peitsch, 1997), DSVIEWER (Accelrys Ltd, UK), and Bobscript (Esnouf, 1999) and in some cases rendered with RASTER3D (Merritt and Bacon, 1997) and POVRAY (Vision Raytracer Pty. Ltd, UK).

2.9 Reduction of Nitrite Reductase

Dithionite solutions were prepared under anoxic conditions in solutions buffered at pH 8-9 or in 10 mM NaOH. Two reducing equivalents are delivered (Mayhew, 1978). The

reductant in dithionite solutions is the dissociation product SO_2^- . Dithionite solutions were calibrated by titration against $\text{K}_3[\text{Fe}(\text{CN})_6]$ ($\epsilon_{420\text{nm}} = 1020 \text{ M}^{-1}\text{cm}^{-1}$, Peck *et al.*, 1965).

A photochemical procedure for reduction employing “5-deazaflavin” as catalyst was carried out according to Massey and Hemmerich (1977). The reaction mixture in a sealed cuvette contained nitrite reductase ($\approx 3 \mu\text{M}$), 10 mM sodium oxalate and 5 μM “5-deazaflavin”. The enzyme was reduced by irradiation in a modified slide projector with a thermostatted cell holder. After reduction, the reaction was started by adding the reactant with a gas-tight syringe (Hamilton, Bonaduz AG, CH) or from the side arm of the cuvette.

2.10 Ultraviolet / Visible Spectroscopy

UV/Vis spectra were recorded with a Cary 50 spectrometer (Varian, Darmstadt). Difference spectra were recorded by using protein solution without reactant as the reference in the reference sample compartment in order to avoid dilution dependent effects. An aliquot of test solution was added to the sample cuvette, and an equal volume of buffer was added to the reference cuvette. Difference spectra were also generated with the program Origin (Microcal Software Inc., Northampton, USA) in the case that buffer served as reference.

2.10.1 Spectrophotometric Titrations

Titration experiments were carried out with a Cary 50 spectrometer (Varian, Darmstadt) at room temperature unless indicated otherwise. The spectrometer was equipped with a water temperature control unit. A home built sample compartment allowed the use of Thunberg cuvettes and thus work under exclusion of dioxygen.

Reaction of cytochrome *c* nitrite reductase (NrfA) with hydroxylamine and derivatives were carried out with 5 μM protein in 100 mM potassium phosphate buffer, pH 7.5 at 25°C in the absence of dioxygen in 1.0 cm Thunberg cuvettes. Substrate was freshly prepared (1.0 M in water) and added in 5 μl steps to give a final concentration of 50 mM.

2.11 Magnetic Measurements

The magnetic properties of paramagnetic substances with more than one magnetic center can give hints to the sometimes very complicated reaction mechanism. Unfortunately, the measurements of biological systems like proteins are disproportional more difficult like these of low-molecular complexes. The main difficulty is the correction of the diamagnetism

of the whole sample, including sample holding system and the amino acid chain. Furthermore, many biological samples are contaminated by adventitious iron and the fact that the measurements are performed in dilute samples. Magnetic susceptibility measurements differ from spectroscopy in that the various contributions cannot be distinguished (e.g.: a signal at $g = 4.3$ in EPR) and all contributions are included in the final number.

To eliminate the contributions of the buffer and the sample holder, the measurement with buffer and the sample holder was correctly performed. The buffer contained 50 mM Hepes/NaOD in D₂O pH 7.5. The use of D₂O and NaOD have two reasons:

- The proton moment is 660 times smaller than the electron moment which translates into a factor $(\mu_H/\mu_e)^2 = (1/660)^2 = 2.3 \cdot 10^{-6}$. But the concentration of protons in water is 110 M and this gives rise to a magnetic contribution equivalent to 0.25 mM spin 1/2 electrons.
- The relaxation of protons near liquid helium temperatures is very slow. Complete relaxation takes several hours and the relaxation time varies in the presence of paramagnetic species.

Fortunately, replacing protons by deuterium solves both problems. Indeed, deuterium nuclear paramagnetism is significantly smaller than that of protons: $(\mu_D/\mu_H)^2 = (0.857/2.793)^2 = 0.094$. Therefore, it contributes only to 24 μ M spin 1/2 electrons and the relaxation of deuterium is rapid due to its electric quadrupole moment. If the protein is stable enough to be lyophilized, the problems introduced by the solvent become irrelevant.

To eliminate the contributions of the protein diamagnetism, the measurement of the apoprotein is the most appropriate way but is not always possible. An estimation of the diamagnetic part can be calculated with the equation 2.1.

The magnetic measurements were carried out with lyophilized enzyme and with enzyme dissolved in 50 mM Hepes/NaOD (D₂O) under exclusion of dioxygen in a helium atmosphere at a Quantum-Design-MPMSR-5S-SQUID magnetometer. Both the soluble (NrfA_S) and the membrane bound (NrfHA) enzyme were used in its oxidized (as isolated) form. The samples were applied as solids in gelatine capsules. All measurements were carried out between 2-200 K at a field strength of 0.5 and 1.0 T, respectively.

The data were corrected for the diamagnetism of the sample holding system. For the diamagnetic correction of the protein an approximation according to equation 2.1 was carried out (Kahn, 1993).

$$X^D = 0,5 \cdot M \cdot 10^{-6} \quad (\text{eq. 2.1})$$

The molar susceptibility of the sample is dependent on the following parameters: the magnetic moment of the sample (M_s), the mass of the sample (m_s), the molar mass of the sample (M), the diamagnetism of the capsule (X_g) and the protein (X^D) (Equation 2.2).

$$X_{mol} = M_s \cdot \frac{M}{(H \cdot m_s)} + X_g + X^D \quad (\text{eq. 2.2})$$

The calculation of the Bohr's magneton is done according to equation 2.3.

$$\mu_{eff} = 2,83 \cdot \sqrt{X_{mol} \cdot T} \quad (\text{eq. 2.3})$$

The theoretically values resulting from the Curie law of two coupling and two non coupling centres are calculated according to equations 2.4 and 2.5, respectively.

$$\mu_{eff} = 2 \cdot \sqrt{S \cdot (S+1)} \quad ; \text{ with } S = S_A + S_B \quad (\text{eq. 2.4})$$

$$\mu_{eff} = 2 \cdot \sqrt{S_A \cdot (S_A + 1) + S_B \cdot (S_B + 1)} \quad (\text{eq. 2.5})$$

The values for NrfA with a total spin of 9/2 (in the oxidized form) are for a coupling system of 9.95 μ_B and for a non coupling system of 6.86 μ_B , respectively. The values for NrfHA with a total spin of 13/2 (in the oxidized form) are for a coupling system of 13.96 μ_B and for a non coupling system of 7.68 μ_B , respectively.

2.12 Electron Paramagnetic Resonance Spectroscopy

A detailed discussion of electron paramagnetic resonance spectroscopy would be beyond the scope of this work and can be found in relevant textbooks (Palmer, 1983; Swartz *et al.*, 1972; Weil *et al.*, 1994; Abragam and Bleaney, 1986; Pilbrow, 1990) and reviews (Beinert *et al.*, 1962; Rowlands and Murphy, 1999; Walker, 1999; Walker, 2004).

2.12.1 Theoretical Background

The technique of electron paramagnetic resonance (EPR) spectroscopy is very similar in concept to the more familiar nuclear magnetic resonance (NMR) technique. Both deal with the interaction of electromagnetic radiation with magnetic moments; in the case of EPR, the magnetic moments arise from electrons. Therefore, typical systems that have been studied include:

- Free radicals in the solid, liquid or gaseous phase
- Transition ions including Actinide ions
- Systems with more than one unpaired electron
- Various point defects
- Systems with conducting electrons.

The applied electromagnetic radiation is in a frequency range of 10^9 to 10^{11} s^{-1} (1-100 GHz), which is generated by microwave sources. Furthermore, the use of a magnetic field is the unique aspect of magnetic-dipole spectroscopy.

The simplest energy-level diagram for a particle of spin 1/2 (e.g.: an organic radical or Fe(III) l.s. ion) in a magnetic field is shown in Figure 2.1. According to quantum theory for isolated electrons, only two orientations exist, parallel or antiparallel to the external magnetic field. The levels are labeled with the numbers $M = \pm 1/2$. Resonant absorption occurs if the frequency is adjusted so that:

$$\Delta E = h \cdot \nu \quad (\text{eq. 2.6})$$

In EPR, the frequency ν is fixed and with the alterable external magnetic field H the energy separation is tuned to “resonance condition”.

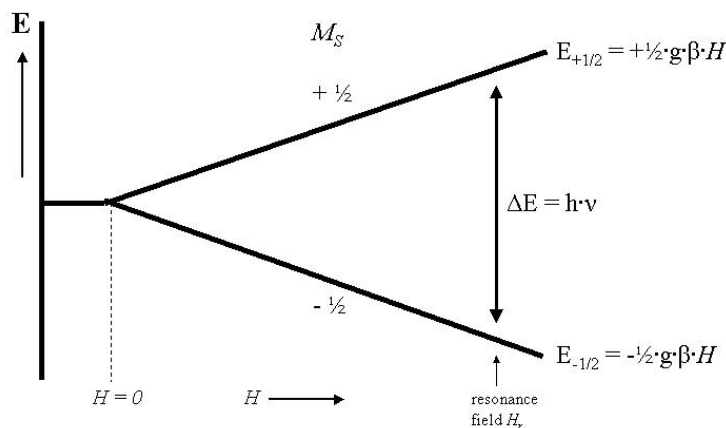


Figure 2.1: Zeeman energy-level scheme for the simplest system (e.g.: free electron) as a function of applied magnetic field H , showing EPR absorption. $E_{+1/2}$ and $E_{-1/2}$ represent the energies of the $M = +\frac{1}{2}$ and $M = -\frac{1}{2}$ states. The constants g are the g -factor and β the Bohr's magneton, respectively.

If, as is normally the case, the lower energy level is more populated, a net increase of electrons at the higher level will result concomitant with absorption of energy $x \cdot h \cdot \nu$. This absorption is then measured.

It follows from the fact that transitions between artificially created energy levels are observed that the gap between these levels is not of a fixed magnitude but depends on and is in fact proportional to the applied magnetic field H , where C is a constant.

$$h \cdot \nu = \Delta E = C \cdot H \quad (\text{eq. 2.7})$$

C includes the constant β (Bohr's magneton) and a factor g , the "spectroscopic splitting" factor, which is determined by the intrinsic properties of the material under study:

$$C = g \cdot \beta \quad (\text{eq. 2.8})$$

$$h \cdot \nu = g \cdot \beta \cdot H \quad (\text{eq. 2.9})$$

$$g = \frac{h \cdot \nu}{\beta \cdot H} \quad (\text{eq. 2.10})$$

The value of g can be calculated when H and ν are measured and will ultimately give information on the state of the electron which absorbs energy. Equation 2.10 describes the so-called "resonance condition".

An important consideration in EPR is the effect of symmetry on the line shapes. In many cases the samples are polycrystalline materials, composed of numerous small crystallites that are randomly oriented in space. The resultant *powder* EPR spectrum is the envelope of spectra corresponding to all possible orientations of the paramagnetic species with respect to the magnetic field. The profile of the powder spectrum is determined by several parameters, including the symmetry of the g -tensor, the actual values of its components, and the line shape and the line width of the resonance. Concerning the symmetry of the g -tensor, three possible cases can be identified (Figure 2.2): isotropic, axial, and rhombic.

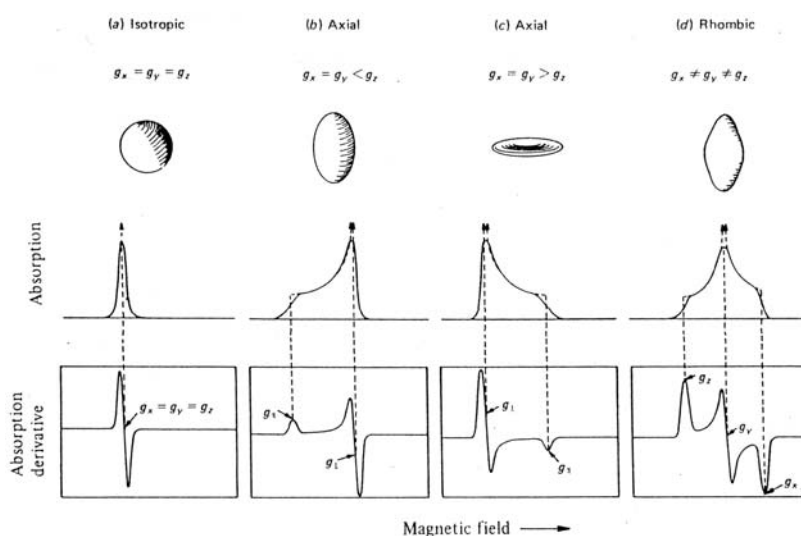


Figure 2.2: Schematic representation of the three possible cases of g -tensor and the resulting EPR spectra.

2.12.2 EPR Spectra of Multiheme Enzymes

Two core motives of heme-heme interaction are observed in different protein environments (Einsle, 1999):

- The almost perpendicular arrangement of hemes as observed for hemes 1 and 3 of cytochrome c_3 (Einsle *et al.*, 2001), in the following referred as the CC3 module (Figure 2.3 (A)).
- The parallel and tight stacking interaction with an iron-iron distance between 9 and 10 Å, as it is seen most clearly in the split-Soret cytochrome (Liu *et al.*, 1988; Matias *et al.*, 1997), in the following referred to as the SSC motif.

The CC3 module is characterized by an iron-iron-distance ranging between 11.1 and 12.8 Å and an angle close to 90° between the heme planes (Figure 2.3 (A)). The heme edge to edge distances around 6.5 Å and the distal histidine ligands are located on the same side of the porphyrin rings, within the module. The SSC motif represents a completely different type of interaction, a stacking arrangement in which the two hemes are almost exactly parallel and related by a local twofold symmetry axis (Figure 2.3). The iron-iron-distances range between 9.0 and 9.5 Å and the closest distance of the porphyrin rings, between the CHB atoms of the hemes, is close to or below 4 Å, allowing for direct resonance transfer.

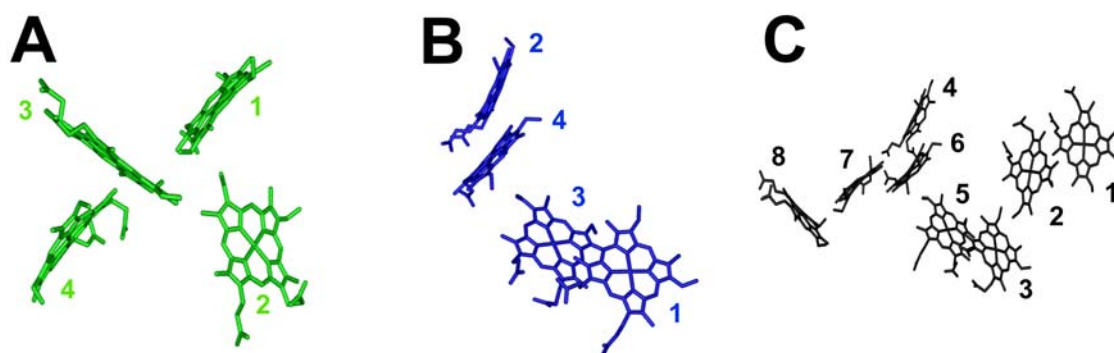


Figure 2.3: Heme arrangement of multiheme enzymes. (A) Cytochrome c_3 from *Desulfovibrio desulfuricans* PDB code: 1I77; (B) Cytochrome c_{554} from *Nitrosomonas europaea* PDB code: 1BVV; (C) Hydroxylamine oxidoreductase from *Nitrosomonas europaea* PDB code: 1FGJ. The heme groups are numbered according to their attachment to the protein chain.

EPR spectroscopy of cytochrome c_3 from *Desulfovibrio desulfuricans* (Einsle *et al.*, 2001) gave a rhombic spectrum with apparent g values at $g_{\max} = 2.95$, $g_{\text{mid}} = 2.29$ and $g_{\min} = 1.54$ and 1.43, consistent with low-spin Fe(III)-heme groups with bis-histidinyll coordination (Figure 2.4 (A)). Furthermore, a broad peak at $g_{\max} = 3.29$ was detected. Because, in bis-histidinyll coordinated porphyrins the g -tensor anisotropy increases with the angle between the normal vectors of the imidazole planes (Walker, 1999; Ogura *et al.*, 2001; Yatsunyk *et al.*, 2003; Walker, 2004), the latter g_{\max} value may be attributed to a heme iron center with approximately perpendicular imidazole planes. In the case of spectra with strong g_{\max} features, only g_z can be observed, g_x and g_y usually being too broad to be resolved. This type of heme center is found in heme 2 of cytochrome c_3 (Figure 2.3 (A)).

In cytochrome c_{554} hemes 1 and 3 build up the SSC motif (Figure 2.3 (B)). The perpendicular mode EPR spectrum (Upadhyay *et al.*, 2003) shows peaks at $g = 3.9$ and 2.7, a

derivative feature at $g = 2.06$ and two valleys at 1.63 and 1.46 (Figure 2.4 (B)). The parallel mode spectrum shows signals at $g = 7.2$ and 3.2, respectively. The observation of a parallel mode signal for ferric hemes requires the presence of spin-spin interactions between hemes. In addition, the perpendicular mode signals are not typical of isolated hemes, indicating that all hemes in oxidized cytochrome c_{554} are spin coupled. The signals at $g = 2.7$, 2.06, 1.63, and 1.46 originate from a spin system separate from that of the $g = 3.9$ and the parallel mode signals. A weak antiferromagnetic exchange interaction between two $S = 1/2$ low-spin heme centers is expected. Furthermore, a second antiferromagnetic exchange interaction between a low-spin heme and a high-spin heme originates the signals $g = 7.2$ in the parallel mode spectrum and $g = 3.9$ in the perpendicular mode spectrum, respectively.

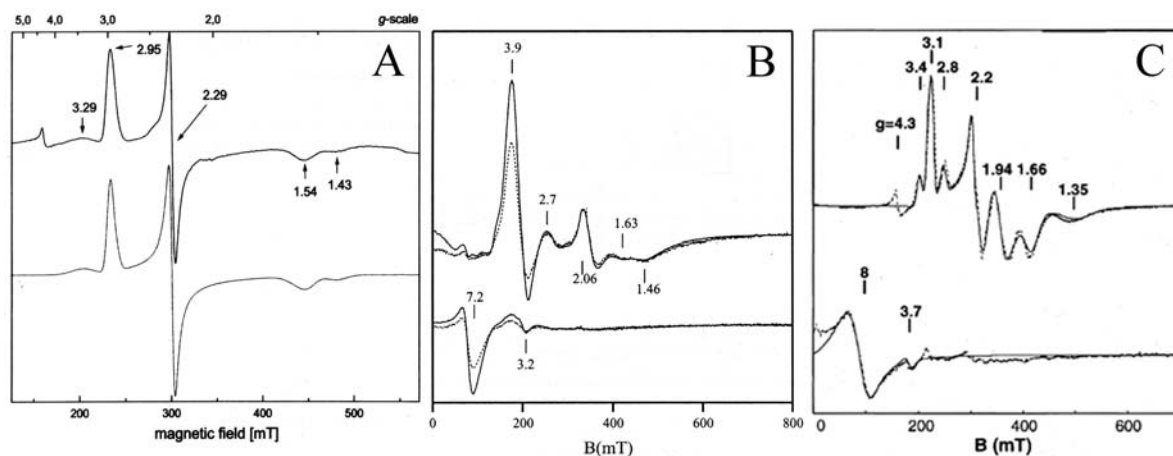


Figure 2.4: EPR spectra of multiheme enzymes. **(A)** experimental and simulated spectra of cytochrome c_3 from *Desulfovibrio desulfuricans* (Einsle *et al.*, 2001); **(B)** experimental and simulated spectra of perpendicular and parallel mode of cytochrome c_{554} from *Nitrosomonas europaea* (Upadhyay *et al.*, 2003); **(C)** experimental and simulated spectra of perpendicular and parallel mode of hydroxylamine oxidoreductase from *Nitrosomonas europaea* (Hendrich *et al.*, 2001).

Hydroxylamine oxidoreductase (HAO) has three CC3-modules (hemes 2/3, 5/6, 7/8 in Figure 2.3 (C)) which all interact through SSC motives (Igarashi *et al.*, 1997). The active site heme group in cytochrome P_{460} (heme 4 in Figure 2.3 (C)) interacts with one of the CC3 modules (hemes 6 and 7) at a distance and orientation that is similar to the SSC motif to form a triplet of stacked hemes. The perpendicular mode EPR spectrum (Figure 2.4 (C)) has resonances at $g = 3.1$, 2.2, and 1.35 (Hendrich *et al.*, 2001), which are typical of low-spin ferric heme complexes (Walker, 1999). Least-squares fitting of the experimental spectra of fully oxidized HAO indicates that these resonances can be assigned to at least two different mononuclear heme species. The set of resonances at $g = 3.4$, 2.8, 1.94, and 1.66 have

frequency dependent g -values, which for $S = 1/2$ spin centers is indicative of a spin-coupled system. From the temperature dependence of the signal, the isotropic exchange coupling between this two hemes is antiferromagnetic. The parallel mode spectrum (Figure 2.4 (C)) shows two signals at $g = 8$ and 3.7, which originate from two different spin systems. The weaker signal at $g = 3.7$ originates from the latter coupling pair. The larger signal near $g = 8$ has been previously assigned to an integer-spin state of an additional pair of exchange-coupled hemes. Nevertheless, this signal originates from the active site heme, namely cytochrome P₄₆₀. To summarize thus far, in HAO there are four distinguishable EPR species, two of them constitute a exchange-coupling pair.

2.12.3 Multifrequency EPR Spectroscopy

The g -values were calculated according to the resonance equation 2.10 (Chapter 2.12.1). The simulation of the spectra was performed with the program WEPR (Neese, 1995).

2.12.3.1 Perpendicular Mode X-Band EPR Spectroscopy

EPR spectra were recorded on a Bruker Eleksys 500 with an ER 049 X microwave bridge (Bruker). The system was equipped with an Oxford Instruments ESR 900 helium cryostat controlled by the ITC 503 temperature device. The modulation frequency was 100 kHz and the modulation amplitude was typically 0.5 mT. The measurements were performed with a Bruker 4122 SHQE cavity at ≈ 9.38 GHz. The sample tubes were Suprasil quartz tubes 705-PQ-9.50 (Wilmad) with a \varnothing_{out} of 4 mm. The sample volume was 250 μl .

2.12.3.2 Parallel Mode X-Band EPR Spectroscopy

EPR spectra were recorded with a Bruker ESP 300 spectrometer connected to a ER 041 MR microwave bridge, a ER 048 H microwave controller, and a ER 032 M field controller. The temperature was maintained with a Helitran-system (model LTD-3-110 C; Air products and Chemicals, Allentown, USA), and was controlled by manually adjusting the flow from the liquid helium storage vessel which was operated at a pressure of ≈ 0.7 bar. The microwave frequency was measured with a Autohet Counter Mode 350 D (microwave frequency; Dana Electronics, Darmstadt), the magnetic field with a Bruker NMR Gaussmeter ER 035 M, and the temperature with a ITC 503 temperature controller (Oxford Instruments). The modulation frequency was always 100 kHz and the modulation amplitude was typically 0.5 mT. Measurements were performed with a Bruker ER 4116 DM bimodal cavity at

≈ 9.38 GHz. The sample tubes were Suprasil quartz tubes 705-PQ-9.50 (Wilmad) with a \varnothing_{out} of 4 mm and the sample volume was 250 μl .

2.12.3.3 Q-Band EPR Spectroscopy

EPR spectra were recorded with a Bruker Elexsys 500 with an ER 051 QG microwave bridge. The system was equipped with an Oxford Instruments CF 935 helium cryostat controlled by an ITC 503 temperature controller. The modulation frequency was 100 kHz and the modulation amplitude was typically 0.5 mT. The measurements were performed with a Bruker ER 5106 QT cavity at ≈ 34 GHz. The sample tubes were Suprasil quartz tubes 705-PQ-6.25 (Wilmad) with a \varnothing_{out} of 3 mm. The sample volume was 70 μl .

2.12.3.4 S-Band EPR Spectroscopy

S-Band EPR spectra were recorded in collaboration with Dr. E. Bill and PD Dr. F. Neese (Max-Planck-Institut für Bioanorganische Chemie, Mülheim/Ruhr) on a Bruker spectrometer. Loop gap resonators were used and the temperature was maintained with a LTD helitran system. The sample tubes were Suprasil quartz tubes 705-PQ-9.50 (Wilmad) with a \varnothing_{out} of 4 mm and the sample volume was 250 μl .

3 Results

3.1 Cytochrome c Nitrite Reductase and Variants from *Wolinella succinogenes*

3.1.1 Cultivation of *W. succinogenes*

Cells grew within one to two days in a 50 l batch culture (Figure 3.1). Ideally, bacterial growth ends in a saturation phase as observed during cultivation of *W. succinogenes*. The fluctuation in pH after 6, 8, 10 and 12 hours arose from the fact that during oxidation of formate, which acts as the electron source, to carbon dioxide, the gaseous CO₂ leaves the solution and the pH increases. For optimal growth, a pH of 7.0 is necessary which was adjusted with 1 M HCl.

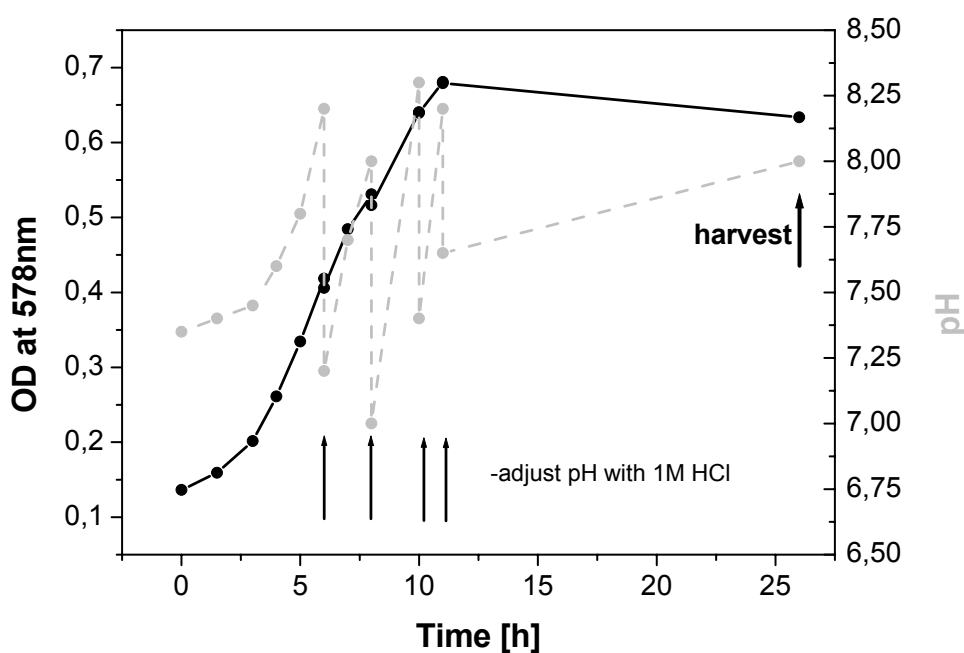


Figure 3.1: Growth curve of *W. succinogenes*. Black line OD (optical density) vs. time, grey line pH vs. time.

The maximum optical density was 0.7, corresponding to a total cell mass of 1.3 g/l (wet weight).

3.1.2 Purification of ccNir from *W. succinogenes*

3.1.2.1 Purification of ccNirWT

Both soluble and membranous ccNir were purified to homogeneity according to SDS-PAGE by a three- or four-step procedure. The protocol included DE52 anion exchange and hydroxylapatite (HAP) column chromatography followed by a gel filtration step. The DE52 anion exchange column and the hydroxylapatite column were coupled. Occasionally, a second more sensitive hydroxylapatite column chromatography step was necessary after gel filtration. After French press treatment of the cells 55-65 % of the nitrite reductase activity was found in the membrane fraction and 35-45 % in the soluble fraction. Triton X-100 was used to solubilize nitrite reductase from the membrane fraction.

Purification step	Protein [mg]	Specific activity [U/mg]	Purification factor	Activity [U]	Yield [%]
Soluble Fraction	1620	5.0	1.0	8100	100
DE52 / HAP	66	67	13	4422	55
Superdex 200	10	309	62	3090	38

Table 3.1: Purification of ccNirWT (NrfA_S). (1 U = 1 $\mu\text{mol NO}_2^- \text{min}^{-1}$).

Table 3.1 and 3.2 show representative purifications of ccNirWT from the soluble and the membrane fraction, respectively. The yield was 10 mg from the soluble fraction and 28 mg from the membrane fraction of 60 g wet weight cell mass. Membranous nitrite reductase eluted from the gel filtration column in two fractions. A high M_r form ($\approx 79\%$) and a low M_r form ($\approx 21\%$) were separated. Both forms of membranous nitrite reductase showed similar specific activities as determined for the enzyme from the soluble fraction. Upon purification, the specific activity of soluble nitrite reductase increased by a factor of 62 from 5.0 to 309 U/mg in the assay with methyl viologen as redox mediator. For the enzyme purified from the membrane fraction a specific activity of 311 U/mg for the monomeric form (NrfA_M) and 325 U/mg for the complex (NrfHA) was obtained.

Purification step	Protein [mg]	Specific activity [U/mg]	Purification factor	Activity [U]	Yield [%]
Membrane Fraction	4055	11	1.0	44605	100
Membrane Extract	1237	25	2.3	30925	69
DE52 / HAP	47	176	16	8272	19
Superdex 200					
NrfHA	22	325	30	7150	16
NrfA _M	5.8	311	28	1804	4

Table 3.2: Purification of ccNirWT (NrfA_M and NrfHA). (1 U = 1 $\mu\text{mol NO}_2^- \text{min}^{-1}$).

3.1.2.2 Purification of ccNirK134H

Table 3.3 and 3.4 show representative purifications of ccNirK134H from the soluble and the membrane fraction, respectively. The yield was 28 mg from the soluble fraction and 13 mg from the membrane fraction of 50 g wet weight cell mass.

Purification step	Protein [mg]	Specific activity [U/mg]	Purification factor	Activity [U]	Yield [%]
Soluble Fraction	2460	1.8	1.0	4428	100
DE52 / HAP	132	27	15	3564	80
Superdex 200	28	105	58	2940	66

Table 3.3: Purification of ccNirK134H (NrfA_S). (1 U = 1 $\mu\text{mol NO}_2^- \text{min}^{-1}$).

The specific activity of ccNirK134H (NrfA_S) is only around 35 % compared to that of ccNirWT. Also the specific activities of ccNirK134H (NrfA_M and NrfHA) were only one third compared to ccNirWT. The yield after the gel filtration step from the soluble fraction is three times higher in ccNirK134H, but the yield from the membrane fraction is only 46 % compared to that of ccNirWT. Upon purification, the specific activity of soluble nitrite reductase increased by a factor of 58 from 1.8 to 105 U/mg in the assay with methyl viologen as redox mediator. For the enzyme purified from the membrane fraction a specific activity of 98 U/mg for the monomeric form (NrfA_M) and 113 U/mg for the complex (NrfHA) was obtained.

Purification step	Protein [mg]	Specific activity [U/mg]	Purification factor	Activity [U]	Yield [%]
Membrane Fraction	3020	2.1	1.0	6342	100
Membrane Extract	1740	3.3	1.6	5742	91
DE52 / HAP	35	66	31	2310	36
Superdex 200					
NrfHA	7.5	113	53	848	13
NrfA _M	5.5	98	47	539	8

Table 3.4: Purification of ccNirK134H (NrfA_M and NrfHA). (1 U = 1 $\mu\text{mol NO}_2^- \text{min}^{-1}$).

3.1.2.3 Purification of ccNirQ276E

Table 3.5 and 3.6 show representative purifications of ccNirQ276E from the soluble and the membrane fraction, respectively. The yield was 24 mg from the soluble fraction and 40 mg from the membrane fraction of 55 g wet weight cell mass.

Purification step	Protein [mg]	Specific activity [U/mg]	Purification factor	Activity [U]	Yield [%]
Soluble Fraction	2481	4	1.0	9924	100
DE52 / HAP	168	41	10	6888	69
Superdex 200	24	183	46	4392	44

Table 3.5: Purification of ccNirQ276E (NrfA_S). (1 U = 1 $\mu\text{mol NO}_2^- \text{min}^{-1}$).

The specific activity of ccNirQ276E (NrfA_S) is only around 60 % compared to that of ccNirWT. The yield after the gel filtration step from the soluble fraction is two times higher in ccNirQ276E, and the yield from the membrane fraction is 150 % compared to ccNirWT. Upon purification, the specific activity of soluble nitrite reductase increased by a factor of 46 from 4 to 183 U/mg in the assay with methyl viologen as redox mediator. For the enzyme purified from the membrane fraction a specific activity of 313 U/mg for the monomeric form (NrfA_M) and 299 U/mg for the complex (NrfHA) was obtained. These activities are in the same range like that of ccNirWT.

Purification step	Protein [mg]	Specific activity [U/mg]	Purification factor	Activity [U]	Yield [%]
Membrane Fraction	2825	16	1.0	45200	100
Membrane Extract	1784	21	1.3	37464	83
DE52 / HAP	44	290	18	12760	28
Superdex 200					
NrfHA	31	299	19	9269	21
NrfA _M	9.6	313	20	3005	7

Table 3.6: Purification of ccNirQ276E (NrfA_M and NrfHA). (1 U = 1 $\mu\text{mol NO}_2^- \text{min}^{-1}$).

3.1.2.4 Purification of ccNirY218F

Table 3.7 and 3.8 show representative purifications of ccNirY218F from the soluble and the membrane fraction, respectively. The yield was 9 mg from the soluble fraction and 43 mg from the membrane fraction of 45 g wet weight cell mass.

Purification step	Protein [mg]	Specific activity [U/mg]	Purification factor	Activity [U]	Yield [%]
Soluble Fraction	2679	1.4	1.0	3751	100
DE52 / HAP	760	3.8	2.7	2888	77
Superdex 200	24	4.7	3.4	113	3
HAP (Merck)	9.0	7.8	5.6	70	2

Table 3.7: Purification of ccNirY218F (NrfA_S). (1 U = 1 $\mu\text{mol NO}_2^- \text{min}^{-1}$).

The specific activity of ccNirY218F (NrfA_S) is only around 3 % compared to that of ccNirWT. The yield after the gel filtration step from the soluble fraction is nearly the same in ccNirY218F, but the yield from the membrane fraction is 150 % compared to ccNirWT. Upon purification, the specific activity of soluble nitrite reductase increased by a factor of 6 from 1.4 to 7.8 U/mg in the assay with methyl viologen as redox mediator. For the enzyme purified from the membrane fraction a specific activity of 23 U/mg for the monomeric form (NrfA_M) and 21 U/mg for the complex (NrfHA) was obtained. This is 7 % of the activity of ccNirWT (NrfA_M and NrfHA).

Purification step	Protein [mg]	Specific activity [U/mg]	Purification factor	Activity [U]	Yield [%]
Membrane Fraction	2662	1.1	1.0	2928	100
Membrane Extract	1307	2.2	2.0	2875	98
DE52 / HAP	122	17	15	2074	71
HAP (Merck)	67	19	17	1273	43
Superdex 200					
NrfHA	26	21	19	546	19
NrfA _M	17	23	21	391	13

Table 3.8: Purification of ccNirY218F (NrfA_M and NrfHA). (1 U = 1 $\mu\text{mol NO}_2^- \text{min}^{-1}$).

3.1.2.5 Purification of ccNirStopI

Table 3.9 and 3.10 show representative purifications of ccNirStopI from the soluble and the membrane fraction, respectively. The yield was 6 mg from the soluble fraction and 7 mg from the membrane fraction of 60 g wet weight cell mass. ccNirStopI has no detectable specific activity in the soluble fraction as well as in the membrane fraction. The yield after the last purification step from the soluble fraction is nearly 50 % of that of ccNirWT, but the yield from the membrane fraction is rather low compared to ccNirWT. Upon purification, the specific activity of the soluble and the membrane fraction of nitrite reductase did not increased in the assay with methyl viologen as redox mediator.

Purification step	Protein [mg]	Specific activity [U/mg]	Purification factor	Activity [U]	Yield [%]
Soluble Fraction	2633	0	1.0	0	100
DE52 / HAP	228	0	---	0	---
Superdex 200	121	0	---	0	---
HAP (Merck)	6.0	0	---	0	---

Table 3.9: Purification of ccNirStopI (NrfA_S). (1 U = 1 $\mu\text{mol NO}_2^- \text{min}^{-1}$).

Purification step	Protein [mg]	Specific activity [U/mg]	Purification factor	Activity [U]	Yield [%]
Membrane Fraction	3960	0	1.0	0	100
Membrane Extract	2480	0	---	0	---
DE52 / HAP	37	0	---	0	---
Superdex 200					
NrfHA	5.6	0	---	0	---
NrfA _M	1.2	0	---	0	---

Table 3.10: Purification of ccNirStopI (NrfA_M and NrfHA). (1 U = 1 $\mu\text{mol NO}_2^- \text{min}^{-1}$).

3.1.3 Metal Content

The metal content of ccNirWT (NrfA_S), ccNirQ276E (NrfA_S), and ccNirStopI (NrfA_S) was determined by ICP-MS. The samples were analyzed for iron, calcium, and molybdenum (in duplicate). The molybdenum content was investigated because of impurities of nitrate reductase in the ccNir samples (Table 3.11).

	Calcium*	Iron	Molybdenum
ccNirWT	0.4 / 0.8	4.7 / 4.5	0.04
ccNirQ276E	0.3 / 1.1	5.1 / 5.2	0.02
ccNirStopI	10.6	4.1	n.d.

Table 3.11: Calcium, iron, and molybdenum content of ccNir (NrfA_S). The values are calculated per monomer. * In the first analysis, the buffer contained calcium, thus the values for calcium are too high (cursive numbers). In the second run, the buffer was free of calcium.

In ccNirWT and ccNirQ276E five Fe atoms per monomer were found as expected for five heme centers. On the other hand, in ccNirStopI there were only four per monomer of ccNir, indicating that one heme site has been successfully deleted (Pisa *et al.*, 2002).

The calcium values of ccNirWT and ccNirQ276E indicate one calcium per monomer ccNir.

The molybdenum content was between 2 and 4 % per monomer ccNir. This corresponds to the impurities detectable in the SDS-PAGE gels and also in the EPR-spectra (Chapter 3.1.6.1-3.1.6.5).

3.1.4 UV-Vis Spectra

Nitrite reductase displayed typical *c*-type cytochrome UV-Vis absorption spectra (Pettigrew and Moore, 1987). ccNirWT (NrfA_S) showed absorption maxima at 280, 409, and 534 nm, and a shoulder at 615 nm in the as isolated state (Figure 3.2 (A1 and A2)). The shoulder at 615 nm was assigned to a high-spin Fe(III) heme center (Blackmore *et al.*, 1990; Brittain *et al.*, 1992). Upon reduction, new maxima appeared at 420, 523, and 553 nm. Nitrite reductase displayed no additional maxima up to 1100 nm. Second derivative spectra revealed minima at 419, 427, 523, 530, 550 and 555 nm. Peaks at 419 and 550 nm were assigned to low-spin Fe(II) heme centers, whereas those at 427 and 555 nm were consistent with high-spin Fe(II) heme (Wood, 1984; Adachi *et al.*, 1993). In principle, the variants show similar UV-Vis spectra with similar absorption maxima (Figure 3.2 (B1/B2-E1/E2)). The maxima of the Soret-band of the reduced enzymes differ in the range from 418 (ccNirStopI) to 423 nm (ccNirQ276E) and the maxima of the α -band of the oxidized (as isolated) enzymes differ in the range from 530 (ccNirStopI) to 535 nm (ccNirQ276E).

ccNirWT (NrfA_S, NrfA_M, and NrfHA) were purified to homogeneity, the variants nearly to homogeneity. The optical purity indices of ccNirWT and variants are summarized in Table 3.12. Clearly, ccNirStopI was less pure compared to the other proteins.

Indices	WT	K134H	Q276E	Y218F	Stop I	ccNir <i>S. deleyianum</i> *
$A_{280\text{nm}}(\text{ox})/A_{409\text{nm}}(\text{ox})$	0.34	0.41	0.37	0.40	0.73	0.30
$A_{553\text{nm}}(\text{red})/A_{280\text{nm}}(\text{ox})$	0.83	0.71	0.80	0.73	0.35	0.86

Table 3.12: Purity indices of ccNirWT (NrfA_S) and variants. * Values obtained by Schumacher (1993).

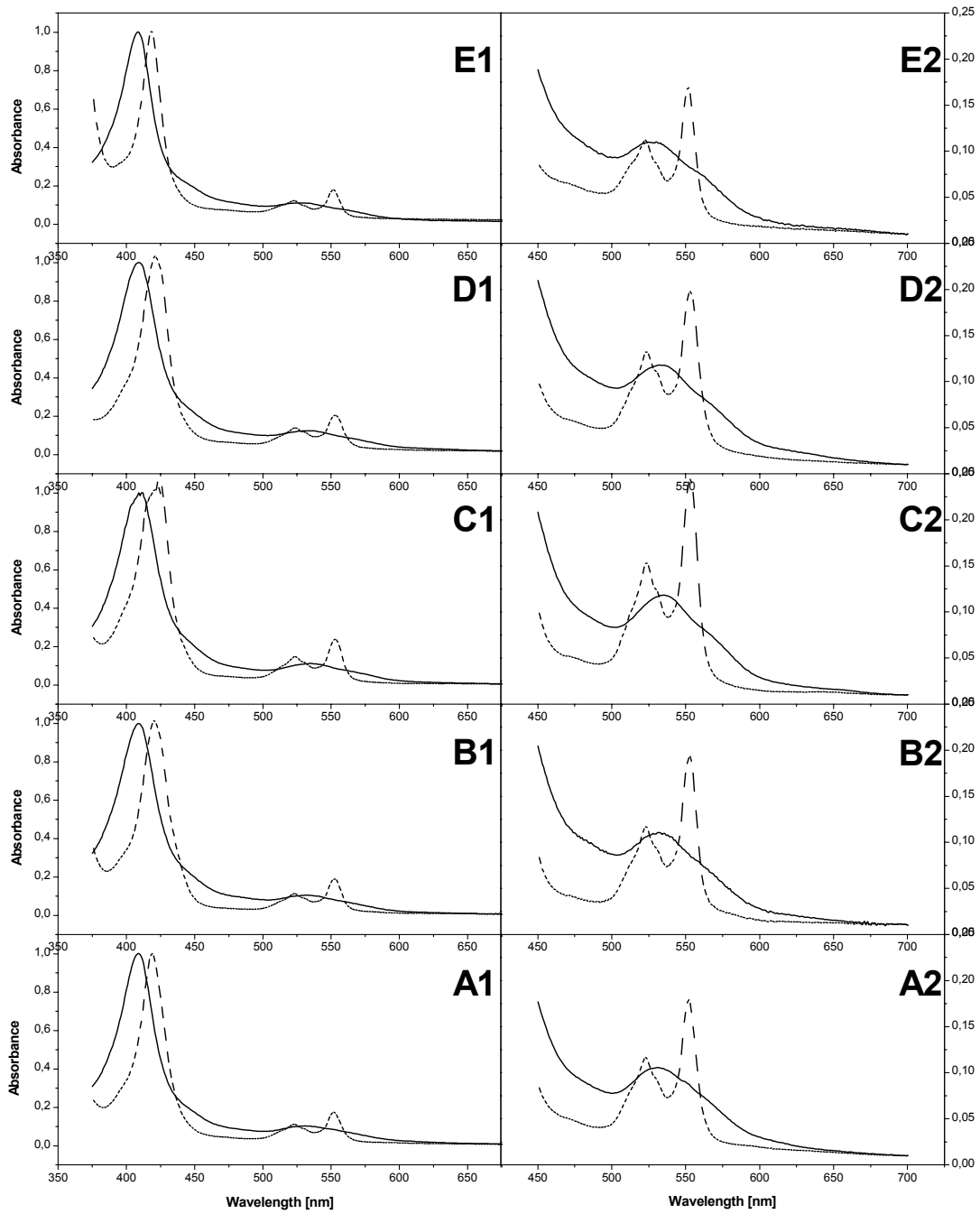


Figure 3.2: UV-Vis spectra of ccNir (NrfA_S). Oxidized as isolated (solid line), reduced with Na₂S₂O₄ (dotted line). **A:** ccNirWT; **B:** ccNirK134H; **C:** ccNirQ276E; **D:** ccNirY218F; **E:** ccNirStopI.

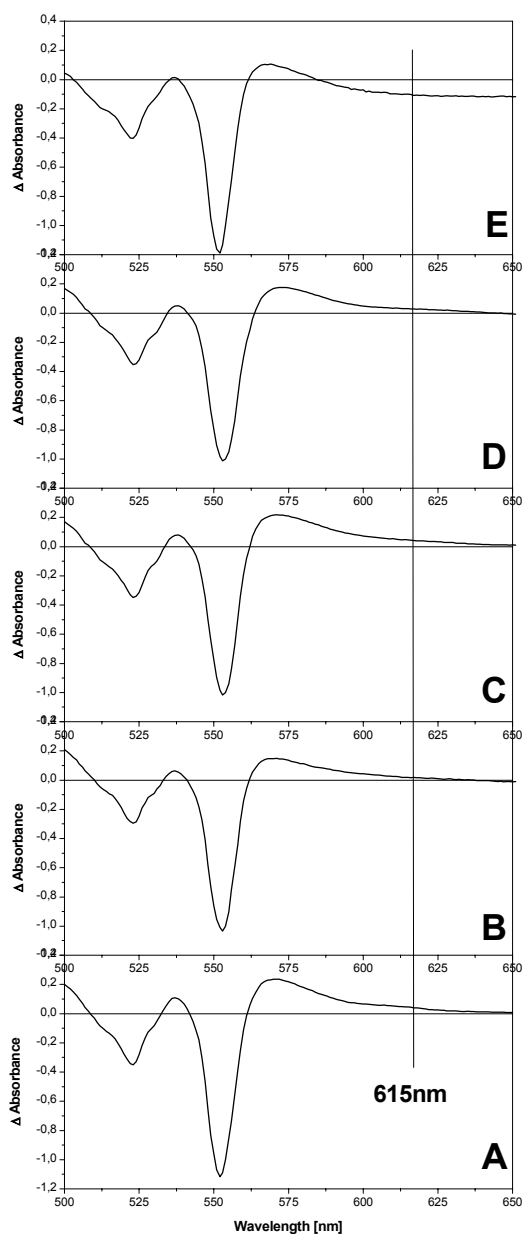


Figure 3.3: Difference spectra (oxidized minus reduced). **A:** ccNirWT; **B:** ccNirK134H; **C:** ccNirQ276E; **D:** ccNirY218F; **E:** ccNirStopI.

The difference spectra (oxidized minus reduced) of ccNir and its variants, with the exception of ccNirStopI, show a shoulder at 615 nm (Figure 3.3 (A-E)). At this wavelength Δ absorbance has to be positive. Therefore, all variants, but not ccNirStopI, carry a Fe(III) high-spin center. In ccNirStopI the active site heme 1 is deleted (Figure 3.3 (E)).

3.1.5 Reaction of ccNir with Hydroxylamine and Derivatives

ccNir can reduce hydroxylamine and nitric oxide to ammonia, with specific activities of ~ 50 % for hydroxylamine but only ~ 1.5 % for nitric oxide relative to that for nitrite (Stach *et al.*, 2000). Both NO and NH₂OH are also potential intermediates of the six-electron reduction of nitrite to ammonia. The existence of an Fe(II)-NO• adduct had been shown by EPR spectroscopy (Schumacher, 1993), and a Fe(III)-NH₂OH complex was obtained by soaking a crystal of ccNirWT with NH₂OH and its X-ray structure could be solved at 2.0 Å resolution (Einsle *et al.*, 2002b). The O-methyl derivative of hydroxylamine was also an active substrate (Stach, 2001).

Figure 3.4 shows hydroxylamine and its derivatives used in this study. Chemically, hydroxylamine usually acts as a strong reducing agent, but can also function as an oxidant, depending on the metal, coordinated ligands, and external conditions such as pH. As oxidation products, N₂, N₂O, NO, NO₂, NO₂⁻ or NO₃⁻ can be formed; the reduction product appears to be solely ammonia. In the case of Fe(III) complexes, hydroxylamine will act as a strong reductant and the corresponding Fe(II) compounds will be formed (Wieghardt, 1984).

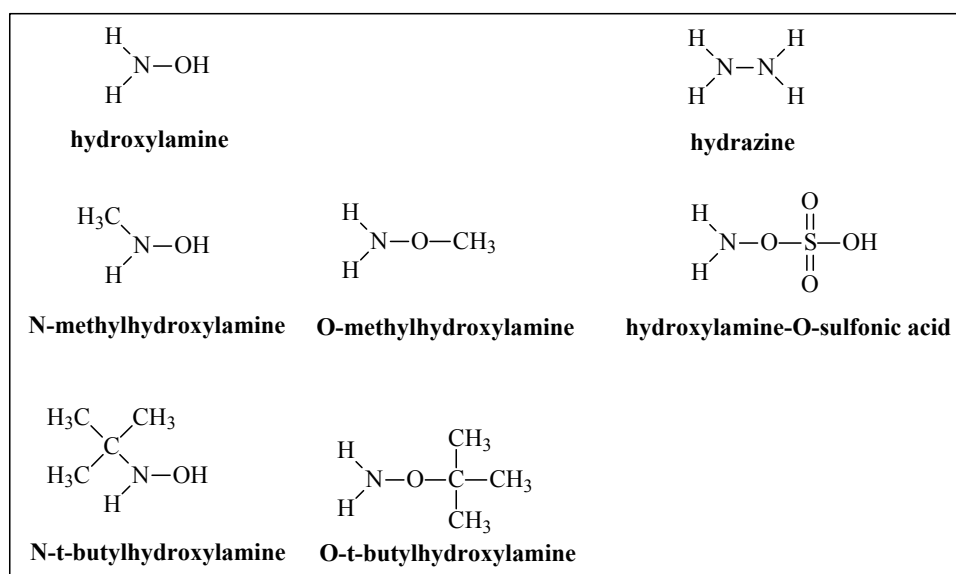


Figure 3.4: Structure of hydroxylamine and its derivatives.

UV/Vis spectroscopy represents a suitable tool for initial investigation of the reactivity of heme proteins because of their distinct electronic properties and intense absorption maxima in the region 400-650 nm, both of the oxidized and reduced enzyme, respectively (Chapter 3.1.4).

In the first set of experiments, the reactivity of hydroxylamine, its derivatives substituted at both the N- and O-position, and hydrazine (Figure 3.4) was investigated in the absence of dioxygen, starting from oxidized (as isolated) ccNir (Figure 3.5 (A)). Both hydroxylamine and derivatives reacted rather poorly, and the maximum reduction of ccNir (16 %; 10^4 excess of substrate) was achieved by hydroxylamine and its N-methyl derivative (Table 3.13), compared to approximately 5 % for the various N- and O-substituted derivatives, including hydroxylamine-O-sulfonic acid. On the other hand, hydrazine proved to be a relatively good reductant (67 %) of ccNir under these conditions.

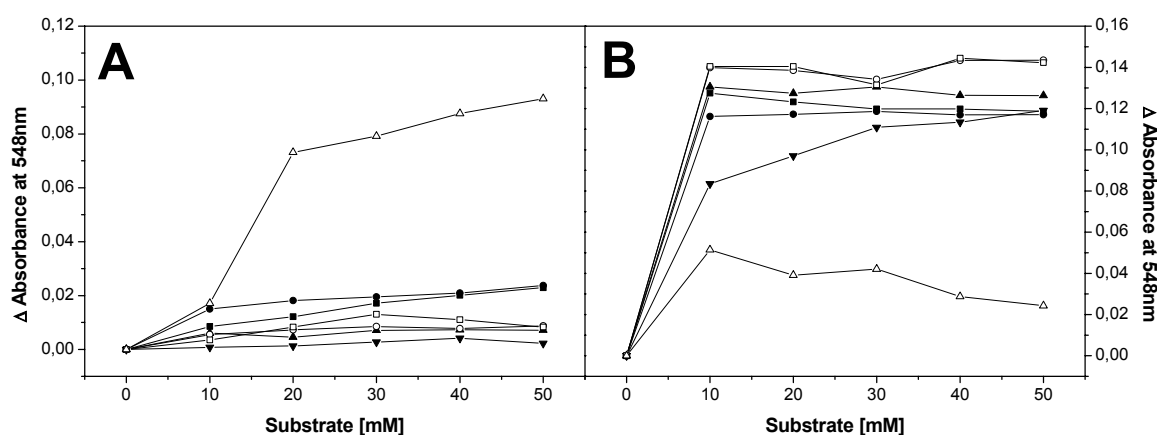


Figure 3.5: Reaction of ccNirWT with hydroxylamine and its derivatives. **A:** Reduction of Fe(III)-ccNir; **B:** Oxidation of Fe(II)-ccNir (produced by photochemical reduction of Fe(III)-ccNir). Enzyme was present at 5 μ m, in 100 mM potassium phosphate buffer, pH 7.0, at 25°C; hydroxylamine (●), N-methylhydroxylamine (■), O-methylhydroxylamine (▲), N-t-butylhydroxylamine (▼), O-t-butylhydroxylamine (○), hydroxylamine-O-sulphonic acid (□), and hydrazine (Δ).

In the oxidative reaction, Fe(II)-ccNir (produced by photochemical reduction of Fe(III)-ccNir) was investigated (Figure 3.5 (B)). Hydroxylamine and the various derivatives, except hydrazine, did re-oxidize the enzyme very rapidly, with an efficiency of close to 100 % (Table 3.13). In most cases, the reoxidation was complete after addition of 5 mM substrate (Figure 3.5).

Substrate	Fe(II)-ccNir ¹ (%)	Fe(III)-ccNir ² (%)
hydroxylamine	16	75
N-methylhydroxylamine	16	76
O-methylhydroxylamine	5	78
N-t-butylhydroxylamine	5	89
O-t-butylhydroxylamine	6	94
hydroxylamine-O-sulfonic acid	6	93
hydrazine	67	20

Table 3.13: Calculated values from ΔA_{548} after stepwise addition of 50mM substrate; 100% = ΔA_{548} for [Fe(II)-ccNir_{photochemically reduced}]-[Fe(III)-ccNir_{as isolated}]. ¹ Reduction of Fe(III)-ccNir as isolated; ² Oxidation of photochemically reduced Fe(II)-ccNir.

3.1.6 Multifrequency EPR Spectroscopy

EPR spectra of ccNir (as isolated) recorded at different microwave frequencies, and applying X-Band (≈ 9 -10 GHz) both in the parallel and perpendicular mode, are documented in Figures 3.6 to 3.10. EPR spectra of ccNir from *W. succinogenes* were in close agreement with the spectra reported for ccNir from *S. deleyianum* (Stach, 2001), *D. desulfuricans* (Costa *et al.*, 1990), *V. fischeri* (Sadana *et al.*, 1986), and *E. coli* (Liu *et al.*, 1987).

The presence of magnetic interactions can be verified by recording EPR spectra at different microwave frequencies. The g -values of interacting systems with $S > 1/2$ will shift with the frequency used.

The better resolution of closely spaced g -values at higher frequencies, e.g. Q-Band (≈ 35 GHz), allows the separation of the complicated and overlapping spectra into their components. Lower microwave frequencies, e.g. S-Band (≈ 2 -4 GHz), can be advantageous for the reduction of experimental linewidth, leading to a better resolution, or for the observation of weak hyperfine features that may be masked by more intense features at higher microwave frequencies.

The EPR spectra of all ccNir samples used in this study had three things in common. Firstly, the signal at $g \approx 4.3$ presumably arises from non-specifically bound Fe(III). Secondly, the significant increase in intensity of the resonance at $g \approx 3.4$ is not observed for every parallel mode spectrum of ccNir, thus may be due to an artefact. And finally, there was an EPR signal at $g \approx 2$ with variable intensity. Generally, the intensity of this feature in spectra of *W. succinogenes* ccNir was higher compared with spectra of the *S. deleyianum* (Stach, 2001)

enzyme. In the earlier literature, this feature was assigned to a contamination by an iron-sulfur protein (Blackmore *et al.*, 1987; Schumacher, 1993). Based on the temperature dependent behaviour of this signal, and with respect to typical resonance features of iron-sulfur clusters (Cammack, 1992), it was concluded that the signal at $g \approx 2$ presumably does not arise from an iron-sulfur cluster (Stach, 2001). In view of the presence of 2-4 % molybdenum in the ccNir samples (Chapter 3.1.3), the sharp signal at $g \approx 2$ most likely arises from nitrate reductase, a well known Mo, Fe-S enzyme, in agreement with the extra band at 96 kDa in the SDS-PAGE gel.

3.1.6.1 EPR Spectra of ccNirWT

The perpendicular mode EPR spectrum at X-Band (Figure 3.6 (A)) showed resonances at $g = 2.98$, 2.32 and ≈ 1.50 and $g = 2.50$, 2.15 and ≈ 1.45 that are typical for low-spin Fe(III) centers (Palmer, 1983) where the bis-histidine ligands have nearly parallel imidazole planes (Walker, 1999). Additional low-spin Fe(III) features are at $g = 3.41$ and 3.22 . These are responsible for two Fe(III) low-spin centers where the bis-histidine ligands have nearly perpendicular imidazole planes (Walker, 1999). The g_{mid} and g_{low} features of this centers are extremely broad and hard to detect. Spin quantification and computer simulations (CuSO_4 standard) of the latter signals from EPR spectra of *S. deleyianum* enzyme yielded 1.80 low-spin Fe(III) heme centers (Schumacher *et al.*, 1997).

In addition to these low-spin Fe(III) features, there was a strong signal at $g = 3.81$ and a broad line around $g = 9.8$ which could not be attributed to any common Fe(III) spin state. A strong signal at $g = 9.4$ was also detected in the parallel mode (Figure 3.6 (D)). The signals at $g = 3.81$ and 9.8 in the perpendicular mode spectrum and the signal at $g = 9.4$ in the parallel mode spectrum were assigned to a pair of exchange-coupled hemes according to Andersson *et al.* (1986), Blackmore *et al.* (1990), and Hendrich *et al.* (2001). Furthermore, a resonance at $g \approx 6$ indicative of high-spin Fe(III) was observed.

Figure 3.6 shows representative spectra of ccNirWT (NrfA_S) at three different microwave frequencies (34, 9.38, and 3.84 GHz) plotted on a g -scale. The samples were taken from one single preparation of ccNir. It is evident that the spectra differ significantly as a function of microwave frequency. Analysis of the EPR data is very complex since even at high frequency (Q-Band) the separation of magnetically coupled heme centers does not occur. The spectrum in Figure 3.6 (B) does not extend below $g \approx 1.87$ due to the magnetic field limit of the Q-Band EPR spectrometer.

To summarize, the set of resonances at $g = 2.98$, 2.32 , and ≈ 1.50 and $g = 2.50$, 2.15 and ≈ 1.45 were assigned to low-spin Fe(III) hemes according to Palmer (1983). These features arise from non-interacting low-spin ferric hemes since they do not depend on the microwave frequency.

The feature at $g \approx 6$ is due to high-spin Fe(III) heme. The origin of this signal is still not understood.

The signals observed at $g = 3.81$ and 9.8 at X-Band have frequency dependent g -values which is indicative of a spin-coupled system, i.e. magnetic coupling between heme groups (Chapter 3.1.7).

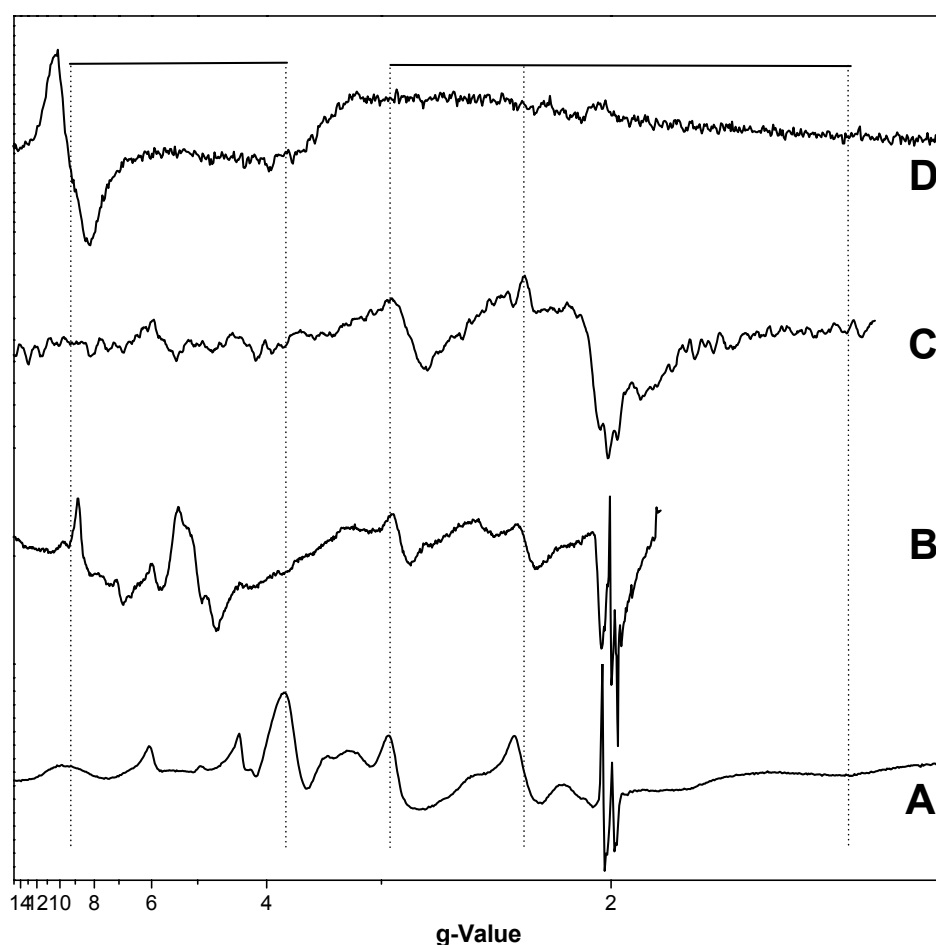


Figure 3.6: Multifrequency EPR spectra of ccNirWT (NrfA_S). Enzyme, 0.17 mM in 50 mM HEPES/NaOH buffer, pH 7.5. **A**: microwave frequency, 9.38 GHz (perpendicular mode); microwave power, 2 mW; temperature, 10 K. **B**: microwave frequency, 34 GHz; microwave power, 5 mW; temperature, 15 K. **C**: microwave frequency, 3.84 GHz; microwave power, 5 mW; temperature, 10 K. **D**: microwave frequency, 9.40 GHz (parallel mode); microwave power, 2 mW; temperature, 8 K.

3.1.6.2 EPR Spectra of ccNirK134H

The perpendicular mode EPR spectrum at X-Band (Figure 3.7 (A)) showed resonances at $g = 2.91$, 2.30 and ≈ 1.46 and $g = 2.74$, 2.12 and ≈ 1.40 that are typical for low-spin Fe(III) centers (Palmer, 1983) with nearly parallel imidazole planes (Walker, 1999). Additional low-spin Fe(III) features are at $g = 3.35$ and 3.16 . These result from two Fe(III) low-spin centers with nearly perpendicular imidazole planes (Walker, 1999).

In addition, signals at $g = 3.87$ and around $g = 9.3$ were present which are weaker compared to ccNirWT. No signal was detected in the parallel mode (Figure 3.7 (D)). The signals at $g = 3.87$ and 9.3 in the perpendicular mode spectrum could be assigned to a pair of exchange-coupled hemes as suggested by Andersson *et al.* (1986), Blackmore *et al.* (1990), and Hendrich *et al.* (2001). Why there was no integer-spin signal in the parallel mode spectrum is still not understood. In addition, a resonance at $g \approx 6.1$ indicative of high-spin Fe(III) was observed.

Figure 3.7 shows representative spectra of ccNirK134H (NrfA_S) at three different microwave frequencies (34, 9.38, and 3.84 GHz) plotted on a g -scale. The samples were taken from one single preparation of ccNir. It is evident that the spectra differ significantly as a function of microwave frequency. Analysis of the EPR data is very complex since even at high frequency (Q-Band) the separation of magnetically coupled heme centers does not occur. The spectrum in Figure 3.7 (B) does not extend below $g \approx 1.87$ due to the magnetic field limit of the Q-Band EPR spectrometer.

To summarize, the set of resonances at $g = 2.91$, 2.30 , and ≈ 1.46 and $g = 2.74$, 2.12 and ≈ 1.40 were assigned to low-spin Fe(III) hemes according to Palmer (1983). These features arise from non-interacting low-spin ferric hemes since they do not depend on the microwave frequency.

The feature at $g \approx 6.1$ is due to high-spin Fe(III) heme. The origin of this signal is still not understood.

The signals observed at $g = 3.87$ and 9.3 at X-Band have frequency dependent g -values which is indicative of a spin-coupled system, i.e. magnetic coupling between heme groups (Chapter 3.1.7).

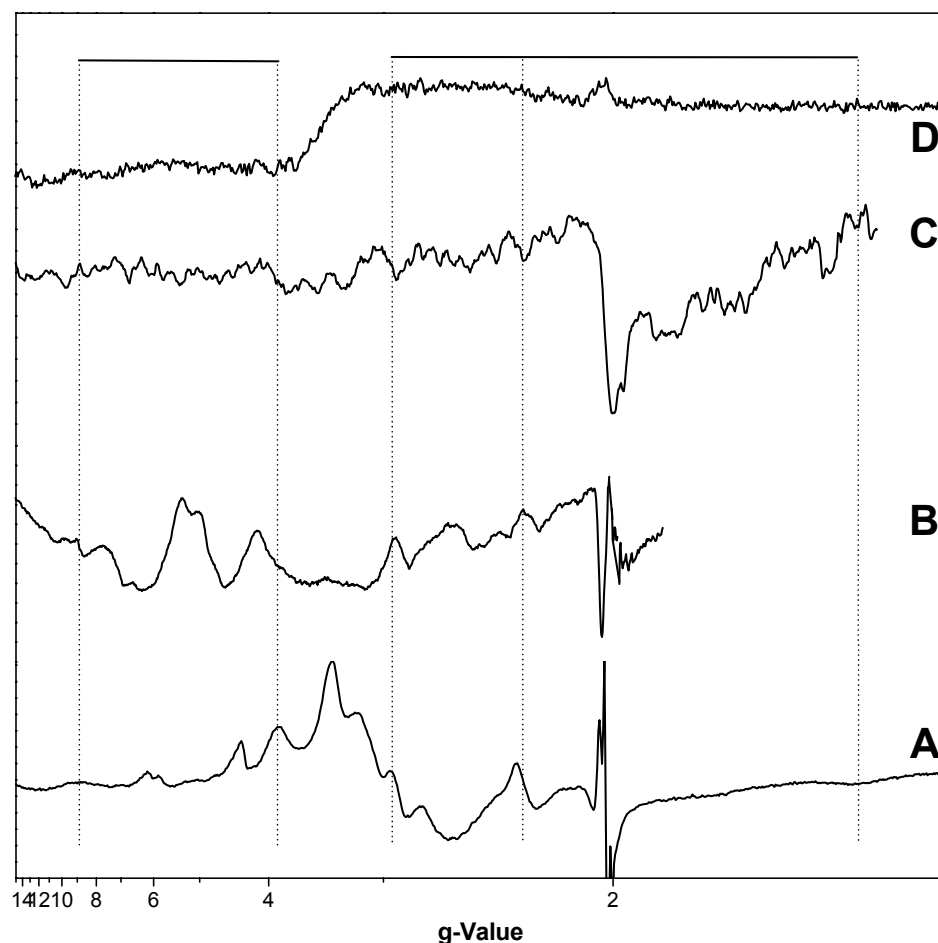


Figure 3.7: Multifrequency EPR spectra of ccNirK134H (NrfA_S). Enzyme, 0.17 mM in 50 mM HEPES/NaOH buffer, pH 7.5. **A**: microwave frequency, 9.38 GHz (perpendicular mode); microwave power, 2 mW; temperature, 10 K. **B**: microwave frequency, 34 GHz; microwave power, 5 mW; temperature, 15 K. **C**: microwave frequency, 3.84 GHz; microwave power, 5 mW; temperature, 10 K. **D**: microwave frequency, 9.40 GHz (parallel mode); microwave power, 2 mW; temperature, 8 K.

3.1.6.3 EPR Spectra of ccNiRQ276E

The perpendicular mode EPR spectrum at X-Band (Figure 3.8 (A)) showed resonances at $g = 2.94$, 2.32 , and ≈ 1.57 that are typical for low-spin Fe(III) centers (Palmer, 1983) with nearly parallel imidazole planes (Walker, 1999). Additional low-spin Fe(III) features are at $g = 3.48$ and 3.26 . These are responsible for two Fe(III) low-spin center with nearly perpendicular imidazole planes (Walker, 1999). The resonances at $g = 2.49$, 2.17 , 1.81 , and ≈ 1.48 are microwave frequency dependent and therefore due to a spin coupled system of two $S = 1/2$ systems.

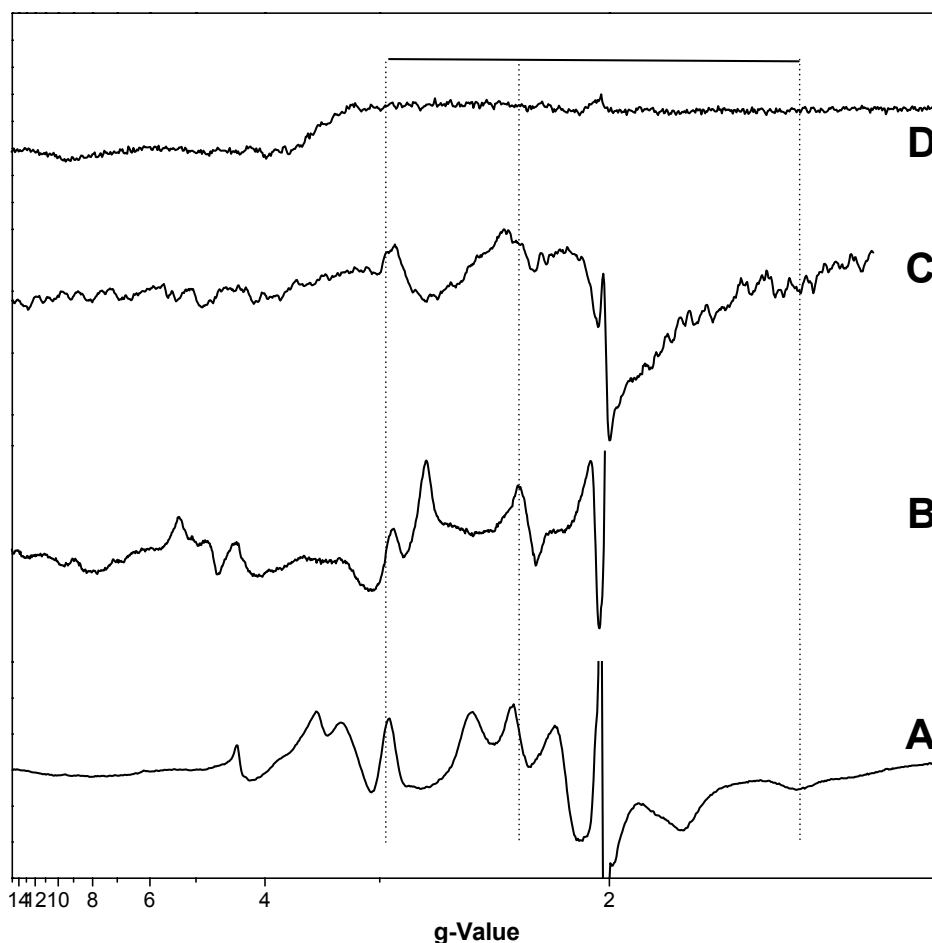


Figure 3.8: Multifrequency EPR spectra of ccNirQ276E (NrfA_S). Enzyme, 0.17 mM in 50 mM HEPES/NaOH buffer, pH 7.5. **A**: microwave frequency, 9.38 GHz (perpendicular mode); microwave power, 2 mW; temperature, 10 K. **B**: microwave frequency, 34 GHz; microwave power, 5 mW; temperature, 15 K. **C**: microwave frequency, 3.84 GHz; microwave power, 5 mW; temperature, 10 K. **D**: microwave frequency, 9.40 GHz (parallel mode); microwave power, 2 mW; temperature, 8 K.

In contrast to ccNirWT and ccNirK134H no signals around $g = 3.8$ and $g = 9.8$ were detected, and there was no signal in the parallel mode spectrum (Figure 3.8 (D)). Furthermore, there was no resonance present at $g \approx 6$ indicative of high-spin Fe(III). Therefore, no coupling system between $S = 5/2$ and $1/2$ exist.

Figure 3.8 shows representative spectra of ccNirQ276E (NrfA_S) at three different microwave frequencies (34, 9.38, and 3.84 GHz) plotted on a g -scale. The samples were taken from one single preparation of ccNir. The spectra differ significantly as a function of microwave frequency in the region around $g = 2.5$ but not around $g = 3.8$. The main difference comes from the line at $g = 2.8$ in the Q-Band spectrum which is found at $g = 2.49$

in the X-Band spectrum. A coupling system of two $S = 1/2$ spins could be responsible for this finding.

To summarize, the set of resonances at $g = 2.94$, 2.32 , and ≈ 1.57 were assigned to low-spin Fe(III) hemes according to Palmer (1983). These features arise from non-interacting low-spin ferric hemes since they do not depend on the microwave frequency, whereas the resonances at $g = 2.49$, 2.17 , 1.81 , and ≈ 1.48 depend on the microwave frequency.

3.1.6.4 EPR Spectra of ccNiRY218F

The perpendicular mode EPR spectrum (Figure 3.9 (A)) showed resonances at $g = 2.95$, 2.33 , and ≈ 1.53 that are typical for low-spin Fe(III) centers (Palmer, 1983) with nearly parallel imidazole planes (Walker, 1999). Additional low-spin Fe(III) features are at $g = 3.39$ and 3.16 . These are responsible for two Fe(III) low-spin center with nearly perpendicular imidazole planes (Walker, 1999). The resonances at $g = 2.58$, 2.17 , 1.80 , and ≈ 1.48 are microwave frequency dependent and therefore due to a spin coupled system of two $S = 1/2$ systems.

In contrast to ccNirWT and ccNirK134H no signals around $g = 3.8$ and $g = 9.8$ were detected, and there was no resonance present at $g \approx 6$ indicative of high-spin Fe(III). A signal at $g = 13$ was detected in the parallel mode spectrum (Figure 3.9 (D)). This signal could be assigned to a pair of exchange coupled hemes. Because of no observed Fe(III) high-spin signal, a coupling of a spin $5/2$ with a spin $1/2$ could be excluded. Instead, a coupling pair of two $1/2$ spins could be assigned to that signal.

Figure 3.9 shows representative spectra of ccNirY218F (NrfA_S) at three different microwave frequencies (34, 9.38, and 3.84 GHz) plotted on a g -scale. The samples were taken from one single preparation of nitrite reductase. The spectra differ not as significantly as in ccNirWT as a function of microwave frequency. The main difference as well as in the spectra of ccNirQ276E is the line at $g = 2.8$ in the Q-Band spectrum which is absent in the X-Band spectrum. A coupling system of two $1/2$ spins could be responsible for this finding.

To summarize, the set of resonances at $g = 2.95$, 2.33 , and ≈ 1.53 were assigned to low-spin Fe(III) hemes according to Palmer (1983). These features arise from non-interacting low-spin ferric hemes since they do not depend on the microwave frequency, whereas the resonances at $g = 2.48$, 2.17 , 1.80 , and ≈ 1.48 depend on the microwave frequency.

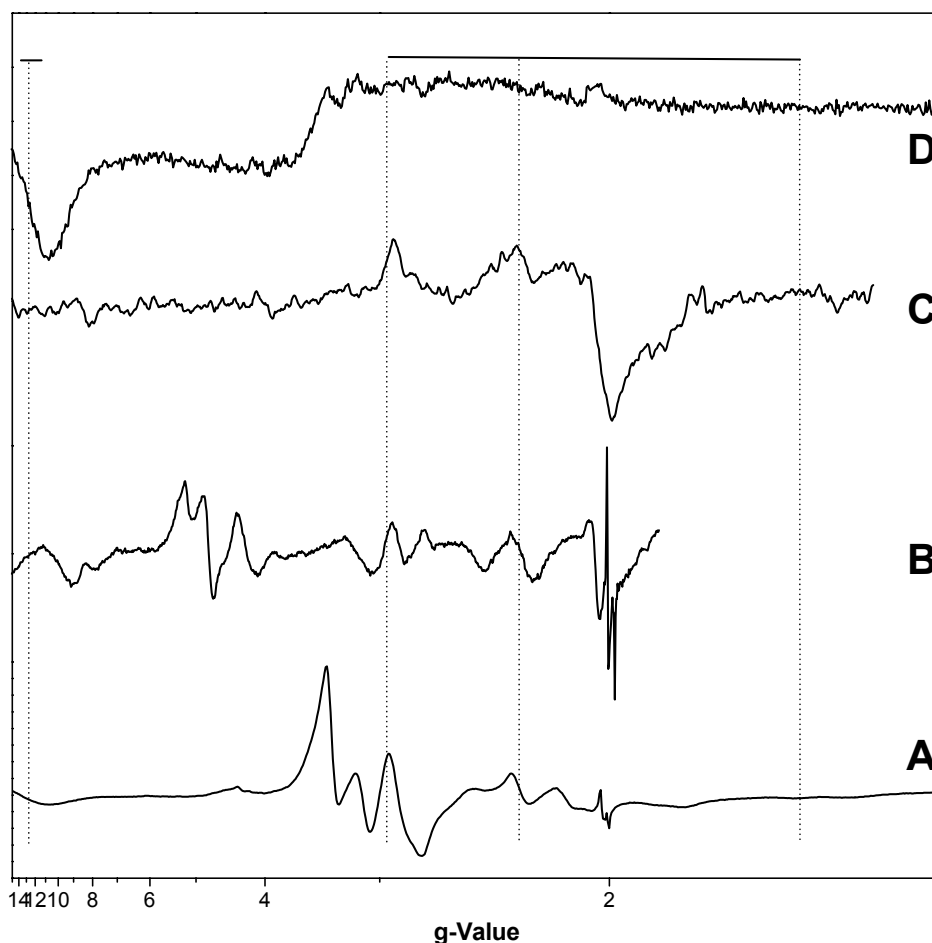


Figure 3.9: Multifrequency EPR spectra of ccNirY218F (NrfA_S). Enzyme, 0.17 mM in 50 mM HEPES/NaOH buffer, pH 7.5. **A**: microwave frequency, 9.38 GHz (perpendicular mode); microwave power, 2 mW; temperature, 10 K. **B**: microwave frequency, 34 GHz; microwave power, 5 mW; temperature, 15 K. **C**: microwave frequency, 3.84 GHz; microwave power, 5 mW; temperature, 10 K. **D**: microwave frequency, 9.40 GHz (parallel mode); microwave power, 2 mW; temperature, 8 K.

3.1.6.5 EPR Spectra of ccNirStopI

The perpendicular mode EPR spectrum (Figure 3.10 (A)) showed resonances at $g = 2.93$, 2.32 and ≈ 1.59 that are typical for low-spin Fe(III) centers (Palmer, 1983) with nearly parallel imidazole planes (Walker, 1999). Additional low-spin Fe(III) features at higher g -values like in ccNirWT and the other variants could not be observed.

In contrast to ccNirWT and ccNirK134H the signals around $g = 3.8$, $g = 9.8$, and $g = 6$ were absent. Additionally, no signal was detected in the parallel mode (Figure 3.10 (D)).

Figure 3.10 shows representative spectra of ccNirStopI (NrfA_S) at three different microwave frequencies (34, 9.38, and 3.84 GHz) plotted on a g -scale. The samples were taken

from one single preparation of nitrite reductase. The spectrum in Figure 3.10 (B) does not extend below $g \approx 1.87$ due to the magnetic field limit of the Q-Band EPR spectrometer. The spectra do not differ significantly as a function of microwave frequency. Therefore, no exchange coupling pair of hemes exist.

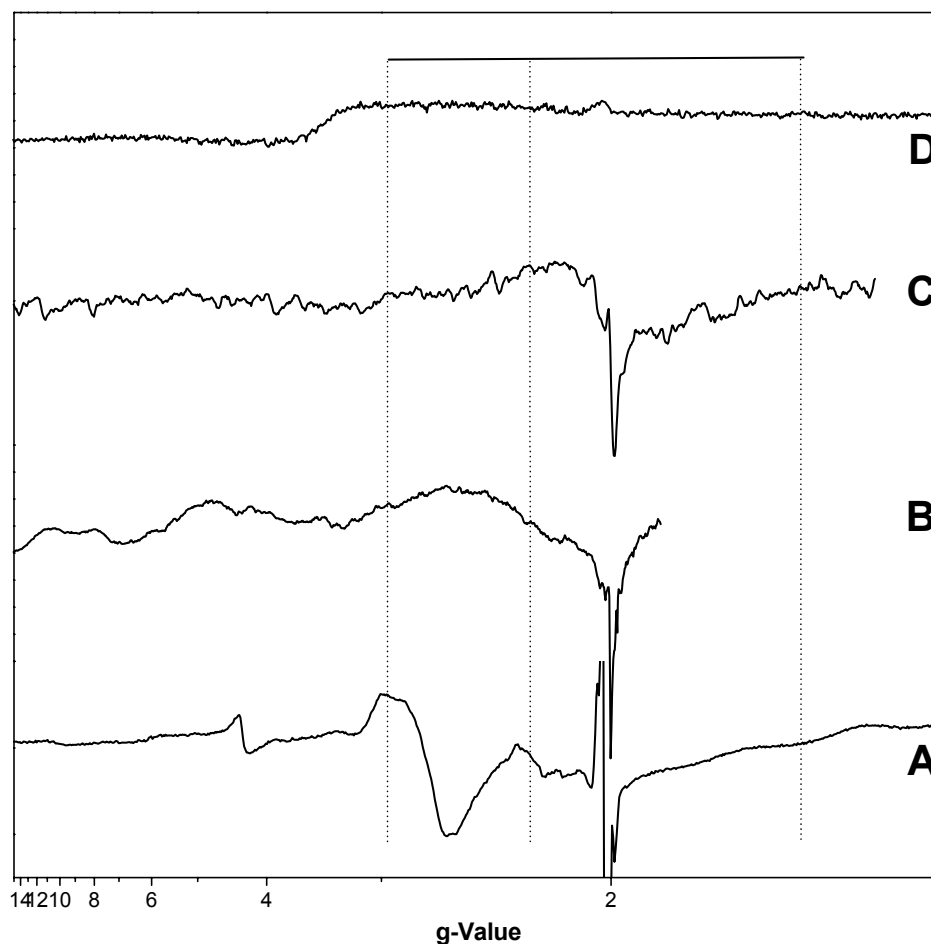


Figure 3.12: Multifrequency EPR spectra of ccNirStopl (NrfA_S). Enzyme, 0.17 mM in 50 mM HEPES/NaOH buffer, pH 7.5. **A:** microwave frequency, 9.38 GHz (perpendicular mode); microwave power, 2 mW; temperature, 10 K. **B:** microwave frequency, 34 GHz; microwave power, 5 mW; temperature, 15 K. **C:** microwave frequency, 3.84 GHz; microwave power, 5 mW; temperature, 10 K. **D:** microwave frequency, 9.40 GHz (parallel mode); microwave power, 2 mW; temperature, 8 K.

3.1.6.6 Comparison of the EPR Parameters for ccNir and Variants

To summarize the results from the multifrequency studies, apparent g -values of all signals from X-Band measurements were listed in Table 3.14 except the lines around $g = 2$. The spectra of ccNirWT and all variants show resonances around $g = 2.98$ to $g = 1.46$ indicating two separate Fe(III) low-spin hemes with nearly parallel imidazole planes (hemes 2

and 3 in the structure (Einsle *et al.*, 2000)). In the spectra of ccNirQ276E and ccNirY218F, the signals around $g = 2.5$, 2.15, 1.8, and 1.48 are microwave frequency dependent, indicating a spin coupled pair of two $S = 1/2$. In the spectrum of ccNirStopI the resonance around $g = 2.5$ could not be resolved. The resonances between $g = 3.5$ to $g = 3.16$ are due to Fe(III) low-spin hemes with nearly perpendicular imidazole planes (hemes 4 and 5 in the structure (Einsle *et al.*, 2000)). These signals are only missing in ccNirStopI. Resonances indicative for a Fe(III) high-spin heme at $g = 6$ could only be found in the spectra of ccNirWT and ccNirK134H. Furthermore, the signals indicative for a $S = 5/2 \leftrightarrow 1/2$ exchange coupled pair around $g = 9.8$ and $g = 3.8$ could only be found in the spectra of ccNirWT and ccNirK134H. In all samples, a signal around $g = 4.3$ indicates non-specifically bound iron.

	g-Value											
WT	9.84	6.04	4.34	3.81	3.41	3.22	2.98	2.50	2.32	2.15	1.83	1.50
K134H	9.28	6.12	4.31	3.87	3.35	3.16	2.91	2.74	2.30	2.12	1.76	1.46
Q276E			4.37		3.48	3.26	2.94	2.49	2.32	2.17	1.81	1.57
Y218F			4.34		3.39	3.16	2.95	2.48	2.33	2.17	1.80	1.53
Stop I			4.36				2.93		2.32	2.17	1.81	1.59

Table 3.14: Apparent g -values of ccNirWT (NrfA_S) and variants.

3.1.6.7 Power Saturation Studies

The dependence of the EPR signal intensity (baseline corrected peak height) on the microwave power P was studied at 10 K. The saturation behavior (half-saturation, $P_{1/2}$) of the two $S = 1/2$ (hemes with nearly parallel imidazole planes), the $S = 5/2$ (Fe(III) high-spin) and the $S = 5/2 \leftrightarrow 1/2$ (exchange coupled pair) systems were rather different. Whereas the lines due to the Fe(III) high-spin heme and the $S = 5/2 \leftrightarrow 1/2$ exchange coupled pair in the region $g = 3.8$ to $g = 9.8$ (68 to 180 mT) saturate at around 16-30 mW, the lines due to the two Fe(III) low-spin hemes with nearly parallel imidazole planes from $g = 2.96$ to $g = 1.50$ (227 to 445 mT) saturate at around 3-7 mW. However, the intensities of the g_{low} signals of the Fe(III) low-spin hemes were very small so there was considerable experimental uncertainty in the baseline corrected peak heights and thus in the $P_{1/2}$ values.

The details of the half-saturation power determination were taken from Figure 3.11 and listed in Table 3.15.

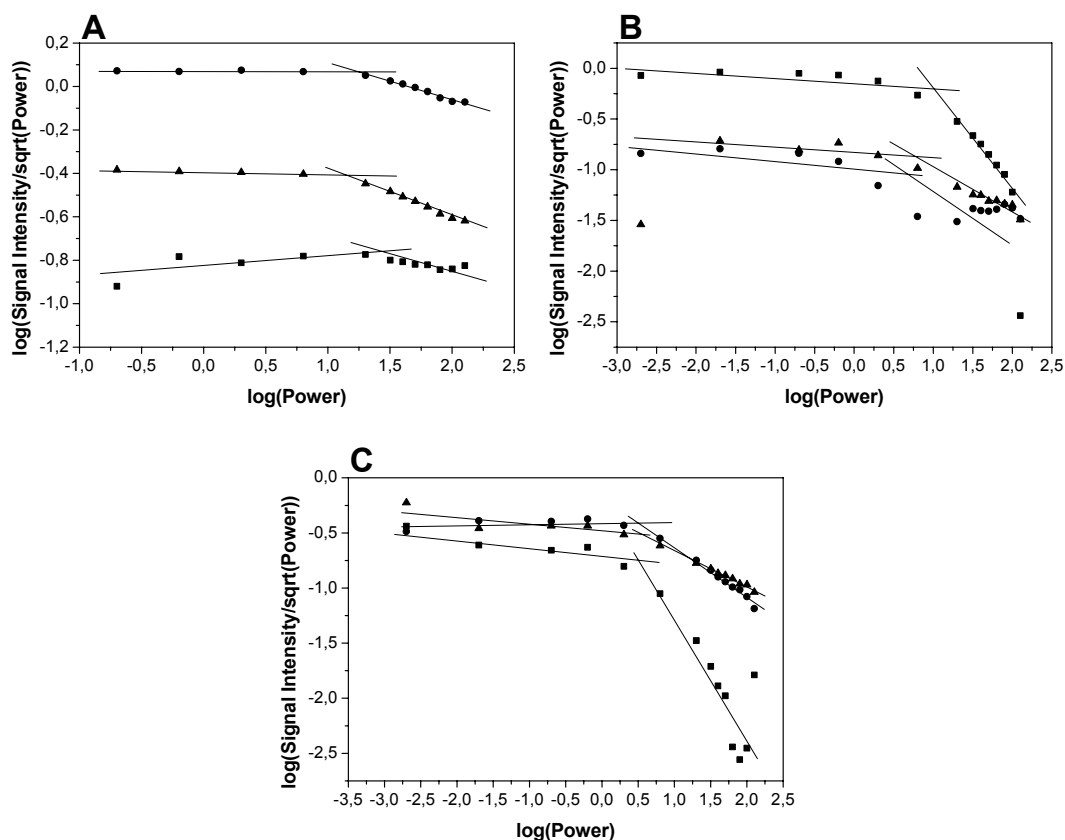


Figure 3.11: Power saturation study on ccNirWT (NrfA_S). **A:** Fe(III) high-spin and $S = 5/2 \leftrightarrow 1/2$ exchange resonances at $g = 9.8$ (■), $g = 3.8$ (●) and $g = 6.0$ (▲). **B:** Fe(III) low-spin resonances at $g = 2.96$ (■), $g = 2.29$ (●) and $g = 1.50$ (▲). **C:** Fe(III) low-spin resonances at $g = 2.49$ (■), $g = 2.10$ (●) and $g = 1.80$ (▲). Enzyme, 0.17 mM in 50 mM HEPES/NaOH buffer, pH 7.5; microwave frequency, 9.38 GHz; microwave power, 0.002-127 mW; modulation amplitude, 0.5 mT; temperature, 10 K.

g -Value	Field [mT]	Spin	P1/2 [mW]
9.84	68	$5/2 \leftrightarrow 1/2$	32
6.04	111	$5/2$	16
3.81	175	$5/2 \leftrightarrow 1/2$	19
2.96	227	$1/2$	7.1
2.49	270	$1/2$	3.3
2.29	293	$1/2$	5.0
2.10	320	$1/2$	3.2
1.80	371	$1/2$	4.0
1.50	445	$1/2$	6.3

Table 3.15: Power saturation parameters of ccNirWT (NrfA_S) at 10 K.

3.1.6.8 Influence of Yttrium(III) on the EPR Spectra of ccNirQ276E (NrfA_S)

During crystallization of ccNirQ276E (Chapter 3.1.8.2) the Ca(II) ion near the active site was exchanged against an Y(III) ion. Note that in all experiments done in solution Y(III) was absent. The question arose whether Y(III) would bind to ccNir in solution and thus might influence the EPR spectrum. Therefore, two identical EPR samples were prepared, one with enzyme as isolated and one with enzyme and 15 mM Y(III). This concentration was used in the crystallization experiments. The corresponding X-Band spectra of ccNirQ276E with and without Y(III) are shown in Figure 3.12.

Two major differences become obvious in the region around $g = 6$ and $g = 3.5$. By addition of Y(III) a small signal at $g = 6.1$ arises from Fe(III) high-spin heme, this signal is absent in the as isolated protein. Furthermore, the sharp signal at $g = 3.48$ in the as isolated sample changes to a shoulder in the sample with Y(III).

Another difference is a shift in the g -values. Whereas the g -values of the Fe(III) low-spin heme with nearly parallel imidazole planes in the spectrum of the as isolated enzyme are $g = 2.94, 2.32$, and 1.57 , the g -values of the enzyme with Y(III) are $g = 3.00, 2.26$, and 1.53 .

Additionally, the relative signal intensities are smaller in the sample with Y(III). Because the g -values at $2.49, 2.17, 1.81$, and 1.48 are due to an exchange coupled system of two $S = 1/2$ centers, the lower signal intensity indicates a lower exchange coupling or a lower relaxation time.

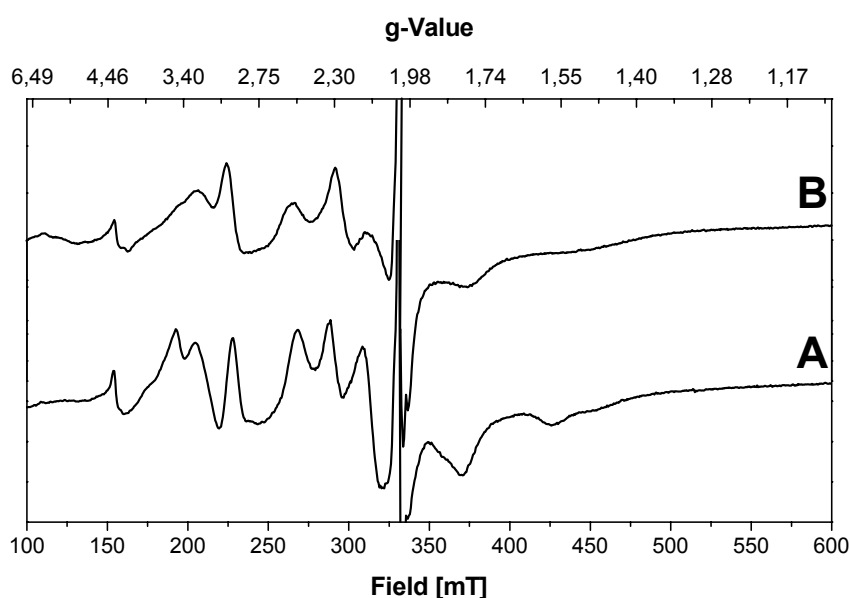


Figure 3.12: X-Band EPR spectra of ccNirQ276E (NrfA_S). **A**: as isolated; **B**: with 15 mM Y(III). Enzyme, 0.17 mM in 50 mM HEPES/NaOH buffer, pH 7.5; microwave frequency, 9.38 GHz; microwave power, 2 mW; temperature, 10 K.

3.1.6.9 Simulation of the X-Band EPR Spectrum of ccNirQ276E (NrfA_S)

The complete X-Band EPR spectrum of ccNirQ276E as isolated (Figure 3.13 (A)) with exception of the $g \approx 2$ part and the signals which are due to a spin coupled pair of two $S = 1/2$ systems was simulated as a sum of three species with $S = 1/2$. The resonances at $g = 2.93$, 2.29, and 1.57 are due to a rhombic Fe(III) low-spin heme signal with nearly parallel imidazole planes (Figure 3.13 (C)). The resonances at $g = 3.47$ and 3.26 are due to two separate rhombic Fe(III) low-spin heme signals with nearly perpendicular imidazole planes (Figure 3.13 (D+E)). Additionally, the resonances from non-specifically bound Fe(III) was simulated with $S = 5/2$. The simulation parameters are listed in Table 3.16.

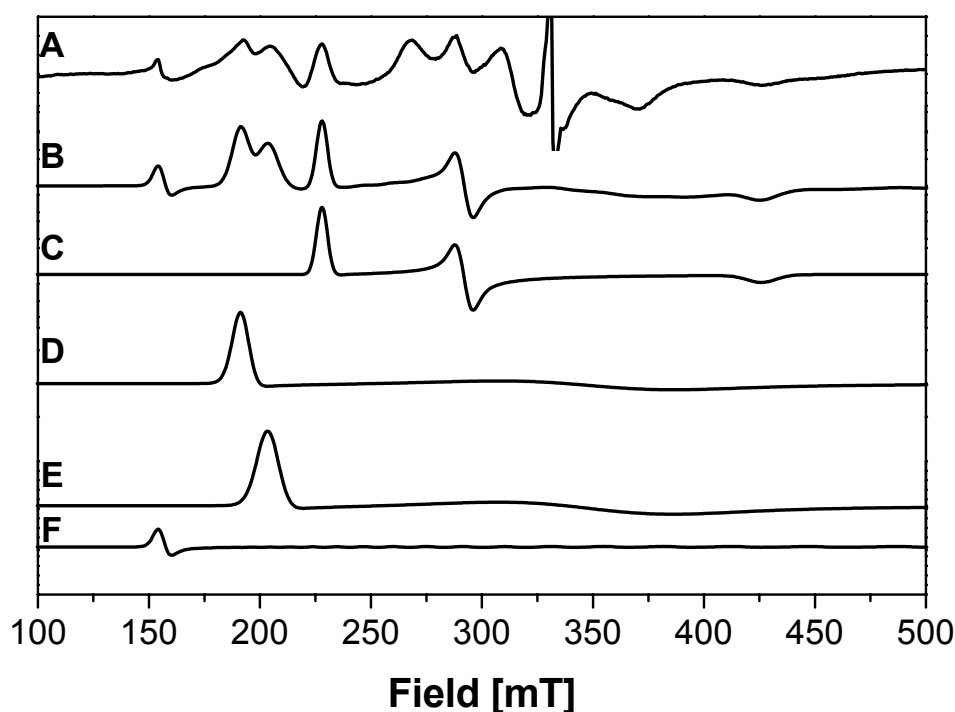


Figure 3.13: Simulation of the X-Band EPR spectrum of ccNirQ276E. **A:** experimental spectrum. **B:** sum of simulations. **C:** simulation of Fe(III) I.s. with parallel imidazole planes (Heme 2). **D:** simulation of Fe(III) I.s. with perpendicular imidazole planes (Heme 4). **E:** simulation of Fe(III) I.s. with perpendicular imidazole planes (Heme 5). **F:** simulation of non-specifically bound iron. Enzyme, 0.17 mM in 50 mM HEPES/NaOH buffer, pH 7.5; microwave frequency, 9.38 GHz; microwave power, 2 mW; temperature, 10 K. Simulation parameters: see Table 3.16.

The signal at $g \approx 2$ was simulated as a sum of two species with $S = 1/2$ (Figure 3.14). The axial signal at $g > 2$ comes from a FeS-cluster of nitrate reductase, the isotropic signal at $g = 2.008$ most likely from a radical.

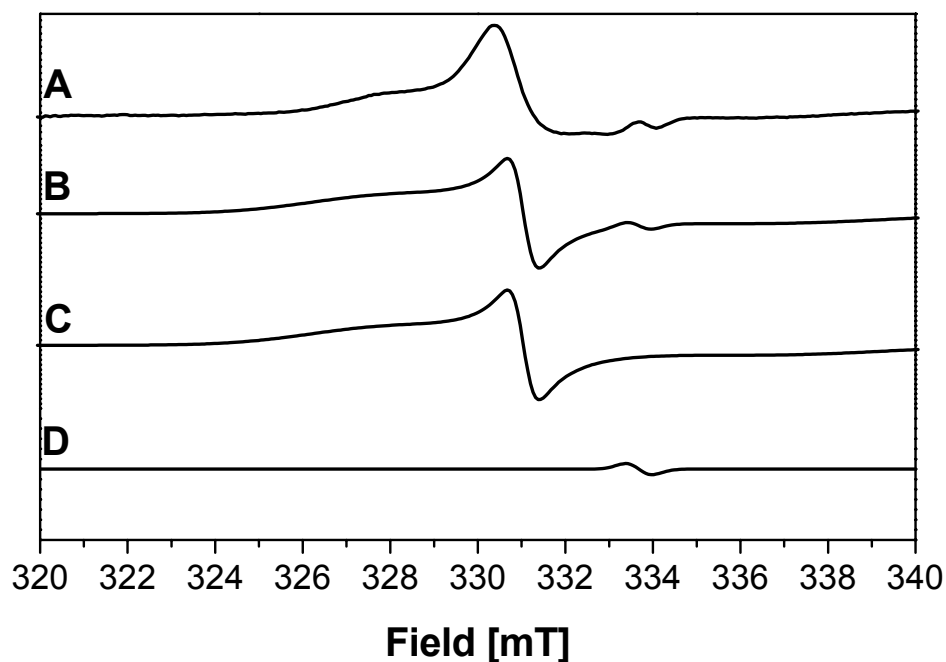


Figure 3.14: Simulation of signals around $g = 2$ of ccNirQ276E. **A:** experimental spectrum. **B:** sum of simulations. **C:** simulation of FeS-cluster. **D:** simulation of a radical. Enzyme, 0.17 mM in 50 mM HEPES/NaOH buffer, pH 7.5; microwave frequency, 9.38 GHz; microwave power, 2 mW; temperature, 10 K. Simulation parameters: see Table 3.16.

Species	Spin	Heme*	Parameter		
Fe(III) l.s. (parallel imidazole planes)	1/2	2 or/and 3	$g_x=2.93$ $W_x=120$	$g_y=2.29$ $W_y=120$	$g_z=1.57$ $W_z=170$
Fe(III) l.s. (perpendicular imidazole planes)	1/2	4 or 5	$g_x=3.47$ $W_x=200$	$g_y=1.9$ $W_y=1000$	$g_z=0.5$ $W_z=500$
Fe(III) l.s. (perpendicular imidazole planes)	1/2	4 or 5	$g_x=3.26$ $W_x=250$	$g_y=1.9$ $W_y=1000$	$g_z=0.5$ $W_z=500$
Fe(III) h.s. (unspezific bound iron)	5/2		$g=2.0$ $W_x=150$	$E/D=0.33333$ $W_y=250$	$D=4$ $W_z=400$
FeS-cluster	1/2		$g_x=2.045$ $W_x=60$	$g_y=2.024$ $W_y=7$	
Radical	1/2		$g_x=2.008$ $W_x=10$	$g_y=2.008$ $W_y=10$	$g_z=2.008$ $W_z=10$

Table 3.16: Simulation parameters of X-Band EPR spectrum of ccNirQ276E. Microwave frequency: 9.3795 GHz. * see Einsle *et al.* (2000).

3.1.7 Magnetic Susceptibility

In the first SQUID experiment the lyophilized NrfA_S enzyme was compared to the lyophilized enzyme complex NrfHA. The shape of the curves in the μ_{eff} vs. temperature diagram points towards an antiferromagnetic coupling between two or more paramagnetic centers (Figure 3.15 (A)). The $X_{\text{mol}} \cdot T$ vs. temperature diagram reveals no Curie dependence indicating an antiferromagnetic coupling, too (Figure 3.15 (B)). The μ_{eff} values at 200 K (highest temperature applied during the measurement) are 9.02 μ_{B} for NrfA_S, and 10.8 μ_{B} for NrfHA, respectively. If we compare these values with the calculated values for NrfA_S with a total spin of 9/2 (in the oxidized form), which are for a coupling system 9.95 μ_{B} and for a non-coupling system 6.86 μ_{B} , respectively, the measured values are in support of a coupled system, where all five heme centers undergo electronic exchange interaction. The comparison of the experimental and the calculated values of NrfHA assuming a total spin of 13/2 (in the oxidized form), with 13.96 μ_{B} (coupling system), or with 7.68 μ_{B} (non-coupling system), respectively, gives a hint that not all heme centers are in an interaction but there exist an electronic exchange. Note that the calculated data represent the situation at room temperature and the measurements were carried out up to 200 K. There could be an increase in μ_{eff} until room temperature is reached. An evidence for that is the unsaturation of the magnetic moment at 200 K.

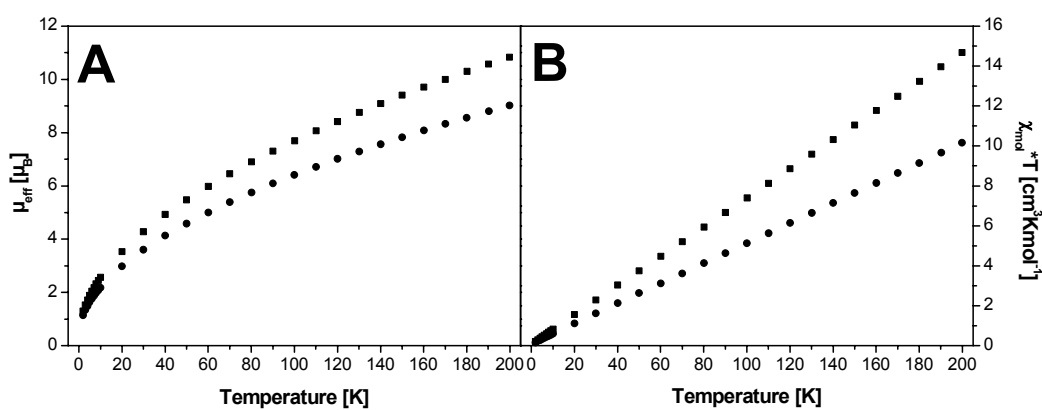


Figure 3.15: Temperature dependence of the magnetic moment of soluble and membranous ccNirWT. **A:** μ_{eff} vs. temperature; **B:** $X_{\text{mol}} \cdot T$ vs. temperature. Lyophilized samples were: ccNirWT (NrfA_S) (●); ccNirWT (NrfHA) (■).

The second experiment was performed to compare the magnetization of lyophilized NrfA_S and NrfA_S frozen in buffer. The shape of the curves and the values at 200 K in the μ_{eff} vs. temperature diagram (Figure 3.16 (A)) reveal practically no difference between the two

samples. The difference of μ_{eff} at 200 K is $0.5 \mu_{\text{B}}$ and of $X \cdot T$ at 200 K is $1.1 \text{ cm}^3 \cdot \text{K} \cdot \text{mol}^{-1}$, respectively (Figure 3.16 (A and B)). This is within the error range of the diamagnetic correction.

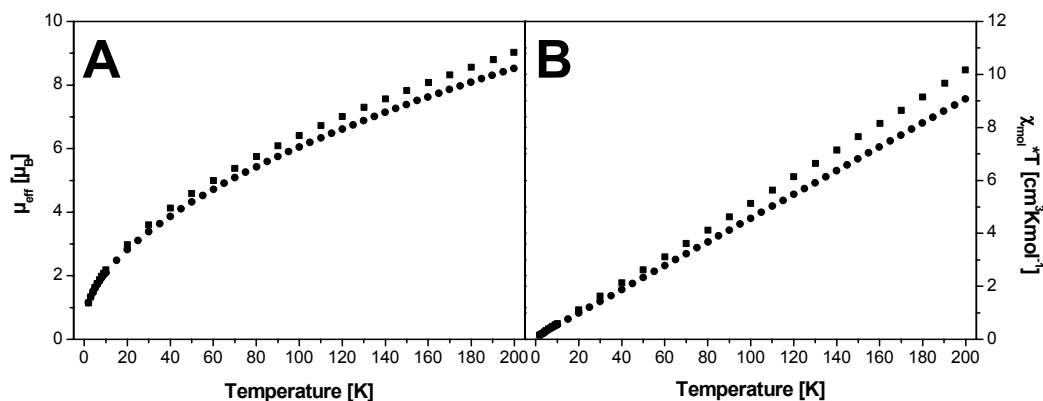


Figure 3.16: Temperature dependence of the magnetic moment of dissolved and lyophilized ccNirWT. **A:** μ_{eff} vs. temperature; **B:** $\chi_{\text{mol}} \cdot T$ vs. temperature. Samples were: dissolved NrfA_S (●); lyophilized NrfA_S (■).

3.1.8 Probing the Active Site of ccNir by X-ray Crystallography – 3D Structures of ccNir Variants

To obtain suitable crystals of *W. succinogenes* nitrite reductase it was necessary to bring the concentration of the protein to higher than 20 mg/ml. Presumably such high concentrations are required for the formation of the dimer that has been detected in all crystal forms known so far. This effect was also observed for all variants of nitrite reductase, where no crystals grew at lower concentrations. Throughout, the crystallization experiments were carried out with protein prepared from the membrane fraction. Furthermore, crystal growth depended on the presence of Y(III) ions.

All variants crystallized in space group $I 4_1 22$ (Table 3.19) which is identical to that of ccNirWT. The overall structure showed no significant differences to ccNirWT and also the 5 hemes in each monomer are oriented in an identical manner.

3.1.8.1 ccNirK134H

The major difference results from the replacement of the lysine 134 residue (sp^3 -nitrogen) by histidine (sp^2 -nitrogen) as the fifth ligand of heme 1 (Figure 3.17). This ligand exchange leads to the regular *c*-type cytochrome binding motif Cys- X_1 - X_2 -Cys-His. The distance between iron and N_{His} is 2.43 Å and therefore relatively long by comparison to

≈ 2.0 Å for the Fe-N distances in the bis-histidinyll coordinated hemes 2-5 (Table 3.17). The C_{α} -positions of the Cys-Trp-Thr-Cys-His motif are identical to the Cys-Trp-Thr-Cys-Lys motif of ccNirWT. The side chain is not flexible enough to bring the histidine closer to the iron to gain a “normal” binding.

A second difference comes from the puckering of heme 1. In comparison to ccNirWT heme 1 in the ccNirK134H appears flattened. The difference of the location of the Fe atoms in both structures is ≈ 0.13 Å. It seems that the iron wants to come closer to the histidine, which is limited by the rather inflexibility of the porphyrine ring because of the covalent fixation by the cysteines 130 and 133 and the stacking with heme 3.

Furthermore, the bond angle $C_{\delta 2}-N_{\epsilon 2}-Fe$ with 150.57° is larger than the bond angle in regular iron-histidine binding motifs with $120-130^{\circ}$.

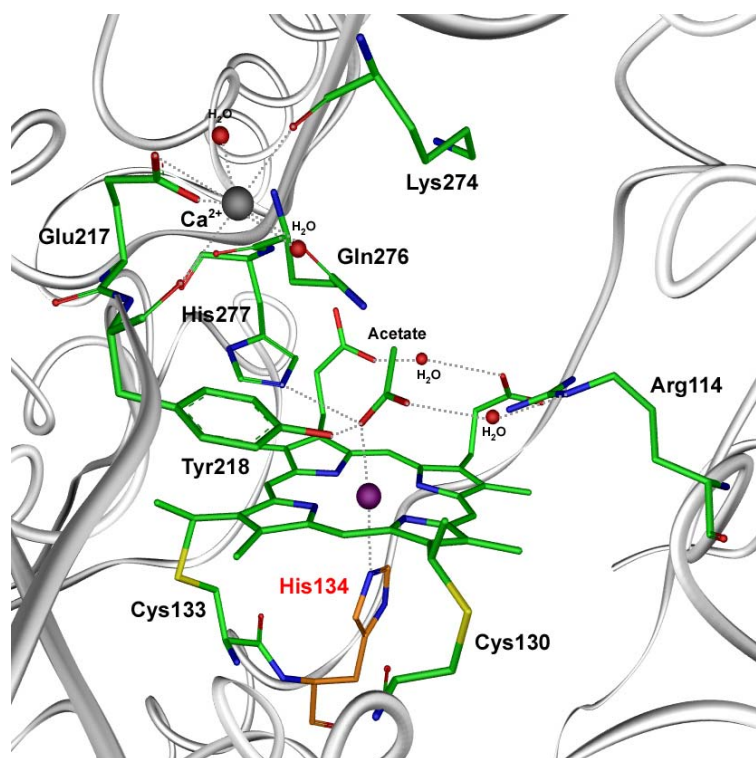


Figure 3.17: Active site (heme 1) of ccNirK134H. The exchanged amino acid is colored in orange.

Another difference was found with regard to the distal ligand. In the X-ray structure of ccNirWT the distal ligand was either a sulfate ion or a water molecule (Einsle *et al.* 2000). In ccNirK134H the distal side was occupied by an acetate ion that came from the crystallization buffer. The bond distance of 2.37 Å between the oxygen atom of the acetate and the iron is rather long compared to 2.03 Å between water and iron in ccNirWT (Table 3.17). The acetate is stabilized by hydrogen bonds to Tyr 218, His 277 and a water molecule that is furthermore hydrogen bonded to Arg 114.

The orientation of the amino acids of the calcium binding site and the calcium ion itself are identical to that of ccNirWT. Therefore, the change from lysine to histidine has no influence to the shape of the inlet channel and the roof of the distal site pocket.

	WT* (PDB 1FS7)	K134H	Q276E	Y218F	Y218F with N-MHA
Ca²⁺/Y³⁺ site					
Glu-217-O _{e1}	2.57	2.56	2.36	2.56	2.31
Glu-217-O _{e2}	2.46	2.40	2.30	2.51	3.05
Tyr-218-O	2.34	2.39	2.29	2.23	2.39
Lys-274-O	2.29	2.37	2.30	2.31	2.43
Gln-276-O _{e1}	2.22	2.30	-----	2.27	2.42
Glu-276-O _{e1}	-----	-----	2.23	-----	-----
Glu-276-O _{e2}	-----	-----	2.23	-----	-----
H ₂ O-1-O	2.42	2.46	2.24	2.50	2.63
H ₂ O-2-O	2.32	2.45	2.09	2.36	2.33
Fe³⁺ site					
Lysine	2.12	-----	2.28	2.15	2.21
Histidine	-----	2.43	-----	-----	-----
H ₂ O	2.03	-----	2.15	2.06	-----
CH ₃ COO ⁻	-----	2.37	-----	-----	-----
N-MHA	-----	-----	-----	-----	2.12
Fe³⁺ to N_{His}/N_{Lys}					
Heme 1 134	2.12	2.43	2.28	2.15	2.21
Heme 2 172	1.96	2.07	2.01	1.97	2.03
313	2.04	1.95	2.05	2.05	2.04
Heme 3 102	2.04	2.09	2.12	2.13	2.20
215	2.04	2.12	2.08	2.12	1.97
Heme 4 299	2.04	2.05	2.13	2.10	2.10
405	2.13	2.15	2.17	2.14	2.33
Heme 5 288	2.04	2.12	2.11	2.06	2.30
330	2.02	2.00	2.04	2.01	1.92
hydrogen bonds from the distal ligand					
OH _(Tyr218)	4.73	3.73	4.41	-----	-----
NH _(His277)	2.88	2.89	2.78	4.32	4.51
H ₂ O	4.36	2.60	3.86	5.18	

Table 3.17: Bond distances [Å] of ccNir and variants. * Data from Einsle *et al.* (2000).

3.1.8.2 ccNirQ276E

The major difference in this variant is the replacement of glutamine 276 by glutamic acid (Figure 3.18). Interestingly, the active site heme 1 and the surrounding residues with exception of the mutated residue are arranged identically in ccNirQ276E and ccNirWT. Whereas the amide group of Gln 276 only coordinates the Ca(II) ion by its carbonyl oxygen atom, the carboxyl-group of Glu 276 in the variant acts as a bidentate ligand. This again opens the binding pocket and the Ca(II) ion can be substituted by an Y(III) ion which comes from the crystallization buffer as the Y(III) ions bound to the protein surface (Einsle *et al.*, 2000). Therefore, the Glu 276 residue must flip to the Y(III) ion by an angle of $\approx 35^\circ$ compared to the position of the Gln 276 residue. All other coordinating ligands remain bound to a total coordination number of eight at the Y(III) ion.

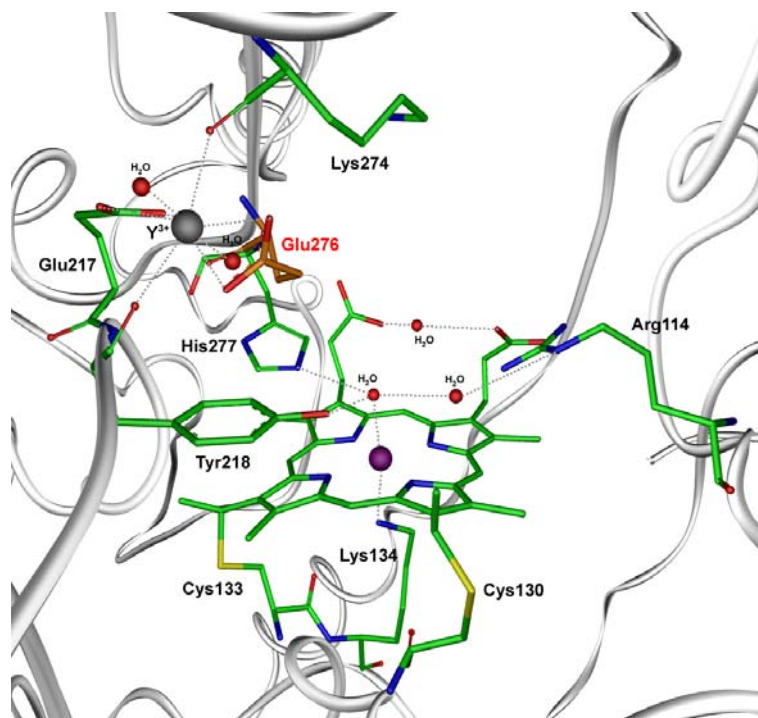


Figure 3.18: Active site (heme 1) of ccNirQ276E. The exchanged amino acid is colored in orange.

Typically, the coordination number of Y(III) ions is six but also coordination numbers of eight and nine have been identified (Cotton *et al.*, 1999). Note that in aqueous solutions only Y(III) ions are stable and are coordinated by eight water molecules with a slightly asymmetric distribution of the Y-O bond distances around 2.368(5) Å (Lindqvist-Reis *et al.*, 2000). The bond distances between the Y(III) ion and the oxygen atoms of the different residues including two waters are in a range of 2.23 to 2.36 Å (Table 3.17).

A second difference can be observed by calculating the electrostatic surface potential of the active site cavity (Figure 3.19). The distribution of the positive and negative potentials as well as the shape of the whole cavity have changed.

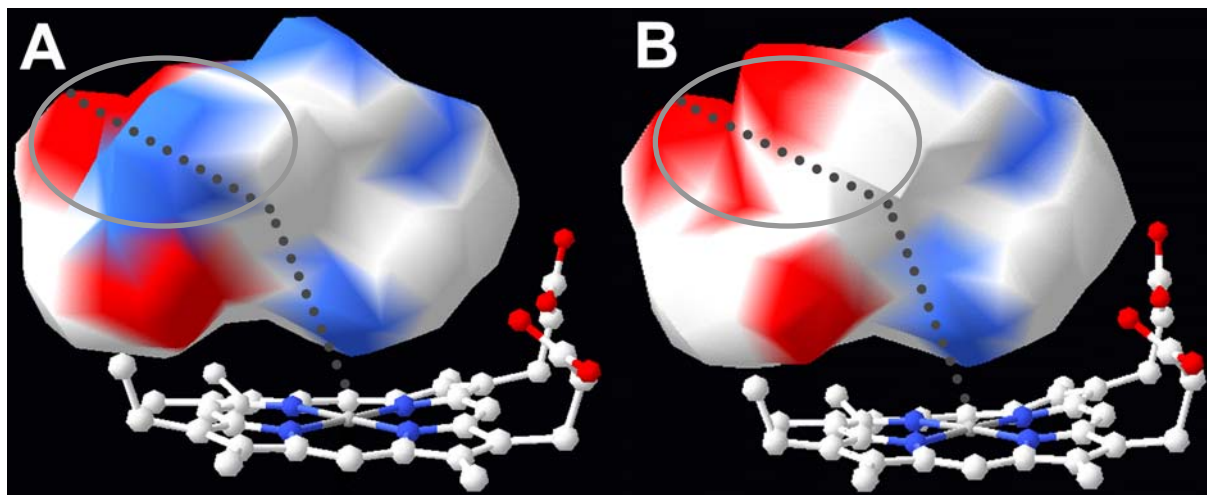


Figure 3.19: Electrostatic surface potential of the active site cavity of ccNir. Positive potential (blue), negative potential (red). **A:** ccNirWT. **B:** ccNirQ276E. The dotted line shows the entry of the negatively charged educt.

This results come from the fact that the residue Glu 276 has one negative charge distributed over two oxygens compared to the partial charges in the amide group of the residue Gln 276 of ccNirWT. Furthermore, the residue of the variant must flip as described above and therefore induces a change of the shape of the distal site pocket. The transition from the inlet channel to the active site cavity is influenced by this mutation to a more negatively charged entry and therefore might influence the protein activity and/or substrate specificity (Stach *et al.*, 2000).

3.1.8.3 ccNirY218F

The major change in this variant is the replacement of the tyrosine 218 residue by phenylalanine (Figure 3.20). Interestingly, the active site heme 1, the surrounding residues and also the C_{α} of the residue 218 are identically in the variant and in ccNirWT. Nevertheless, the benzene ring of Phe 218 comes 0.26 Å closer to His 277 compared to the distance between the benzene ring of Tyr 218 and His 277 in ccNirWT. Furthermore, the benzene ring in Phe 218 is twisted by an angle of 20.74° compared to the ring of Tyr 218.

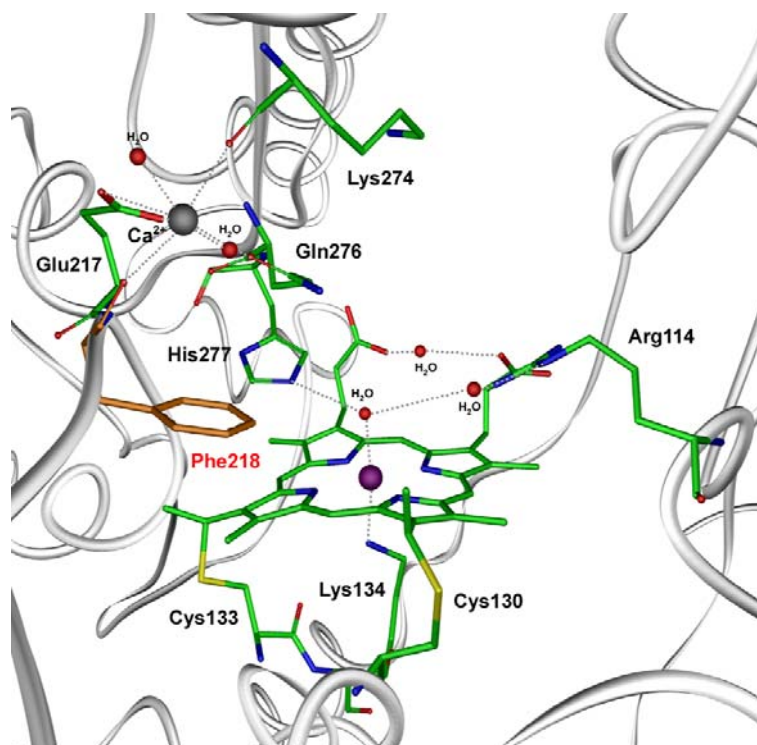


Figure 3.20: Active site (heme 1) of ccNirY218F. The exchanged amino acid is colored in orange.

A second difference is the arrangement of the hydrogen bonds in the active site cavity. Because of the loss of the hydroxyl-group by mutation of tyrosine to phenylalanine no hydrogen bond can be formed to the distal water ligand. Consequently, the incoming substrate nitrite cannot be oriented by this hydrogen bond which might result in a decrease in activity (Chapter 3.1.2.4).

3.1.8.4 Crystal Structure of ccNirY218F N-Methylhydroxylamine Complex

The N-methylhydroxylamine complex of ccNirY218F was prepared by soaking the crystals of the protein with 1 mM N-methylhydroxylamine for 20 minutes. The crystal had the same space group like the uncomplexed ccNirY218F, $I 4_1 22$ (Table 3.19).

The arrangement of the active site heme 1 and the surrounding residues does not change significantly upon binding of N-methylhydroxylamine (Figure 3.21). N-methylhydroxylamine, which is also a substrate of ccNir, binds to the iron atom via its oxygen atom with a distance of 2.12 Å (Table 3.17). It is further stabilized by a hydrogen bond to His 277 as observed for the water molecule in the uncomplexed ccNirY218F.

To get further insights into the binding modes of hydroxylamine, N-methylhydroxylamine, and O-methylhydroxylamine to the active site iron, DFT calculations were carried out by F. Neese (MPI of Bioinorganic Chemistry, Mülheim/Ruhr) under different conditions. As

well as the oxidation state of the iron and the spin state of the iron were varied, also the two binding possibilities (N-binding or O-binding) were checked.

With hydroxylamine and O-methylhydroxylamine as ligands, the N-binding to low-spin iron(II) or iron(III) are preferred (Table 3.18). This was shown crystallographically by Einsle *et al.* (2002b) for hydroxylamine as substrate. So far, the crystal structure of ccNirY218F with O-methylhydroxylamine has not been solved yet.

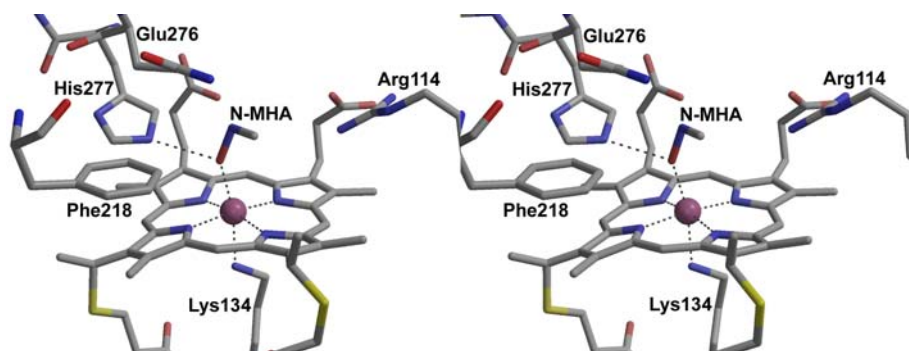


Figure 3.21: Stereo view of the active site (heme 1) of ccNirY218F with bound N-methylhydroxylamine.

Substrate	Redox State	Spin State	N-Bound	O-Bound
Hydroxylamine	Fe(II)	l.s.	0.0	7.2
		h.s.	6.9	8.3
	Fe(III)	l.s.	0.0	8.7
		h.s.	6.4	11.0
N-Methylhydroxylamine	Fe(II)	l.s.	1.2	0.0
		h.s.	5.3	1.6
	Fe(III)	l.s.	0.0	3.9
		h.s.	5.4	0.7
O-Methylhydroxylamine	Fe(II)	l.s.	0.0	5.3
		h.s.	6.9	6.5
	Fe(III)	l.s.	0.0	6.8
		h.s.	20.2	9.1

Table 3.18: Relative energies of the binding of hydroxylamine and derivatives to the active site iron in kcal/mol.

In the case of N-methylhydroxylamine a different binding mode was found. Because of the methyl group at the nitrogen atom, the O-binding to low-spin Fe(II) is preferred but the N-binding to low-spin Fe(III). The differences in energy are very small and are in the error range of this theoretical method (Table 3.18). In view of these results the theoretical

calculations cannot predict whether N-methylhydroxylamine binds via its oxygen or its nitrogen atom to the iron. This was investigated by solving the crystal structure (Figure 3.21).

Whether the iron is in the Fe(II) or Fe(III) state is still unknown and had to be investigated by using single crystal UV-Vis spectroscopy (Stach, 2001).

3.1.9 Crystallization of ccNirQ276E (NrfHA)

Cytochrome *c* nitrite reductase (NrfA) forms a membrane associated complex with a second multiheme cytochrome (NrfH) that functions as the direct electron donor (Simon *et al.*, 2001). Such a complex will allow fast electron transfer which is not limited by diffusion and docking of redox partners.

Crystallization of the NrfHA nitrite reductase complex was achieved with ccNirQ276E enzyme complex. With this variant production of crystals was quite reproducible and the crystals were larger (Figure 3.22) compared to crystals obtained from ccNirWT NrfHA complex (Einsle *et al.*, 2002a).

On SDS-PAGE these crystals (Figure 3.22), when dissolved in sample buffer, exhibited two bands at 62 kDa and 22 kDa corresponding to NrfA and NrfH, respectively (Figure 3.22).

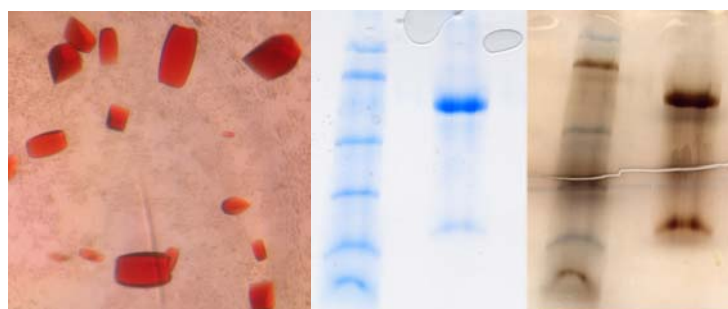


Figure 3.22: Crystals of ccNirQ276E (NrfHA); SDS-PAGE gel of crystals from ccNirQ276E (NrfHA) dissolved in sample buffer: Coomassie stain (left), silver stain (right).

First crystals from *W. succinogenes* NrfHA wild-type were obtained with Triton X-100 as detergent (Einsle *et al.*, 2002a). Further experiments were carried out to improve the crystallization in combination with Triton X-114. The best result was obtained with 2 μ l of a protein solution (10-20 mg/ml) in 10 mM HEPES/NaOH buffer, pH 7.5 and 2 μ l of a reservoir solution containing 4-4.5 % PEG 300, 1.9-2.0 M $(\text{NH}_4)_2\text{SO}_4$, 0.1 M HEPES/NaOH buffer, pH 7.0 plus 0.5 % Triton X-114. The crystals grew within seven to eight days but did not diffract. Lower the concentration of PEG 300 to 2.5-3.0 % and therefore lengthen the duration of growth to two to three month, the crystals became larger and diffracted to a

maximum resolution of 6.0 Å. They belonged to space group *I* 4₂2, with unit cell dimensions of *a* = 244.2 Å, *b* = 244.2 Å, and *c* = 248.9 Å. This work is still in progress.

Parameter	K134H	Q276E	Y218F	Y218F N-Methylhydroxylamine
Data collection				
Space group	<i>I</i> 4 ₂ 2	<i>I</i> 4 ₂ 2	<i>I</i> 4 ₂ 2	<i>I</i> 4 ₂ 2
Unit cell dimensions	<i>a</i> = 119.97 Å	<i>a</i> = 120.41 Å	<i>a</i> = 120.07 Å	<i>a</i> = 120.20 Å
	<i>b</i> = 119.97 Å	<i>b</i> = 120.41 Å	<i>b</i> = 120.07 Å	<i>b</i> = 120.20 Å
	<i>c</i> = 186.24 Å	<i>c</i> = 186.95 Å	<i>c</i> = 186.80 Å	<i>c</i> = 187.43 Å
	α, β, γ = 90°	α, β, γ = 90°	α, β, γ = 90°	α, β, γ = 90°
Resolution range [Å]	24.81 – 2.05	24.91 – 2.03	24.86 – 2.10	46.63 – 2.40
No. of reflections All	42984	44539	40094	27223
No. of reflections Observed	38514	42669	39974	26216
Completeness (%)	89.6	95.8	99.7	96.3
R _{merge} (%)	(2.16-2.05 Å)	(2.14-2.03 Å)	(2.21-2.10 Å)	(2.53-2.40 Å)
Total	9.8	13.2	13.3	17.0
Last shell	54.0	54.3	58.7	50.7
I/σ(I)	(2.16-2.05 Å)	(2.14-2.03 Å)	(2.21-2.10 Å)	(2.53-2.40 Å)
Total	6.8	4.9	5.5	3.7
Last shell	1.4	1.4	1.3	1.5
Data used in refinement				
Resolution range (Å)	24.82 – 2.20	24.91 – 2.03	20.33 – 2.10	24.91 – 2.40
Data cutoff σ(F)	0.0	0.0	0.0	0.0
Completeness (working + test set) (%)	99.6	95.6	99.6	96.2
Number of reflections (observed)	34673	42299	39925	26165
R-value (working set)	0.178	0.206	0.180	0.206
Free R-value (test set)	0.231 (9.9%)	0.253 (10.1%)	0.228 (10.0%)	0.279 (9.8%)
Fit in highest resolution bin				
Resolution range (Å)	2.24 – 2.20	2.16 – 2.03	2.23 – 2.10	2.55 – 2.40
Bin completeness (working + test set) (%)	98.9	73.9	98.5	77.5
Bin R-value	0.263	0.292	0.270	0.333
Bin Free R-value	0.303	0.316	0.306	0.370
r.m.s.d. Bond length [Å]	0.006	0.006	0.006	0.008
r.m.s.d. Bond angles [°]	1.1	1.2	1.2	1.3
R _{merge} = Σ(I – <I>)/ΣI.		R-value = Σ(F _{obs} – F _{calc})/Σ F _{obs} .		

Table 3.19: Data collection and refinement statistics for all ccNir variants and the N-Methylhydroxylamine complex.

3.2 Cytochrome cd_1 Nitrite Reductase

3.2.1 Crystallization of cd_1 Nir from *Pseudomonas stutzeri* and *Thiobacillus denitrificans*

Cytochrome cd_1 nitrite reductase from *P. stutzeri* was crystallized with the sitting drop vapor diffusion method. After three to four days crystals were obtained (Figure 3.23). The crystals diffracted to a resolution of 3.5 Å and belonged to space group $P 4_122$ with unit cell dimensions of $a = 127.3$ Å, $b = 127.3$ Å, and $c = 137.5$ Å.

The color of the crystals from cd_1 nitrite reductase changed from green (heme d_1 contribution) to red (heme c) depending on the orientation of the crystals. This feature was verified by polarized single-crystal optical spectroscopy of *P. aeruginosa* cd_1 nitrite reductase (Makinen *et al.*, 1983) that showed that the two hemes of the monomer are oriented roughly perpendicular to each other in the oxidized and reduced state of the enzyme. However, the crystal structure of *P. pantotrophus* enzyme revealed that the angle between the two hemes was about 60° within the monomer (Fülöp *et al.*, 1995). The angle formed by the tetrapyrrole planes of the c and d_1 hemes in *P. aeruginosa* cytochrome cd_1 is roughly 70° (Nurizzo *et al.*, 1997).

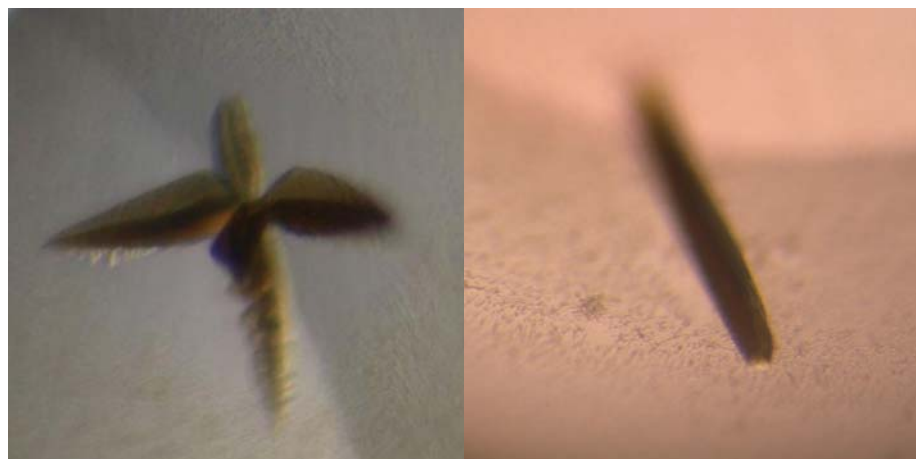


Figure 3.23: Crystal of cytochrome cd_1 nitrite reductase from *P. stutzeri* (left) and *T. denitrificans* (right).

Cytochrome cd_1 nitrite reductase from *T. denitrificans* was crystallized with the sitting drop vapor diffusion method. After four to five days crystals were obtained (Figure 3.23). The crystals diffracted to a resolution of 3.0 Å. Crystals belonged to space group $C 222$ with unit cell dimensions of $a = 155.1$ Å, $b = 204.7$ Å, and $c = 167.8$ Å.

4 Discussion

4.1 Crystal Structure of Cytochrome c Nitrite Reductase

4.1.1 Assembly of the Wild-Type Protein

Nitrite reductase (NrfA) is a homodimer of $\approx 100 \text{ \AA} \times 80 \text{ \AA} \times 50 \text{ \AA}$ (Figure 4.1), with ten hemes in remarkably close packing (Einsle *et al.*, 2000). The protein folds into one compact domain, with α -helices as the predominant secondary structural motif, ranging from short helical turns to four long helices at the carboxy-terminal end of the peptide chain. There are eight 3_{10} helices three or four residues long, seven of which occur within the first 200 residues. β -sheet structures are found only in two short, antiparallel strands, where one is part of a funnel-like cavity leading to the active site. Dimer formation is mediated by helices $\alpha 22$ and $\alpha 25$, with helix $\alpha 25$ as the key element, as it interacts with its counterpart in the other monomer over its full length of 28 residues, corresponding to 42 \AA . The contact surface has an area of $\approx 1.700 \text{ \AA}^2$, or 8.5 % of the total accessible surface area of a monomer. Helix $\alpha 27$ runs along the protein surface with a kink at Lys 470. Whereas this helix does not participate in the formation of any functional features or in covering the heme groups, its conservation indicates a possible stabilizing effect on the protein as a whole.

Y(III) ions play a crucial role in mediating crystal contacts. They took part in every single intermolecular contact in the crystal packing, including the contact between two monomers forming the dimer, where Y(III) ion was coordinated by a propionate side chain of heme 5 from each monomer. Another Y(III) ion bound close to the exit of the product channel, coordinated by propionate side chains from both hemes 3 and 4.

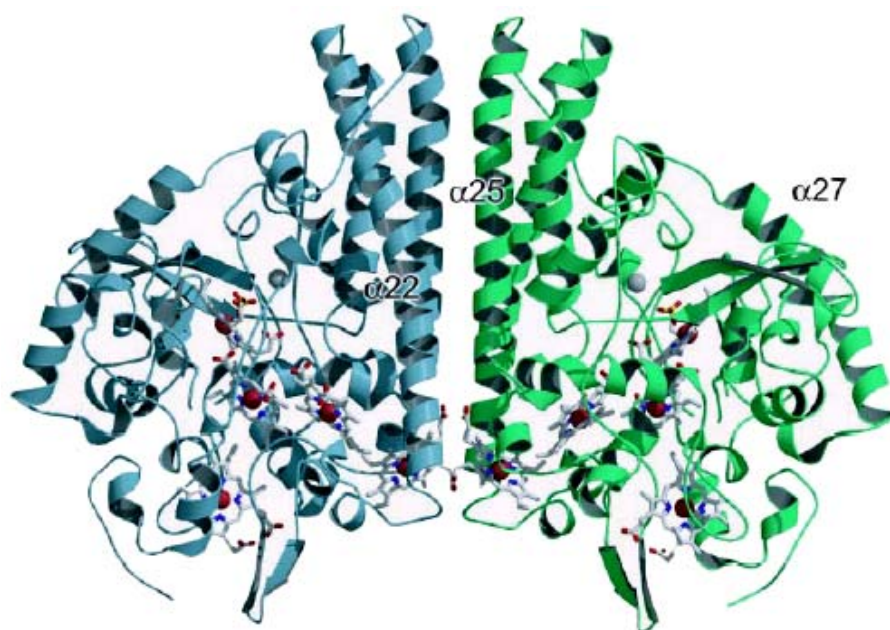


Figure 4.1: The ccNir dimer. A front view with the dimer axis oriented vertically, the five hemes in each monomer (white), the Ca(II) ions (grey). The dimer interface is dominated by three long α -helices per monomer. All hemes in the dimer are covalently attached to the protein. Figure was taken from Einsle *et al.* (2000).

The five hemes in the monomer of ccNir are in close contact, with Fe-Fe distances of between 9.3 and 12.5 Å (Figure 4.2). They are arranged as a group of three, almost coplanar, hemes (1, 3, 4), with heme 1 forming the active site. Hemes 2 and 5 are further apart and are not coplanar with hemes 1, 3, and 4. All hemes except heme 1 are bis-histidinyll coordinated and are linked to the peptide backbone by thioether bonds to the cysteine residues of a classical heme-binding motif for periplasmic proteins, Cys-X₁-X₂-Cys-His. With edge-to-edge distances below 4 Å, hemes 1, 3, and 4 are close enough to allow direct π -electron interaction of the porphyrin rings. The propionate side chains of heme 1 form part of the active site cavity, while those of heme 4 are exposed to the solvent and those of heme 3 are hydrogen-bonded inside the protein. All porphyrins show a slight distortion from ideal planarity, most strongly in heme 2 and least in the active site heme 1. Heme 2 could function as the entry point for electrons. The short Fe-Fe distance of 11.7 Å between hemes 5 within the dimer suggests an electronic interaction of these centers which might be functionally relevant. Hemes 5 interact across the dimer interface with a distance closer than hemes 2 and 3 within each monomer. Furthermore, both hemes interact directly through hydrogen bonds between their propionate side chains.

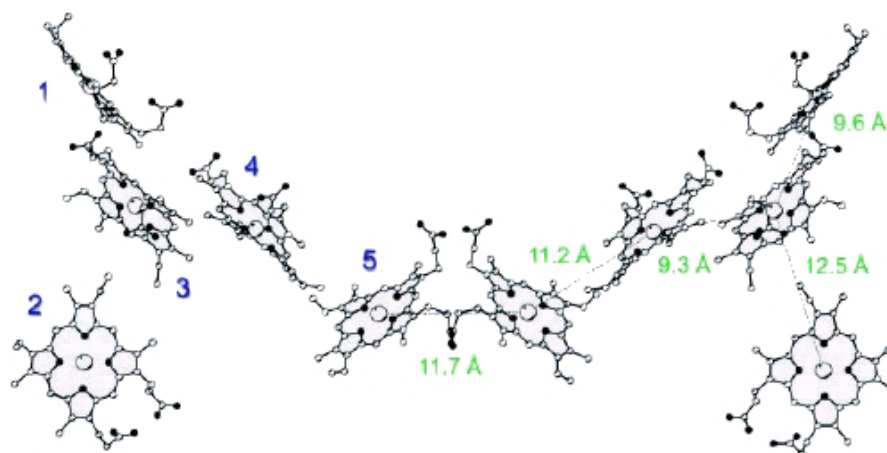


Figure 4.2: Heme arrangement in ccNir. The overall orientation corresponds to Figure 4.1, with the active site located at heme 1. Hemes in the left monomer are numbered according to their attachment to the protein chain. In the right monomer, the Fe-Fe distances between the hemes are given. Figure was taken from Einsle *et al.* (2000).

The site of nitrite reduction is clearly heme 1, with the N_ζ atom of Lys 134, replacing a histidine in the classical binding motif, and an oxygen atom of a water ion (Figure 4.3). Water binds to the iron at a bond length of 2.03 Å. It is further coordinated to both His 277 and Tyr 218. Arg 114 also forms a hydrogen bond to one of the propionates and is bonded to the distal water by another water molecule.

An additional electron-density maximum detected close to the active site was assigned to Ca(II). The roof of the active site cavity is formed by Phe 92 and Gln 276, which coordinates the Ca(II) by its carboxamide oxygen such that the amino group faces the active site. The cavity as a whole shows a strong positive surface potential.

The active site accommodates anions and uncharged molecules. The preference for anions is reflected by a positive electrostatic potential around and inside the active site cavity. This is induced by the residues forming the cavity: Tyr 218, His 277, Arg 114, Gln 276, and Lys 274. These residues will serve as stores for protons required for the reduction of nitrite to ammonia and can be resupplied by water molecules. Considering the good accessibility of the active site for water molecules and the presumably lowered pH on the periplasmic side of the cytoplasmic membrane, the product of nitrite reduction will be the positively charged ammonium ion rather than uncharged ammonia. The cationic product might make use of a second channel leading to the protein surface opposite to the entry channel.

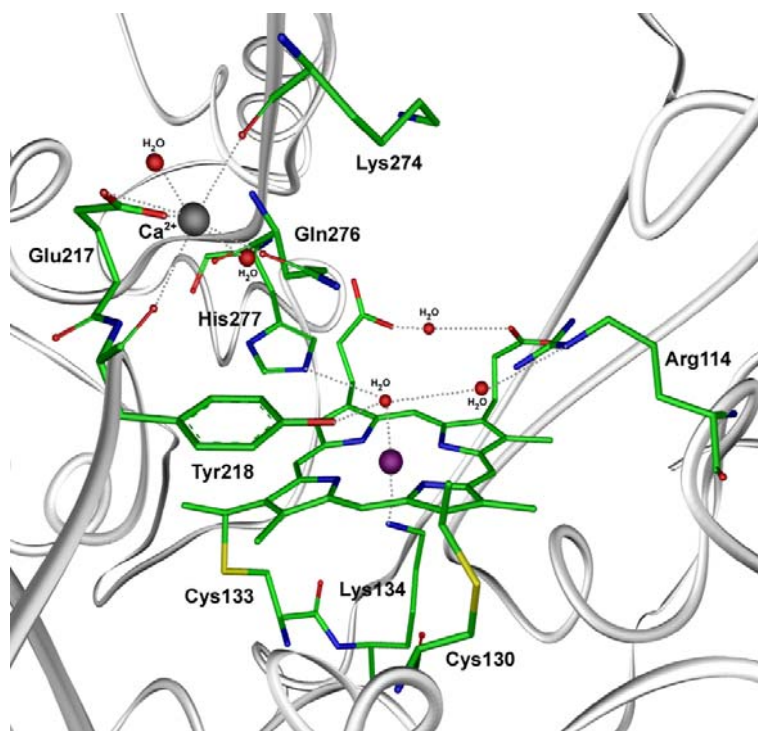


Figure 4.3: Active site (heme 1) of ccNirWT. Structure from Einsle *et al.*, 2000 (PDB code: 1FS7).

This second channel is lined by Met 76, Lys 80, Leu 83, Lys 348, Gln 352, Ile 397, and His 400, and filled with coordinated water molecules. It branches before reaching the protein surface and ends with both arms in areas possessing a significantly negative electrostatic surface potential. The existence of separate pathways for substrate and product with matched electrostatic potential could also contribute to the enzyme's high specific activity compared with the siroheme-containing nitrite reductases that catalyze the same reaction. Another remarkable feature close to the active site is a set of tyrosine residues, which are conserved in all cytochrome *c* nitrite reductase sequences known to date. The tyrosine residues close to the active site might play a role in dealing with possible radical intermediates of the stepwise reduction of nitrite to ammonia by forming tyrosyl radicals during the catalytic cycle.

4.1.2 Comparison of the Crystal Structures of ccNir Variants

The crystal structures of ccNir (NrfA) from the sulfur reducing ϵ -proteobacterium *S. deleyianum* (Einsle *et al.*, 1999), the closely related enteric ϵ -proteobacterium *W. succinogenes* (Einsle *et al.*, 2000), the γ -proteobacterium *E. coli* (Bamford *et al.*, 2002), and the sulfate reducing δ -proteobacterium *D. desulfuricans* ATCC 27774 (Almeida *et al.*, 2003) have been determined recently. The former bacteria share 78 % identical residues in the amino acid sequence (Einsle *et al.*, 2000). The amino acid sequences of the NrfA proteins

from *W. succinogenes* and *E. coli* are 43 % identical. As expected the structures of nitrite reductase from all organisms are similar. The structurally and functionally important features are conserved between all species. In a superposition of the structures from *W. succinogenes* and *S. deleyianum*, the root mean square displacement of all C $_{\alpha}$ atoms is 1.19 Å with each of the three monomers in the asymmetric unit of the *S. deleyianum* crystals (Einsle, 1999). Note that the three “identical” monomers in the asymmetric unit of the *S. deleyianum* crystals themselves have a root mean square displacement of the C $_{\alpha}$ atoms of 0.37 Å among each other (Einsle, 1999).

The special feature of the active site heme in ccNir is that it only shows a fivefold coordination with an axial lysine ligand provided by a novel heme binding motif (Cys-X₁-X₂-Cys-Lys). The other four hemes have the usual motif (Cys-X₁-X₂-Cys-His) and show bis-histidinyll coordination. Both features were found throughout all ccNir’s structural investigated so far. It was suggested that the lysine in the heme binding motif is of crucial importance in promoting the binding of anions, and the environment of this heme contributes to the provision of a reduction potential low enough to reduce substrate nitrite to ammonia (Jafferri *et al.*, 2000). It was demonstrated for *E. coli* cytochrome *c*₅₅₂ that the lysine residue is required for normal rates of nitrite reduction (Eaves *et al.*, 1998). If lysine was altered to histidine, the enzyme was inactive.

The unusual lysine residue has an important significance for nitrite reduction because of the rare examples of ccNir’s with a histidine residue as the proximal ligand. The ccNir from *Campylobacter jejuni* (Parkhill *et al.*, 2000), a ϵ -proteobacterium, has the usual Cys-X₁-X₂-Cys-His motif at the active site. Pisa *et al.* (2002) constructed a mutant (K134H) from *W. succinogenes* which contained a *nrfA* gene encoding a CWTCH motif instead of CWTCK. The specific nitrite reductase activity from the cell homogenate, the membrane fraction as well as the soluble fraction of strain K134H did not exceed 40 % of that of ccNirWT. Similarly, the purified enzymes NrfA_S, NrfA_M, and NrfHA had only 30-40 % of the wild-type activity (Chapter 3.1.2.2, Figure 4.9). Surprisingly, ccNirK134H did not grow with nitrite as acceptor and its electron transport activity from formate to nitrite was about 5 % of ccNirWT activity. Therefore, one possible function of lysine 134 may be to raise the mid-point potential of the active site heme group to a value more positive than of any of the four bis-histidinyll ligated heme groups. The drastic inhibition of electron transfer may therefore be caused by a decreased redox potential of heme 1. By comparison of the structures of ccNirWT and ccNirK134H (Chapter 3.1.8.1, Figure 4.4) the only significant difference is the increased bond distance iron-histidine by 0.31 Å compared to the distance iron-lysine in ccNirWT.

Therefore, the weak coordination of histidine to the active site iron may cause a decreased redox potential. This has to be investigated by redox titration experiments.

Other biologically important heme proteins have axial ligands connected to the iron via tetrahedral nitrogen. Examples are the alkaline forms of cytochrome *c* where lysine 73 or 79 coordinates the iron (Ferrer *et al.*, 1993; Rossell *et al.*, 1998), cytochrome *f* where the polypeptide N-terminus binds the iron and not a lysine residue is involved in electron transfer in photosynthesis (Martinez *et al.*, 1994), and CooA, a transcription factor of the CAP family in which the iron is coordinated by the main chain nitrogen of a proline (Lanzilotta *et al.*, 2000). Furthermore, it was reported on a Met100Lys mutant of cytochrome *c*₅₅₀ from *Paracoccus versutus* (Ubbink *et al.*, 1994; Louro *et al.*, 2002). This protein contains a single, covalently bound heme and is involved in bacterial electron transport. By replacing the methionine by a lysine, the midpoint potential of the mutant has shifted -329 mV compared to wild-type. EPR spectroscopy revealed two species of the mutant with $g_z = 3.53$, $g_y = 1.69$, $g_x = 0.82$ (form I) and $g_z = 3.30$, $g_y = 2.00$, $g_x = 1.18$ (form II). However, crystal structures of the wild-type as well as of the mutant protein are not available, but the structure of the highly homologous cytochrome *c*₅₅₀ from *P. denitrificans* (84 % amino acid sequence identity) (Ubbink *et al.*, 1992).

Crystallization of nitrite reductase from *S. deleyianum* and *W. succinogenes* was carried out at different pH values (Einsle *et al.*, 1999; Einsle *et al.*, 2000). The *S. deleyianum* enzyme was crystallized at pH 7.5, whereas crystals of *W. succinogenes* enzyme were grown at pH 5.7. Slight differences in binding mode of substrate were observed arising presumably from different protonation state of the imidazole nitrogen of His 282 and His 277, respectively. The pK_a of histidine is around 6.5. The distal site in the structure of ccNir from *E. coli* (Bamford *et al.*, 2002) and ccNir from *D. desulfuricans* ATCC 27774 (Almeida *et al.*, 2003) is occupied by a water molecule and unoccupied, respectively. Crystals of ccNir from both organisms were obtained at pH 7.5. Therefore it can be assumed that nitrite and sulfate, an inhibitor of ccNir, would bind to the active site iron in the same arrangement like it is the case in ccNir from *S. deleyianum*.

The presence of a Ca^{2+} ion as an essential constituent in ccNir was first discovered in the X-ray structure of the *S. deleyianum* (Einsle *et al.*, 1999) enzyme and confirmed by ICP-MS (Chapter 3.1.3). As all calcium-coordinating residues are strictly conserved between *S. deleyianum* and *W. succinogenes nrfA* sequences, it was no surprise to find calcium at the same position in the enzyme from *W. succinogenes*. That the calcium binding site appears to be an essential structural feature in the overall architecture of ccNir and an essential feature

for catalysis was shown by Einsle *et al.* (2000) and Stach (2001). Another heme containing protein which is also dependent on the presence of calcium ions is horseradish peroxidase (Howes *et al.*, 2001). It contains two calcium binding sites, one at the distal site and the other at the proximal site of the heme, both sevenfold coordinated. The calcium-depleted ferrous form displays a low-spin bis-histidinyI heme state and a small proportion of high-spin heme. Furthermore, the $\nu(\text{Fe-Im})$ stretching mode downshifts 27 cm^{-1} upon calcium-depletion revealing a significant structural perturbation of the proximal cavity near the histidine ligand. The specific activity of the calcium-depleted enzyme is 50 % that of the native form. In ccNir during mutation from Gln 276 to Glu 276 the coordination number of the calcium binding site changes from seven to eight (Chapter 3.1.8.2, Figure 4.4). It was surprisingly that in the X-ray structure not only the residue 276 was changed but also the Ca(II) to Y(III) which was present in the crystallization buffer. Y(III) is more likely eightfold coordinated than Ca(II) and also the bond distances of this site decreased to values specific for an yttrium binding (Cotton *et al.*, 1999). Not only the structural feature was different from ccNirWT but also the spectroscopic (EPR) properties by adding Y(III) to a solution containing ccNir Q276E (Chapter 3.1.6.8). Therefore it can be assumed that Y(III) binds also in solution to the former calcium binding site. During mutation a change in activity was not observed (Figure 4.9).

A remarkable feature in the crystal structure of *W. succinogenes* ccNir is the presence of several yttrium ions. Addition of YCl_3 to the crystallization buffer improves crystal growth. In general, yttrium ions are situated at every single intermolecular contact in the crystal packing (Einsle *et al.*, 2000).

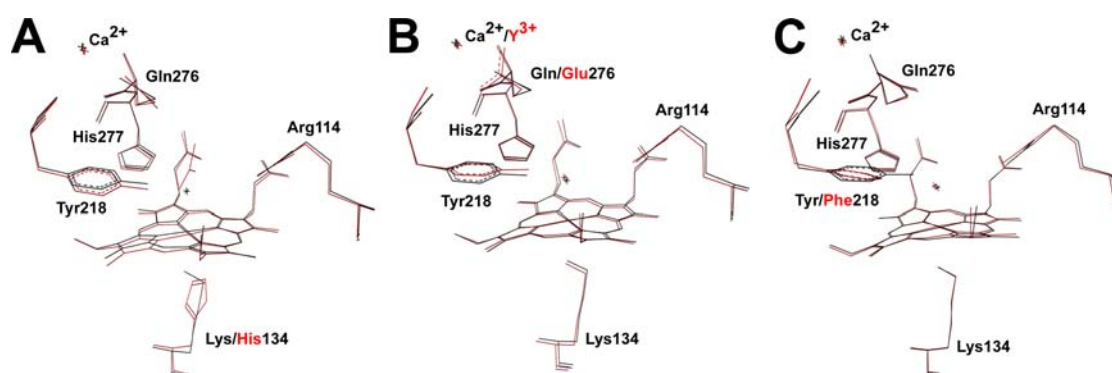


Figure 4.4: Superposition of the active sites from ccNirWT (black) with its variants (red). **A:** with ccNirK134H; **B:** with ccNirQ276E; **C:** with ccNirY218F.

The tyrosine residues close to the active site, especially tyrosine 218, might play a role in dealing with possible radical intermediates of the stepwise reduction of nitrite to ammonia by forming tyrosyl radicals during the catalytic cycle (Einsle *et al.*, 2000). This hypothesis is

supported by the observation that in all crystals of ccNir from *W. succinogenes* partial *ortho*-hydroxylation of Tyr 219 seems to occur. In ccNirY218F the hydroxyl-group of Tyr 218 was depleted by substitution of tyrosine by phenylalanine (Figure 4.4). Thus, the formation of a radical species at this position is suppressed and the specific activity decreases to about 3-5 % that of ccNirWT (Figure 4.9).

4.1.3 Substrate Binding Motifs

The three types of dissimilatory nitrite reductase are the cytochrome *c* nitrite reductase, the cytochrome *cd*₁ nitrite reductase and the copper nitrite reductase. The former enzyme catalyzes the six-electron reduction of nitrite to ammonia whereas the latter enzymes catalyze the one-electron reduction of nitrite to nitric oxide. Nitrite can bind to the active site metal (iron or copper) either via its nitrogen atom, which is the case in ccNir and *cd*₁Nir, or via one oxygen atom, which is the case in copper Nir (Figure 4.5).

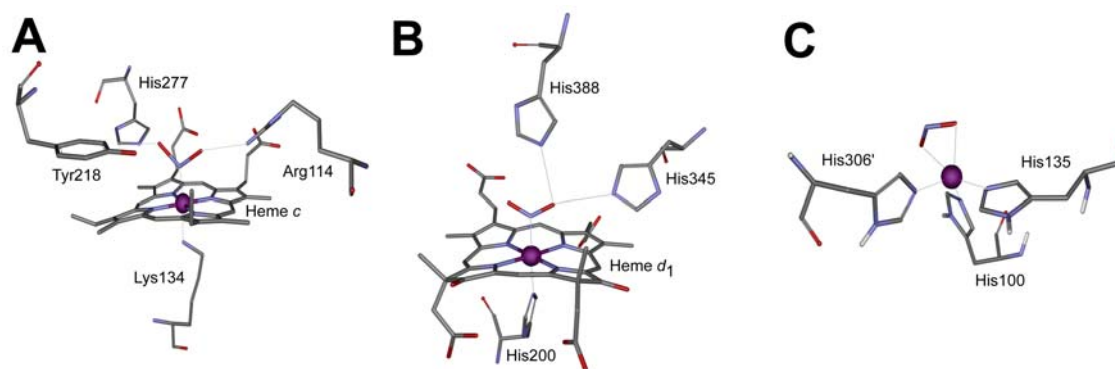


Figure 4.5: Binding of nitrite to dissimilatory nitrite reductases. **A:** cytochrome *c* Nir (Einsle *et al.*, 2002b); **B:** cytochrome *cd*₁ Nir (Williams *et al.*, 1997); **C:** copper Nir (Murphy *et al.*, 1997).

In ccNir from *W. succinogenes* nitrite is further stabilized by hydrogen bonds from one oxygen to His 277 and from the other one to Arg 114 (Figure 4.5 (A)). The protons for the first reaction step including the heterolytic cleavage of a N-O bond most likely come from His 277 and Tyr 218 (Einsle *et al.*, 2002b). After the release of a water molecule and the formation of a Fe-NO species, rapid electron transfer is necessary to overcome the problem of a very stable {FeNO}⁷ species (Chapter 4.3.1). A fast electron transfer is favoured by the arrangement of the five hemes within a monomer and also the arrangement of the two hemes in the dimer interface (Figure 4.2). All hemes are in a distance of around 4 Å that effective electron transfer becomes possible (Chapter 4.1.1).

In cd₁Nir from *P. pantotrophus* nitrite is further stabilized by hydrogen bonds from one oxygen to both His 345 and His 388 (Figure 4.5 (B)). These two histidines are the proton donors for the first reaction step with the cleavage of one N-O bond (Allen *et al.*, 2001). So far, ccNir and cd₁Nir seems to have nearly the same assembly of nitrite binding. A remarkable difference is the intramolecular electron transfer rate. In the *P. aeruginosa* enzyme, the rate is around 1 s⁻¹, both in the presence and the absence of nitrite (Allen *et al.*, 2001). The minimum edge-to-edge distance between hemes in different monomers in *P. pantotrophus* cd₁Nir is 38 Å, a distance which is not suitable for efficient electron transfer. This is incompatible with the turnover of the enzyme, strongly suggesting that catalytic processes only involve electron transfer within a single monomer of the dimer. In contrast there might be a cooperative effect in ccNir within the dimer, leading to a faster reduction and ammonia as the reduction product instead of nitric oxide. Another remarkable difference is the heme-ligand switching in cd₁Nir from *T. pantotropha* during catalysis (Williams *et al.*, 1997). Upon reduction, the tyrosine ligand of the d₁ heme is released to allow substrate binding. Concomitantly, a refolding of the cytochrome *c* domain takes place, resulting in an unexpected change of the *c* heme iron coordination from His 17/His 69 to Met 106/His 69. This structural change decelerates the reaction rate compared to ccNir where no significant structural changes occur during catalysis.

In copper Nir, nitrite is bound primarily by a single oxygen atom that is protonable, and after reduction and cleavage of that N-O bond, NO is released leaving the oxygen atom bound to the copper site as hydroxide or water (Murphy *et al.*, 1997). Normally, NO cannot be further reduced by the copper Nir. However, the enzyme can produce nitrous oxide (N₂O) if nitric oxide is allowed to accumulate.

4.2 Spectroscopic Properties of Cytochrome *c* Nitrite Reductase

4.2.1 UV-Vis Spectroscopy

The UV-Vis absorption spectra of nitrite reductase from *W. succinogenes* were typical for cytochrome *c* in the oxidized as well as in the reduced state (Pettigrew and Moore, 1987). Of special interest is the absorption shoulder at 615 nm which is indicative of a high-spin heme group according to Blackmore *et al.* (1990). This shoulder is absent in the spectrum of ccNirStopI (NrfA_S) because of the deletion of the active site heme 1 (Pisa *et al.*, 2002) (Chapter 3.1.4). This five coordinated heme must be responsible for the high-spin signals at

$g = 6$ in the EPR spectrum of ccNirWT (Bamford *et al.*, 2002). The broad Soret band at 409 nm of the enzyme in the oxidized state suggests that this absorption could arise from several unresolved bands originating from different heme types within the protein. This different heme types also might result in different EPR signals, according to the orientation of the imidazole planes of the coordinated histidines (Chapter 4.2.2.1).

Second derivative spectra of nitrite reductase in the fully reduced state revealed minima at 550 and 555 nm. Furthermore, a split Soret band was observed with minima at 419 and 427 nm. By comparison with the spectra reported for horse heart cytochrome *c* (Wood, 1984), the bands observed for ccNir at 419 and 550 nm were assigned to low-spin heme centers. The maxima at 427 and 555 nm are typical for high-spin heme centers which have been observed for deoxymyoglobin (Adachi *et al.*, 1993). Note that there is a cytochrome *c* which also shows a split Soret band. This protein called split-Soret cytochrome *c* was isolated from the sulfate- and nitrate-reducing bacterium *D. desulfuricans* ATCC 27774 (Liu *et al.*, 1988). Upon its reduction the Soret band did not only reveal a maximum at 424 nm, but also a shoulder at 415 nm.

The molar absorption coefficient $\epsilon_{553\text{nm}}$ of the monomeric cytochrome *c* nitrite reductase in the reduced state (Schumacher, 1993) was $\approx 3\times$ the coefficient $\epsilon_{550\text{nm}}$ of reduced horse heart cytochrome *c* (Margoliash and Frohwirt, 1959). Furthermore, it was smaller than $\epsilon_{552\text{nm}}$ of the reduced tetraheme cytochrome *c*₃ from *D. desulfuricans* Norway (Bruschi *et al.*, 1977). This result indicates that the absorption coefficient does not increase in a complete linear fashion with the number of heme groups. This observation is consistent with the described $\epsilon_{552\text{nm}}$ of reduced nonaheme cytochrome *c* from *D. desulfuricans* (Fritz *et al.*, 2001) which corresponds to $\approx 7\times$ the coefficient $\epsilon_{550\text{nm}}$ of reduced horse heart cytochrome *c*.

4.2.2 EPR Spectroscopy

Cytochrome *c* nitrite reductase and its variants show highly complex EPR spectra over a broad range of frequencies. The presence of five heme centers per monomer and the possibility of multiple electronic interactions between these hemes complicate their interpretation. Complex EPR spectra have also been reported for other multiheme nitrite reductases involved in dissimilatory nitrate-ammonification (Sadana *et al.*, 1986; Blackmore *et al.*, 1987; Liu *et al.*, 1987; Costa *et al.*, 1990; Bamford *et al.*, 2002; Almeida *et al.*, 2003).

4.2.2.1 Microwave Frequency Independent Resonances

The resonances at $g = 2.94$, 2.29 , and ≈ 1.50 were found in all variants of ccNir. These g -values are characteristic of low-spin ferric hemes (Palmer, 1983) where the two bound histidines have nearly parallel imidazole planes (Walker, 1999). They were assigned to magnetically isolated hemes since this set of resonances has frequency independent g -values (Chapter 3.1.6). From spin quantification and computer simulations of these signals (CuSO_4 standard), 1.80 ± 0.2 low-spin Fe(III) heme centers were determined for *S. deleyianum* nitrite reductase (Nath, 1996). Similar results were obtained by Blackmore *et al.* (1987) who reported on 1.7 low-spin Fe(III) heme centers in *W. succinogenes* nitrite reductase using Fe(III) myoglobin cyanide as standard. The candidates where the bound histidines have nearly parallel imidazole planes are hemes 2 and 3 (Figure 4.6).

A second set of resonances at $g = 2.48$, 2.13 and ≈ 1.45 was frequency independent in variants ccNirWT and ccNirK134H, or frequency dependent in ccNirQ276E and ccNirY218F. For the former proteins these signals can be attributed to typical low-spin heme centers as in the case of the resonances at $g = 2.94$, 2.29 , and ≈ 1.50 . Why these signals are frequency independent and therefore indicative of a spin uncoupled system, and which hemes are involved in this interaction, remains unclear. One possible explanation could be that they are coupled to a high-spin Fe(III) center that is absent in the other proteins.

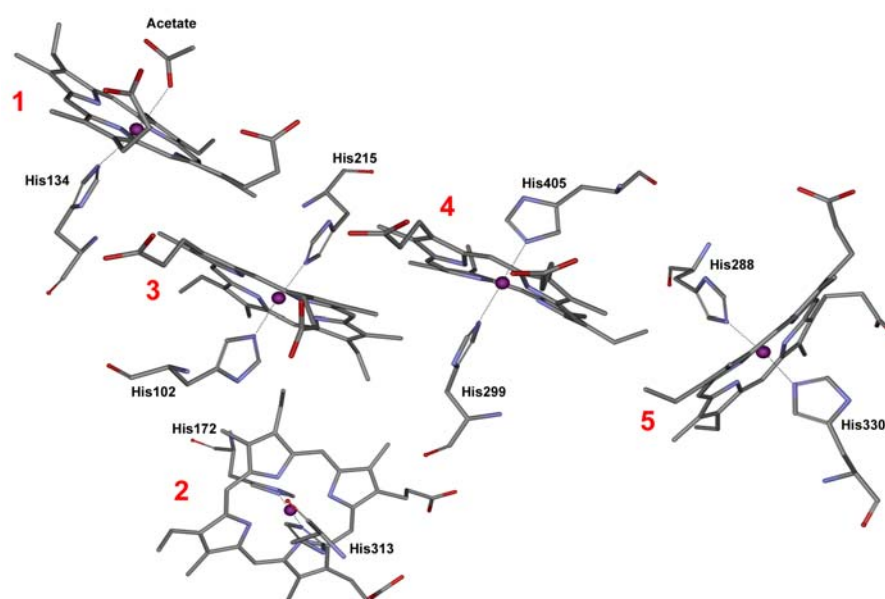


Figure 4.6: Coordination of the bound histidines of ccNirK134H. The hemes are numbered according to their attachment to the amino acid chain.

The signals with high g_{\max} values at $g = 3.5$ and 3.2 are attributed to low-spin ferric hemes where the two bound histidines have nearly perpendicular imidazole planes as observed for hemes 4 and 5 (Figure 4.6) (Walker, 1999).

Simulation of the ferric low-spin signals with the assumption of isolated, non-coupling hemes, fits quite well with the experimental data from ccNirQ276E (Chapter 3.1.6.9). The remaining signals can be attributed either to the $S = 3/2 \leftrightarrow S = 1/2$ spin-coupled pair or to the $S = 1/2 \leftrightarrow S = 1/2$ spin-coupled pair.

The feature at $g \approx 2$ most likely results from a contamination with nitrate reductase which contains several [4Fe-4S] clusters (Blackmore *et al.*, 1987). All eukaryotic and bacterial nitrate reductases are molybdenum-dependent enzymes and possess a unique cofactor, the so-called molybdopterin (Kisker *et al.*, 1999). The amount of molybdenum with 2-4 % in ccNirWT and ccNirQ276E supports this assumption. Four types of nitrate reductases catalyze the two-electron reduction of nitrate to nitrite. These are the eukaryotic assimilatory nitrate reductases and three distinct bacterial enzymes, comprising the cytoplasmic assimilatory (Nas), the membrane-bound (Nar), and the periplasmic dissimilatory (Nap) nitrate reductases (Moreno-Vivián, 1999). Nap is necessary during reduction of nitrate to ammonia and therefore present in cells of *W. succinogenes*.

Generally, [2Fe-2S] clusters give only rise to a signal in the reduced state, whereas [3Fe-4S] clusters show an axial signal below 20 K (Cammack, 1992; Beinert *et al.*, 1997; Sticht and Rösch, 1998). Even at higher temperatures (70 K) only oxidized [4Fe-4S] clusters exhibit a signal. The resonance at $g \approx 2$ in nitrite reductase samples could only be detected below 20 K. Simulation of an axial [3Fe-4S] spectrum with g -values at 2.05 and 2.02 fits quite well with the experimental data (Chapter 3.1.6.9).

The signal at $g = 2.008$ most likely arises from a tyrosine radical which was also observed for example in ribonucleotide reductase, or photosystem II (Stubbe and van der Donk, 1998). Since the crystal structure of nitrite reductases from *S. deleyianum* and *W. succinogenes* revealed several tyrosine residues close to the active site (Einsle *et al.*, 1999; Einsle *et al.*, 2000), a putative role of these residues in catalysis has been discussed (Einsle *et al.*, 2002b). These tyrosine residues are conserved throughout all NrfA sequences known to date (Einsle *et al.*, 2000). They might play a role in stabilization of radical intermediates during the catalytic reduction of nitrite to ammonia by forming tyrosyl radicals. Observation of partial ortho-hydroxylation of Tyr 219 in *W. succinogenes* enzyme supports this hypothesis (Einsle *et al.*, 2000). However, the simulation of an isotropic signal at $g = 2.008$ fits quite well with the experimental data (Chapter 3.1.6.9).

4.2.2.2 Microwave Frequency Dependent Resonances

Interestingly, with the set of resonances at $g = 2.48$, 2.13 and ≈ 1.45 , a further signal at $g \approx 1.8$ could only be observed in the spectra of ccNirQ276E and ccNirY218F and was assigned to the group of frequency dependent signals. The apparent g -values are indicative of a spin coupled system between two $S = 1/2$ centers (Upadhyay *et al.*, 2003). According to the results of the magnetic measurements (Chapter 3.1.7), the low-spin hemes in ccNirWT exhibit a antiferromagnetic exchange interaction with $J > 0.1 \text{ cm}^{-1}$ (Neese, personal communication).

The most characteristic features in the EPR spectra of ccNirWT and ccNirK134H are the signal at $g = 3.8$ and the broad line at $g = 9.8$. These resonances have frequency dependent g -values, indicative of a spin-coupled system. In general, high-spin heme centers have five coordinate Fe(III) as reported for the active site heme (heme 1) of ccNir. Evidence for the involvement of the active site heme in the prominent feature at $g = 3.8$ came from the EPR spectrum of the ccNirK134H. This variant has a histidine residue instead of the unusual lysine ligand (Chapter 3.1.8.1) in the axial position of heme 1. EPR spectra of ccNirK134H revealed a decrease in intensity of the signal at $g = 3.8$ (Chapter 3.1.6.2). The origin of these prominent signals was assigned to heme-heme interactions (Blackmore *et al.*, 1987, 1990; Costa *et al.*, 1990; Brittain *et al.*, 1992; Moura *et al.*, 1997). Costa *et al.* (1990) concluded that the high-spin ferric heme center must be involved in this interaction.

Although the existence of a high-spin Fe(III) heme in nitrite reductase was clearly demonstrated by room temperature MCD spectroscopy (Stach, 2001), the EPR spectra of nitrite reductase did only reveal a more or less minor resonance at $g \approx 6$ indicative for a Fe(III) high-spin heme center. This resonance was only present in ccNirK134H but could not be observed in ccNirQ276E, ccNirY218F, and ccNirStopI. In the latter variant the active site heme (heme 1) is deleted by constructing a *nrhHAIJ* gene cluster with the *nrfl* codons 47 and 48 altered to stop codons (Pisa *et al.*, 2002). Therefore, the resonance at $g \approx 6$ is assigned to the active site heme.

There is evidence for an exchange-coupled heme cluster in the parallel mode spectra. An integer-spin EPR signal was observed at $g = 9.8$ in the ccNirWT. Presumably, the integer-spin resonance arises from a pair of spins because all the irons of oxidized nitrite reductase are ferric with half-integer spin. The signal shifted to $g = 8.8$ upon addition of CN^- (Nath, 1996), supporting the idea that the high-spin heme contributes to the integer-spin feature. As one possible explanation for the resonances at $g = 3.8$ and 9.8 , one can propose spin-spin interaction between the active site heme group and a low-spin heme center close by. Since the

crystal structure of ccNirWT revealed hemes with very short edge to edge distances ($\approx 4 \text{ \AA}$) and short Fe-Fe distances ($\approx 12 \text{ \AA}$) (Einsle *et al.*, 2000), the EPR signals at $g = 3.8$ and 9.8 arise from an interaction between heme 1 and heme 3 (Figure 4.7). A second plausible explanation for the existence of the coupled signals the interaction between the active site heme group and an organic radical, e.g. a tyrosyl radical, could be assumed. A good candidate is Tyr 218 which is close to the distal site of the active site heme (Chapter 3.1.8.3). By replacement of Tyr 218 to Phe 218 (ccNirY218F) the key resonances for an exchange coupled pair disappears (Chapter 3.1.6.4). Nevertheless, an integer-spin EPR signal was observed at $g = 13$ in the ccNirY218F. The ccNirK134H shows the relevant signals in the perpendicular mode at $g = 3.8$ and 9.8 but no integer-spin EPR signal was observed. Furthermore, the ccNirQ276E has no EPR signals indicating an exchange coupled pair between a high-spin heme and a $S = 1/2$ center while no changes occurred at the active site heme or a tyrosine.

Another possibility is the existence of an intermediate spin $S = 3/2$ at the active site heme. A hint is the signal around $g = 4$. Taking into account the facts, a spin-coupled system of $S = 3/2$ and $S = 1/2$ could also exist in ccNirY218F and can be explained by the observation of an integer-spin EPR signal at $g = 13$. Nevertheless, there are still open questions concerning the kind of interaction.

At least the question remained whether the Fe(III) high-spin signals had any biological significance and therefore an influence to the catalytic cycle. There are two arguments that exclude this assumption. (i) ccNirQ276E has nearly the same specific activity like ccNirWT (Chapter 3.1.2.3). However, the EPR spectrum shows no specific resonances that result from high-spin Fe(III) (Chapter 3.1.6.3), (ii) during reduction of ccNir with H_2/Pd -reduced methylviologen the prominent signals at $g = 9.8$, 6 , and 3.8 disappeared because of the received diamagnetic Fe(II) low-spin center. Reoxidation with nitrite could not reconstitute the former “oxidized” EPR spectrum (Schumacher, 1993). Hence, a possible second turnover with substrate has to start with Fe(III) low-spin or Fe(III) intermediate-spin. Consequently, for reduction of nitrite to ammonia it isn't necessary to start the catalytic cycle with a Fe(III) high-spin species. It is also possible that during catalysis the active site iron is always in the ferrous state (Einsle *et al.*, 2002b).

4.2.2.3 Comparison of the EPR Spectra from Multiheme Enzymes

Other multiheme proteins, such as cytochrome c_{554} and hydroxylamine oxidoreductase (HAO) from *N. europaea*, also reveal similar complex EPR spectra (Upadhyay *et al.*, 2003; Hendrich *et al.*, 2001). In comparison, the multiheme protein cytochrome c_3 from

D. desulfuricans (Einsle *et al.*, 2001) reveals a rather simple EPR spectrum (Chapter 2.12.2). Heme arrangement of these proteins resembles that of nitrite reductase. Hemes 1 and 3 of cytochrome c_3 align well with hemes 7 and 8 of HAO and also with hemes 4 and 5 of ccNir, and the four hemes of cytochrome c_{554} align well with hemes 3 to 6 of HAO and also with hemes 1 to 3 of ccNir (Figure 4.7). Despite the similarities in heme packing for the four proteins, the EPR spectrum of cytochrome c_3 shows no coupling and the EPR spectrum of HAO shows moderate coupling while the EPR spectra of both cytochrome c_{554} and ccNir are exceedingly complex, suggesting substantial coupling between all hemes in the latter proteins (Einsle *et al.*, 2001; Upadhyay *et al.*, 2003; Hendrich *et al.*, 2001).

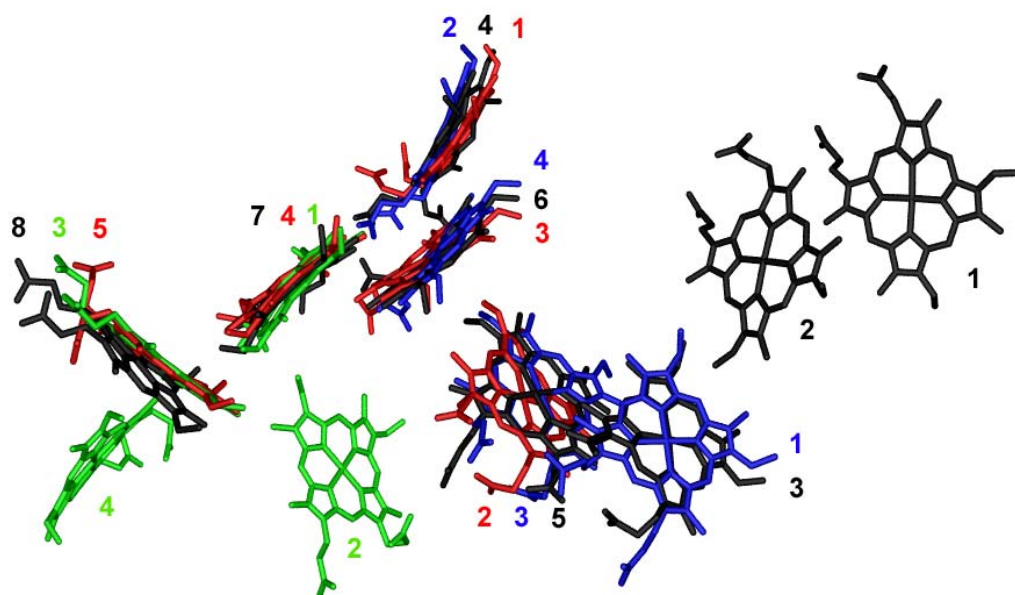


Figure 4.7: Heme arrangement of cytochrome c_3 (green, PDB code 1I77), cytochrome c_{554} (blue, PDB code 1BVB), hydroxylamine oxidoreductase (black, PDB code 1FGJ) and cytochrome c nitrite reductase (red, PDB code 1FS7). The heme groups are numbered according to their attachment to the protein chain.

	g-Value												
ccNir	9.84	6.04	4.34	3.81	3.41	3.22	2.98	2.50	2.32	2.15	1.83	1.50	1.45
Cc ₃			4.3			3.29	2.95		2.29			1.54	1.43
Cc ₅₅₄			4.3	3.9				2.7		2.06		1.63	1.46
HAO			4.3		3.4		3.1	2.8	2.2		1.94	1.66	1.35

Table 4.1: X-Band g-Values from multiheme enzymes. Cc₃: cytochrome c_3 (Einsle *et al.*, 2001); Cc₅₅₄: cytochrome c_{554} (Upadhyay *et al.*, 2003); HAO: hydroxylamine oxidoreductase (Hendrich *et al.*, 2001).

The rather simple EPR spectrum of the tetraheme protein cytochrome c_3 from *Desulfovibrio desulfuricans* (Einsle *et al.*, 2001) showed resonances with apparent g -values at $g_{\max} = 2.95$, $g_{\text{mid}} = 2.29$ and $g_{\min} = 1.54$ and 1.43 , consistent with low-spin Fe(III)-heme groups with bis-histidiny coordination and parallel orientation of the imidazole planes. This feature is found in all multiheme enzymes (Table 4.1). Furthermore, a broad peak at $g_{\max} = 3.29$ was detected and this feature is also found in all other multiheme enzymes because of a low-spin Fe(III)-heme group with bis-histidiny coordination and perpendicular orientation of the imidazole planes (Walker, 1999; Ogura *et al.*, 2001; Yatsunyk *et al.*, 2003; Walker, 2004). This type of heme center is found in heme 2 of cytochrome c_3 , hemes 1 and 4 of cytochrome c_{554} , heme 6 of HAO and hemes 4 and 5 of ccNir (Upadhyay *et al.*, 2003).

Similarities in heme arrangement between ccNir and cytochrome c_{554} resulted in comparable spectroscopic properties. The characteristic feature at $g = 3.8$ was also reported for the tetraheme cytochrome c_{554} (Table 4.1). Furthermore, Mössbauer spectroscopy indicated a mix of low-spin to high-spin iron in the protein in the ratio of approximately 3:1 (Andersson *et al.*, 1986). Optical spectra for cytochrome c_{554} are consistent with such a low-spin/high-spin mix: the protein exhibited an absorption shoulder at 645 nm and a Soret maximum at 420 nm together with a distinct shoulder at approximately 430 nm (Arciero *et al.*, 1991). Andersson *et al.* (1986) also assigned the prominent resonance at $g = 3.8$ in the EPR spectrum to an exchange-coupled pair of low- and high-spin Fe(III) heme centers. Furthermore, the parallel mode spectrum of cytochrome c_{554} shows signals at $g = 7.2$ and 3.2 (Upadhyay *et al.*, 2003) which correspond to the parallel mode signals in ccNir at $g = 9.4$. The observation of a parallel mode signal for ferric hemes requires the presence of spin-spin interactions between hemes. EPR spectra of cytochrome c_{554} did not reveal high-spin hemes in comparison to the signals at $g = 6$ in ccNir, but instead were consistent with a complex spin-paired system (Andersson *et al.*, 1986). If the signal at $g = 3.8$ originates from the same heme-heme interaction in both ccNir and cytochrome c_{554} , it could be assumed that coupling of the hemes 1 and 3 in ccNir and of the hemes 2 and 4 in cytochrome c_{554} (parallel stacking) may be responsible for these interaction signals (Einsle, 1999; Upadhyay *et al.*, 2003).

In addition, the signals at $g = 2.7$, 2.06 , 1.63 , and 1.46 (Table 4.1) originate from a spin system separate from that of the $g = 3.9$ and the parallel mode signals. A weak antiferromagnetic exchange interaction ($J = -0.7 \text{ cm}^{-1}$) between two $S = 1/2$ low-spin heme centers is expected and were assigned to hemes 1 and 3 in cytochrome c_{554} (Upadhyay *et al.*, 2003) (Figure 4.7). Because only heme 3 of cytochrome c_{554} correspond to heme 2 of ccNir

but not heme 1 of cytochrome *c*₅₅₄ correspond to any heme in ccNir, this interaction could not be found in ccNirWT. However, in ccNirQ276E and ccNirY218F comparable signals were found and could be assigned to an antiferromagnetic exchange interaction. In cytochrome *c*₅₅₄ one of the two interacting hemes have bis-histidiny axial coordination with crossed imidazole planes, the other with parallel imidazole planes, and they build a SSC motif (Chapter 2.12.2). The same situation is found between hemes 3 and 4 in ccNir (Figure 4.7). Therefore, the $S = 1/2 \leftrightarrow S = 1/2$ heme-heme interaction in ccNir could be assigned to hemes 3 and 4.

Both heme-heme interactions in cytochrome *c*₅₅₄ originate from edge-to-edge overlap of porphyrin orbitals. There is no evidence for a spin interaction between the pairs (Upadhyay *et al.*, 2003). Most likely, a similar situation is present in ccNir.

Comparable features have been reported for HAO (Arciero *et al.*, 1998). The perpendicular EPR spectrum has a set of resonances at $g = 3.1$, 2.2 , and 1.35 (Hendrich *et al.*, 2001) (Table 4.1), which are typical of low-spin ferric heme complexes (Walker, 1999). Least-squares fitting of the experimental spectra of fully oxidized HAO indicates that this resonances can be resolved into at least two different mononuclear heme species. In ccNir spin quantification and computer simulations of these signals indicates 1.80 ± 0.2 low-spin Fe(III) heme centers for *S. deleyianum* ccNir (Nath, 1996).

Two integer-spin resonances at $g = 8.0$ and 3.7 originate from two different spin systems. The weaker signal at $g = 3.7$ originates from a coupling pair with a set of resonances at $g = 3.4$, 2.8 , 1.94 , and 1.66 (Table 4.1) in the perpendicular mode that are frequency dependent. From the temperature dependence of the signal, the isotropic exchange coupling between this two hemes is antiferromagnetic. The EPR spectra of ccNirQ276E and ccNirY218F show also frequency dependent signals at equal g -values. Anyway, both samples generate no integer-signal at $g = 3.7$. The larger signal near $g = 8$ which vanished upon reduction or in the presence of substrates and inhibitors was assigned to an additional pair of exchange-coupled hemes (Hendrich *et al.*, 2001). The P₄₆₀ heme (heme 4) and heme 6 have been shown to be a component of this exchange-coupled cluster (Figure 4.7). In this case the interacting spins are both low-spin (Hendrich *et al.*, 2001). Further on, the integer-spin at $g = 13$ of ccNirY218F which was not observed in ccNirQ276E, can be assigned to an additional pair of exchange-coupled hemes as it is the case in HAO. Again, the exchange interaction originate from an edge-to-edge overlap of porphyrin orbitals (Hendrich *et al.*, 2001).

Cytochrome *c* nitrite reductase from *E. coli* shows prominent derivative features at $g = 3.5$ and $g = 10.8$ (Bamford *et al.*, 2002) in contrast to the g -values of 3.8 and 9.8 in the spectrum of ccNir from *W. succinogenes* and *S. deleyianum* that are atypical of the spin states of any magnetically isolated hemes. Parallel mode EPR spectroscopy shows only a derivative feature at $g \sim 10.8$ compared to the signal at $g = 9.4$ in ccNir from *W. succinogenes*. The presence of two derivative signals at g -values $\sim 3-4$ and $10-12$, of which the latter is allowed in the parallel mode and the former is forbidden, are a very pattern similar to those observed from a weakly exchanged coupled high-spin heme Fe(III) ($S = 5/2$) and Cu_B(II) ($S = 1/2$) in *E. coli* quinol oxidase (Oganessian *et al.*, 1998). Bamford *et al.* (2002) assign these features to a weakly exchange coupled pair of paramagnets of $S = 5/2$ (heme 1) and $S = 1/2$ (heme 3 or a radical species) (Figure 4.7).

The quantification of the signals at $g = 2.92$, 2.3, and 1.5 from *E. coli* ccNir, which are due to a rhombic Fe(III) low-spin bis-histidinyll coordinated center with nearly parallel imidazole planes (Walker, 1999), gave an integer value of 1 mol spin per mol of enzyme. In contrast, *S. deleyianum* ccNir spin quantification indicates 1.80 mol spin per mol of enzyme (Nath, 1996).

The weak signals at $g = 2.52$ and 1.8 from *E. coli* ccNir probably arise from low levels of low-spin Lys-OH⁻ ligated heme (Bamford *et al.*, 2002). These signals are stronger in ccNirQ276E (Chapter 3.1.6.3) and therefore the amount of low-spin Lys-OH⁻ ligated heme could be increased. The factor of this increased amount must be the glutamate, which no longer be a part of the active site cavity but a bidentate ligand to the yttrium (Chapter 3.1.8.2). However, the electronic structure of the active site heme must be changed a probably resulted in an increased amount of low-spin Lys-OH⁻ ligated heme.

4.3 Mechanism and Reactivity of Cytochrome *c* Nitrite Reductase

In the periplasm of *W. succinogenes*, ccNir (NrfA) forms a stable, membrane-associated complex with its electron donor NrfH, a member of the NapC/NirT family of tetraheme cytochromes, which serves as a quinole oxidase to obtain electrons directly from the membranous quinone pool (Simon *et al.*, 2000; Simon *et al.*, 2001). Most likely, this complex consists of a heterotetrameric unit, NrfH₂A₂ (Einsle *et al.*, 2002b), with a total of eighteen coupled heme centers which guarantee a fast and efficient electron transfer to two independent Fe-Lys active sites (Einsle *et al.*, 2000). The effective electron transfer and the coupling between all heme centers could confirmed by measuring the magnetic properties

(Chapter 3.1.7). It was shown that in NrfA all heme centers interact antiferromagnetically and in the whole NrfHA complex most of them interact also antiferromagnetically.

The six-electron reduction of nitrite to ammonia requires the breaking of two N-O bonds and the formation of three N-H bonds. It is likely that this process occurs in several steps. The first step in the reaction pathway of ccNir is similar to that observed in cytochrome *cd₁* Nir (Allen *et al.*, 2001). In both cases an one-electron reduction of nitrite to nitric oxide and the liberation of the first oxygen atom as water takes place. In contrast to cytochrome *cd₁* Nir, NO is not released from ccNir but is further reduced to ammonia. It is proposed that the reduction of nitrite to ammonia occurs via nitric oxide and hydroxylamine. The reactivity of the enzyme towards these intermediates is ~ 50 % for hydroxylamine but only ~ 1.2 % for nitric oxide relative to the one for nitrite (Stach *et al.*, 2000). However, no intermediates are released during nitrite turnover. In general, NO has an extremely high affinity for heme iron which increases when Fe(III) is reduced to Fe(II) (Ribeiro *et al.*, 1993).

Einsle *et al.* (2002b) proposed a first possible reaction mechanism (Figure 4.8). The reaction starts with the reduction of nitrite coordinated to the Fe(II)-Lys active site (Einsle *et al.*, 1999) and has been suggested to begin with the heterolytic cleavage of the N-O bond. Two rapid one-electron reductions will lead to the production of a {FeNO}⁸ species and, by protonation, to a HNO adduct. A further two-electron two-proton step will produce hydroxylamine, the only bound intermediate which loses water to give the final product, ammonia.

4.3.1 Substrate Binding and Reactivity

Nitrite is predicted by crystallography (Einsle *et al.*, 1999; Einsle *et al.*, 2000) to be N-bound in agreement with the crystal structure obtained after soaking of the substrate into oxidized crystals of *W. succinogenes* and *S. deleyianum* (Einsle, 1999). In the *S. deleyianum* structure (2.5 Å resolution) nitrite is coordinated with one oxygen to both His 282 and Tyr 217 and to a water molecule. However, in the structure of *W. succinogenes* (1.7 Å resolution) one oxygen is only bound to His 277 and the other one to Arg 114. Therefore, the nitrite ion's plane is twisted by 45° with respect to the *S. deleyianum* enzyme. During mutation of His 277 or Arg 114 to leucine no enzyme activity is detectable (Pisa *et al.*, 2004). This documents the importance of the stabilization effect from nitrite by the hydrogen bonds.

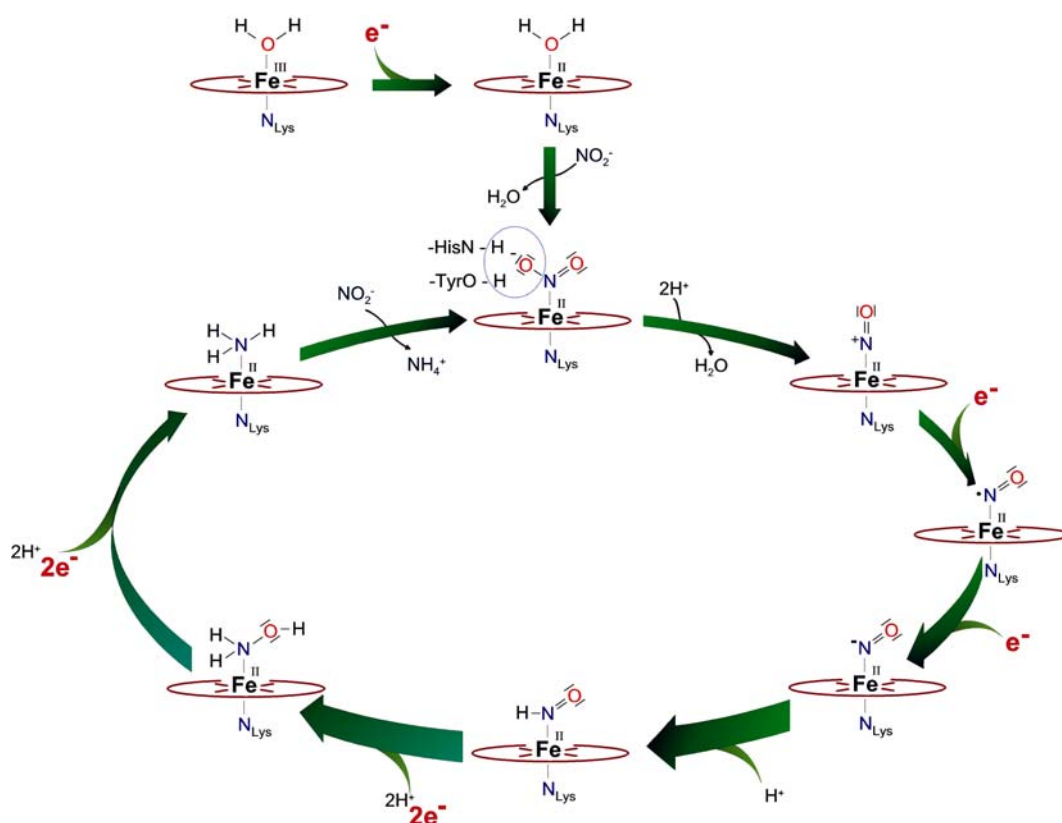


Figure 4.8: Proposed reaction mechanism of ccNir. Figure was taken from Einsle *et al.* (2002b).

The specific activity of the ccNirY218F, where the tyrosine near the active site is mutated by a phenylalanine, is only 3-5 % compared to ccNirWT (Figure 4.9). If the heterolytic cleavage of nitrite to water and a Fe(II)-NO species starts with the dual protonation of one of the two oxygens, the protons most likely come from His 277 and Tyr 218. Because of the deletion of the hydroxyl-group by substitution of tyrosine to phenylalanine, the protonation is blocked. The remaining activity of 3-5 % can be explained by the possible proton supply from one of the other three tyrosines (Tyr 219, Tyr 254, Tyr 258) near the active site. Faller *et al.* (2003) could show that in photosystem II a tyrosine can act both as an electron and a proton transfer unit. This property can also be assigned to the Tyr 218 in ccNir from *W. succinogenes*.

As described in Figure 3.17 the bond length between acetate and the active site iron in ccNirK134H is elongated by 0.34 Å compared to the distance between water and Fe(III) in ccNirWT. The distance of the substrate nitrite to the active site iron in ccNirWT is 1.9 Å (Einsle *et al.*, 2002b) and therefore shorter as the water-iron distance. Because of the decreased enzyme activity of ccNirK134H with about 35 % compared to ccNirWT (Figure 4.9), it is possible that the substrate nitrite is bound less strongly to the active site iron as it is the case with acetate. This effect could result in a weakened back-bonding effect. The initial catalytic step, the cleavage of the first N-O bond, is not as favored as in ccNirWT.

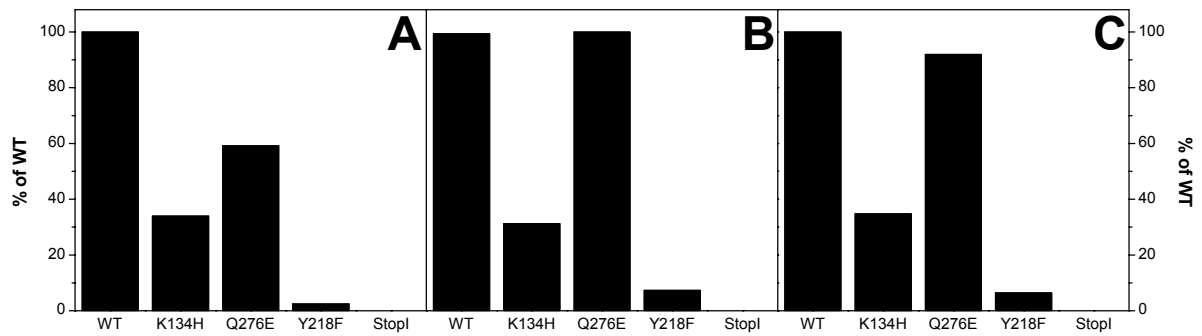


Figure 4.9: Nitrite reductase activity of ccNirWT and variants. **A:** NrfA_S; **B:** NrfA_M; **C:** NrfHA.

Binding of the substrate to the oxidized (as isolated) nitrite reductase turned out to be rather poor (Stach, 2001). In contrast, reduced enzyme was rapidly reoxidized upon addition of nitrite. Stopped-flow investigations on the reoxidation of photochemically reduced *S. deleyianum* ccNir with nitrite were carried out (Steinbach, 2001). The bimolecular step, binding of substrate to the active site, was very fast ($k \geq 8.9 \cdot 10^7 \text{ M}^{-1} \text{ s}^{-1}$), being lost in the dead time of a rapid mixing apparatus. A reaction intermediate with an absorption maximum at 649 nm was described for the first time and was assigned to a Fe(II)-NO₂⁻-complex.

These results support that nitrite binds to the reduced enzyme (Figure 4.8). Nitrite reductase from *S. deleyianum* which had been reduced with H₂/methyl viologen prior to incubation with nitrite and rapid freezing, gave a characteristic triplet signal at $g = 2.016$ (hyperfine splitting $A^N = 1.67 \text{ mT}$) due to the coordination of NO to heme iron producing a low-spin Fe(II) nitrosyl center (Schumacher *et al.*, 1997). Spectroscopic studies on nitrite reductase from *V. fischeri* (Sadana *et al.*, 1986), *W. succinogenes* (Liu *et al.*, 1987), and *D. desulfuricans* (Costa *et al.*, 1990) also revealed such a triplet EPR signal under turnover conditions. The low-spin ferric heme signals at $g = 2.94$, 2.29 , and 1.5 and all the lesser prominent features, which were observed when the enzyme was in its isolated state, reappeared in the case of the nitrite-reacted sample, indicating that most of the hemes were reoxidized. However, the resonance at $g = 3.8$ was absent and the intense signal with hyperfine structure was observed at $g \approx 2$. Furthermore, additional low-spin heme signals were described. Using ¹⁵N-labelled nitrite, a doublet signal at $g \approx 2$ was observed indicating that this feature is due to the nitric oxide-bound ferrous heme. Since the signal at $g = 3.8$ is absent in the nitrite-reacted enzyme, it is likely that the high-spin ferric heme must be involved in the heme-heme interaction which presumably produces this prominent feature (Chapter 4.2.2.2). The disappearance of the $g = 3.8$ signal coincides with the observation of

new resonances. It was suggested that a conversion of high-spin to low-spin heme occurred upon substrate binding (Schumacher, 1993).

Mössbauer data also indicate that a high-spin heme is involved in substrate binding (Costa *et al.*, 1990). This is reasonable since high-spin hemes are usually five-coordinate and therefore can bind substrate at the distal site of the heme iron. Anyway, the EPR spectrum of ccNirQ276E did not show the prominent signals at $g = 9.8$, 6, and 3.8 that are indicative for a high-spin Fe(III) heme. Nevertheless, the specific activity is nearly comparable to that of ccNirWT (Figure 4.9). Therefore, for substrate binding it isn't crucial to start with a high-spin Fe(III) species. Reduction of nitrite can also start by binding to a Fe(III) intermediate-spin or a Fe(III) low-spin species, respectively.

4.3.2 Reactivity Towards NO

Depending on the reducing agent used under turnover conditions, NO was reduced to either ammonia or nitrous oxide. Nitrite reductases from *D. desulfuricans* ATCC 27774, *W. succinogenes*, and *E. coli* have been reported to reduce nitric oxide to ammonia when low-potential electron donors (e.g. dithionite) are available, or like denitrifiers, to N₂O when high-potential electron donors (e.g. ascorbate) serve as sources (Costa *et al.*, 1990).

An Fe(II)-NO adduct which was obtained after reaction of oxidized (as isolated) nitrite reductase with NONOates has been identified by EPR spectroscopy (Stach *et al.*, 2000). It shows an intense resonance at $g = 2.014$, and a hyperfine splitting $A^N = 1.55$ mT. Nitrite reductase (oxidized as isolated) reacted slowly with nitric oxide as documented in UV-Vis spectra by the decrease of the Soret maximum at 409 nm and the band around 615 nm, with isosbestic points at 333, 393, 510, and 539 nm. Obviously, the enzyme underwent partial reduction, and the paramagnetic Fe(II)-NO species was formed.

Synthetic Fe(III) porphyrins are known to be strong O-atom transfer agents (Finnegan *et al.*, 1990). A viable O-atom acceptor in the present case would be nitrite itself leading to a Fe(II)-NO complex and nitrate as the primary reaction products (homolytic cleavage). The alternative reaction would involve binding of nitrite to the reduced enzyme and the subsequent heterolytic scission of the N-O bond (oxo-transfer) to give water and a Fe(III)-NO species (heterolytic cleavage). The two possibilities can be experimentally distinguished by monitoring nitrate formation. Under turnover conditions as well as in the reaction of the oxidized enzyme with nitrite no nitrate was formed (Stach, 2001). Therefore, O-atom transfer is not physiological and the heterolytic cleavage is favored. Einsle *et al.* (2002b) obtained this by density functional calculations. The computations predict high-spin states for the

precursors and low-spin states for the nitrite and NO adducts. The calculations were carried out with NH_3 as one of the axial ligands of the porphyrin. Hydroxide ion, or water, served as distal ligand in the as isolated state. According to these calculations binding of nitrite to the reduced enzyme is much more favorable (Figure 4.8). Heterolytic cleavage of the nitrite N-O bond give a low-spin Fe(II)-NO^+ ($=\{\text{FeNO}\}^6$) species. This is further reduced to Fe(II)-NO^\bullet ($=\{\text{FeNO}\}^7$) which is known to be highly stable. To overcome this problem Einsle *et al.* (2002b) propose a further rapid one-electron reduction step to give Fe(II)-NO^- ($=\{\text{FeNO}\}^8$). This species is known nucleophilic and its protonation yields an Fe(II)-HNO species.

4.3.3 Hydroxylamine as Reaction Intermediate

The assumption of hydroxylamine as an intermediate in the reaction cycle of ccNir becomes plausible by the observation that it is reduced to ammonia by ccNir with about half the specific activity that is observed for nitrite (Stach *et al.*, 2000). By soaking oxidized crystals of ccNir, Einsle *et al.* (2002b) obtained an $\text{Fe(III)-hydroxylamine}$ complex with an end-on bound $\text{Fe-NH}_2\text{OH}$ unit. At the resolution obtained, a distinction between the nitrogen and oxygen atoms of hydroxylamine is not possible, but the binding of the molecule is highly similar to the one of nitrite, with the one oxygen atom missing that was found to interact with His 277 and a hydrogen bond to N_ϵ atom of Arg 114 with a bond length of 3.0 Å. Soaking experiments with N-methylhydroxylamine to ccNirY218F (Chapter 3.1.8.4) clearly show an oxygen binding. This is in agreement with calculations based on the model system iron-porphyrin with a proximal ammonia nitrogen ligand. The calculations predict for hydroxylamine itself and the O-methylated derivative a nitrogen binding (Chapter 3.1.8.4). Interestingly, the enzyme was found to reduce O-methylhydroxylamine (Stach *et al.*, 2000). An exception is the N-methylated derivative where an oxygen binding is predicted. This is in good agreement with the X-ray structure (Chapter 3.1.8.4). We are not aware of structurally characterized model hemes with bound hydroxylamine but we note a number of complexes synthesized by Wieghardt and co-workers that show a large structural variability (Wieghardt, 1984).

The proposed reaction mechanism also includes the three-electron reduction of nitric oxide to hydroxylamine, which is a known substrate of cytochrome *c* nitrite reductase (Stach *et al.*, 2000). Subsequently reduction of hydroxylamine to ammonia takes place.

Nitrite reductase catalyzes the six-electron reduction of nitrite to ammonia with hydroxylamine as possible reaction intermediate whereas HAO performs the four-electron oxidation of hydroxylamine to nitrite. The two-electron step from hydroxylamine to ammonia

occurs only in the reductase. However, nitrite reductase does not catalyze the oxidation of hydroxylamine to nitrite, the reverse direction of the physiologically relevant reaction.

Hydroxylamine is generally considered to be a rather strong reducing agent (Equation 4.1; Wieghardt, 1984).



The reduction of Fe(III) has long been used for the quantitative determination of hydroxylamine (Bengtsson, 1973). In general, hydroxylamine acts as reducing agent in acidic solution and as oxidizing agent in alkaline solution (Jones, 1973). In the presence of NH_2OH and derivatives only partial reduction (5-16 %) of nitrite reductase occurred (Chapter 3.1.5). On the other hand, starting with reduced enzyme, spontaneous reoxidation of ccNir up to 95 % occurred. Binding of hydroxylamine to the enzyme was confirmed by EPR spectroscopy (Stach, 2001). The spectral changes are consistent with binding of hydroxylamine to the active site heme. All features in the UV-Vis as well as in the EPR spectra which were assigned to the high-spin heme were lost. Furthermore, another low-spin heme signal in EPR spectra increased in intensity.

4.3.4 Binding of Ammonium

Iron(III)-porphyrin complexes with NH_3 as a ligand have been reported (Kim and Goff, 1990) but have not been structurally characterized. Structures with ammonia bound to iron(III)-porphyrins have been reported for the protein nitrophorin 4 (Andersen *et al.*, 1998; Roberts *et al.*, 2001). This results and the calculations (Einsle *et al.*, 2002b) favor a low-spin Fe(III) configuration of the complex. However, binding of ammonium to oxidized (as isolated) nitrite reductase is very weak and the complexes show a strong tendency to hydrolyze (Kim and Goff, 1990). As the activity did not decrease even in the presence of 200 mM ammonium chloride (Stach, 2001), it can be assumed that ammonium, if bound to the active site, can easily dissociate and can be replaced by nitrite. Product inhibition was not observed. This is reasonable since the crystal structure revealed separate channels for substrate and product (Einsle *et al.*, 2000): an entry channel with significantly positive electrostatic surface potential for anionic and neutral substrates and a second channel with significantly positive electrostatic surface potential leading to the protein surface opposite to the entry channel. The existence of separate pathways for reaction educt and product may also contribute to the enzyme's high specific activity.

5 References

Abraham, A., Bleaney, B. (1986) Electron paramagnetic resonance of transition ions. Dover Publications Inc., New York.

Adachi, S.I., Nagano, S., Ishimori, K., Watanabe, Y., Morishima, I., Egawa, T., Kitagawa, T., Makino, R. (1993) Roles of proximal ligand in heme proteins: replacement of proximal histidine of human myoglobin with cysteine and tyrosine by site-directed mutagenesis as models for P-450, chloroperoxidase and catalase. *Biochemistry* 32, 241-252.

Adman, E.T., Godden, J.W., Turley, S. (1995) The structure of copper-nitrite reductase from *Achromobacter cycloclastes* at five pH values, with NO_2^- bound and with type II copper depleted. *J. Biol. Chem.* 270, 27458-27474.

Adman, E.T., Murphy, M.E.P. (2001) Copper nitrite reductase. in Handbook of Metalloproteins (Messerschmidt A., Huber R., Poulos T., Wieghardt K., eds.) Wiley-VCH Verlag GmbH, Weinheim.

Allen, J.W.A., Ferguson, S.J., Fülöp, V. (2001) Cytochrome *cd*₁ nitrite reductase. in Handbook of Metalloproteins (Messerschmidt A., Huber R., Poulos T., Wieghardt K., eds.) Wiley-VCH Verlag GmbH, Weinheim.

Almeida, M.G., Macieira, S., Gonçalves, L.L., Huber, R., Cunha, C.A., Romão, M.J., Costa, C., Lampreia, J., Moura, J.J.G., Moura, I. (2003) The isolation and characterization of cytochrome *c* nitrite reductase subunits (NrfA and NrfH) from *Desulfovibrio desulfuricans* ATCC 27774. Re-evaluation of the spectroscopic data and redox properties. *Eur. J. Biochem.* 270, 3904-3915.

Anbar, A.D., Knoll, A.H. (2002) Proterozoic ocean chemistry and evolution: a bioinorganic bridge? *Science* 297, 1137-1142.

Andersen, J.F., Weichsel, A., Balfour, C.A., Champagne, D.E., Montfort, W.R. (1998) The crystal structure of nitrophorin 4 at 1.5 Å resolution: transport of nitric oxide by a lipocalin-based heme protein. *Structure* 6, 1315-1327.

Andersson, K.K., Lipscomb, J.D., Valentine, M., Münck, E., Hooper, A.B. (1986) Tetraheme cytochrome *c*₅₅₄ from *Nitrosomonas europaea*. Heme-heme interactions and ligand binding. *J. Biol. Chem.* 261, 1126-1138.

Arciero, D.M., Collins, M.C., Haladjian, J., Bianco, P., Hooper, A.B. (1991) Resolution of the four hemes of cytochrome *c*₅₅₄ from *Nitrosomonas europaea* by redox potentiometry and optical spectroscopy. *Biochemistry* 30, 11459-11465.

- Arciero, D.M., Golombek, A., Hendrich, M.P., Hooper, A.B.** (1998) Correlation of optical and EPR signals with the P₄₆₀ heme of hydroxylamine oxidoreductase from *Nitrosomonas europaea*. *Biochemistry* 37, 523-529.
- Arth, I., Frenzel, P., Conrad, R.** (1998) Denitrification coupled to nitrification in the rhizosphere of rice. *Soil Biol. Biochem.* 30, 509-515.
- Averill, B.A.** (1996) Dissimilatory nitrite and nitric oxide reductases. *Chem. Rev.* 96, 2951-2964.
- Bamford, V.A., Angove, C.H., Seward, H.E., Thomson, A.J., Cole, J.A., Butt, J.N., Hemmings, A.M., Richardson, D.J.** (2002) Structure and spectroscopy of the periplasmic cytochrome *c* nitrite reductase from *Escherichia coli*. *Biochemistry* 41, 2921-2931.
- Beinert, H., Heinen, W., Palmer, G.** (1962) Application of combined low temperature optical and electron paramagnetic resonance spectroscopy to the study of oxidative enzymes. In *Enzyme models and enzyme structure*. Brookhaven Symposia in Biology: No. 15.
- Beinert, H., Orme-Johnson, W.H., Palmer, G.** (1978) Special techniques for the preparation of samples for low-temperature EPR spectroscopy. *Meth. Enzymol.* 54, 111-150.
- Beinert, H., Holm, R.H., Münck, E.** (1997) Iron-sulfur clusters: nature's modular, multipurpose structures. *Science* 277, 653-659.
- Bengtsson, G.** (1973) A kinetic study of the reaction between iron(III) and hydroxylamine in strongly acid perchlorate solutions. *Acta Chem. Scand.* 27, 1717-1724.
- Berks, B.C., Ferguson, S.J., Moir, J.W.B., Richardson, D.J.** (1995) Enzymes and associated electron transport systems that catalyse the respiratory reduction of nitrogen oxides and oxyanions. *Biochim. Biophys. Acta - Bioenergetics* 1232, 97-173.
- Bertero, M.G., Rothery, R.A., Palak, M., Hou, C., Lim, D., Blasco, F., Weiner, J.H., Strynadka, N.C.J.** (2003) Insights into the respiratory electron transfer pathway from the structure of nitrate reductase A. *Nat. Struct. Biol.* 10, 681-687.
- Blackmore, R.S., Brittain, T., Gadsby, P.M.A., Greenwood, C., Thomson, A.J.** (1987) Electron paramagnetic resonance and magnetic circular dichroism studies of a hexaheme nitrite reductase from *Wolinella succinogenes*. *FEBS Lett.* 219, 244-248.
- Blackmore, R.S., Gadsby, P.M.A., Greenwood, C., Thomson, A.J.** (1990) Spectroscopic studies of partially reduced forms of *Wolinella succinogenes* nitrite reductase. *FEBS Lett.* 264, 257-262.
- Blankenhorn, G.** (1976) Nicotinamide-dependent one-electron and two-electron (flavin) oxidoreduction: thermodynamics, kinetics and mechanism. *Eur. J. Biochem.* 67, 67-80.
- Blatt, Y., Pecht, I.** (1979) Allosteric cooperative interactions among redox sites of *Pseudomonas* cytochrome oxidase. *Biochemistry* 18, 2917-2922.

- Blundell, T.L., Johnson, L.N.** (1994) Crystallization of proteins. In *Protein Crystallography 4. Edition*. Edited by Blundell, T.L., Johnson, L.N., pp. 59-82. Academic Press Inc., San Diego.
- Boltz, D.F., Taras, M.J.** (1978) Nitrogen. In *Colorimetric determination of nonmetals. Chemical analysis*. Edited by Boltz, D.F., Howell, J.A., Vol. 8, pp. 197-251. John Wiley & Sons Inc., New York, Chichester, Brisbane, Toronto.
- Boulanger, M.J., Murphy, M.E.P.** (2002) Crystal structure of the soluble domain of the major anaerobically induced outer membrane protein (AniA) from pathogenic *Neisseria*: a new class of copper-containing nitrite reductases. *J. Mol. Biol.* 315, 1111-1127.
- Brittain, T., Blackmore, R., Greenwood, C., Thomson, A.J.** (1992) Bacterial nitrite-reducing enzymes. *Eur. J. Biochem.* 209, 793-802.
- Brune, A., Frenzel, P., Cypionka, H.** (2000) Life at the oxic-anoxic interface: microbial activities and adaptations. *FEMS Microbiol. Rev.* 24, 691-710.
- Brünger, A.T.** (1992) Free R value: a novel statistical quantity for assessing the accuracy of crystal structures. *Nature* 355, 472-475.
- Brünger, A.T.** (1993) Assessment of phase accuracy by cross validation: the free R value. Methods and applications. *Acta Cryst. D* 49, 24-36.
- Brünger, A.T., Adams, P.D., Clore, G.M., DeLano, W.L., Gros, P., Grosse-Kunstleve, R.W., Jiang, J.S., Kuszewski, J., Nilges, M., Pannu, N.S., Read, R.J., Rice, L.M., Simonson, T., Warren, G.L.** (1998) Crystallography and NMR system: A new software suite for macromolecular structure determination. *Acta Cryst. D* 54, 905-921.
- Bruschi, M., Hatchikian, C.E., Golovleva, L.A., LeGall, J.** (1977) Purification and characterization of cytochrome c_3 , ferredoxin, and rubredoxin isolated from *Desulfovibrio desulfuricans* Norway. *J. Bacteriol.* 129, 30-38.
- Cammack, R.** (1992) Iron-sulfur clusters in enzymes: themes and variations. *Adv. Inorg. Chem.* 38, 281-322.
- Campbell, W.H.** (2001) Structure and function of eukaryotic NAD(P)H:nitrate reductase. *Cell Mol. Life Sci.* 58, 194-204.
- Cardinale, J.A., Clark, V.L.** (2000) Expression of AniA, the major anaerobically induced outer membrane protein of *Neisseria gonorrhoeae*, provides protection against killing by normal human sera. *Infect. Immun.* 68, 4368-4369.
- Cole, J.A.** (1968) Cytochrome c_{552} and nitrite reduction in *Escherichia coli*. *Biochim. Biophys. Acta* 162, 356-368.
- Cole, J.A., Brown, C.M.** (1980) Nitrite reduction to ammonia by fermentative bacteria: a short circuit in the biological nitrogen cycle. *FEMS Microbiol. Lett.* 7, 65-72.
- Cole J.A.** (1996) Nitrate reduction to ammonia by enteric bacteria: redundancy, or a strategy for survival during oxygen starvation? *FEMS Microbiol. Lett.* 136, 1-11.

- Collaborative Computational Project No. 4.** (1994) The CCP4 Suite: Programs for protein crystallography. *Acta Cryst. D* 50, 760-763.
- Conrad, R.** (1996) Soil microorganisms as controllers of atmospheric trace gases (H₂, CO, CH₄, OCS, N₂O, and NO). *Microbiol. Rev.* 60, 609-640.
- Costa, C., Moura, J.J.G., Moura, I., Liu, M.Y., Peck Jr., H.D., LeGall, J., Wang, Y., Huynh, B.H.** (1990) Hexaheme nitrite reductase from *Desulfovibrio desulfuricans*. Mössbauer and EPR characterization of the heme groups. *J. Biol. Chem.* 265, 14382-14388.
- Cotton, F.A., Wilkinson, G., Murillo, C.A., Bochman, M.** (1999) Advanced inorganic chemistry, 6th ed. Wiley Interscience, New York.
- Coyle, C.L., Zumft, W.G., Kroneck, P.M.H., Korner, H., Jakob, W.** (1985) Nitrous oxide reductase from denitrifying *Pseudomonas perfectomarina*. Purification and properties of a novel multicopper enzyme. *Eur. J. Biochem* 153, 459-467.
- Crane, B.R., Siegel, L.M., Getzoff, E.D.** (1995) Sulfite reductase structure at 1.6 Å - Evolution and catalysis for reduction of inorganic anions. *Science* 270, 59-67.
- Crane, B.R., Siegel, L.M., Getzoff, E.D.** (1997a) Probing the catalytic mechanism of sulfite reductase by X-ray crystallography: structures of the *Escherichia coli* hemoprotein in complex with substrates, inhibitors, intermediates, and products. *Biochemistry* 36, 12120-12137.
- Crane, B.R., Siegel, L.M., Getzoff, E.D.** (1997b) Structures of the siroheme- and Fe₄S₄-containing active center of sulfite reductase in different states of oxidation: heme activation via reduction-gated exogenous ligand exchange. *Biochemistry* 36, 12101-12119.
- Darwin, A., Hussain, H., Griffiths, L., Grove, J., Sambongi, Y., Busby, S., Cole, J.A.** (1993) Regulation and sequence of the structural gene for cytochrome *c*₅₅₂ from *Escherichia coli*: not a hexahaem but a 50 kDa tetrahaem nitrite reductase. *Mol. Microbiol.* 9, 1255-1265.
- Devol, A.H.** (2003) Nitrogen cycle: Solution to a marine mystery. *Nature* 422, 575-576.
- Dias, J.M., Cunha, C.A., Teixeira, S., Almeida, G., Costa, C., Lampreda, J., Moura, J.J.G., Moura, I., Romão, M.J.** (2000) Crystallization and preliminary X-ray analysis of a membrane-bound nitrite reductase from *Desulfovibrio desulfuricans* ATCC 27774. *Acta Crystallogr. Biol. Crystall.* 56, 215-217.
- Dodd, F.E., Hasnain, S.S., Abraham, Z.H.L., Eady, R.R., Smith, B.E.** (1997) Structures of a blue-copper nitrite reductase and its substrate-bound complex. *Acta Cryst. D* 53, 406-418.
- Drenth, J.** (1994) Principles of Protein X-ray Crystallography. Springer Verlag, Heidelberg.
- Einsle, O.** (1999) Structure and function of cytochrome *c* nitrite reductase. PhD thesis, Universität Konstanz, Konstanz.
- Einsle, O., Messerschmidt, A., Stach, P., Bourenkov, G.P., Bartunik, H.D., Huber, R., Kroneck, P.M.H.** (1999) Structure of cytochrome *c* nitrite reductase. *Nature* 400, 476-480.

- Einsle, O., Stach, P., Messerschmidt, A., Simon, J., Kröger, A., Huber, R., Kroneck, P.M.H. (2000) Cytochrome *c* nitrite reductase from *Wolinella succinogenes*. Structure at 1.6 Å resolution, inhibitor binding, and heme-packing motifs. *J. Biol. Chem.* 275, 39608-39616.
- Einsle, O., Foerster, S., Mann, K., Fritz, G., Messerschmidt, A., Kroneck, P.M.H. (2001) Spectroscopic investigation and determination of reactivity and structure of the tetraheme cytochrome *c*₃ from *Desulfovibrio desulfuricans* Essex 6. *Eur. J. Biochem.* 268, 3028-3035.
- Einsle, O., Stach, P., Messerschmidt, A., Klimmek, O., Simon, J., Kröger, A., Kroneck, P.M.H. (2002a) Crystallization and preliminary X-ray analysis of the membrane-bound cytochrome *c* nitrite reductase complex (NrfHA) from *Wolinella succinogenes*. *Acta Cryst. D.* 58, 341-342.
- Einsle, O., Messerschmidt, A., Huber, R., Kroneck, P.M.H., Neese, F. (2002b) Mechanism of the six-electron reduction of nitrite to ammonia by cytochrome *c* nitrite reductase. *J. Am. Chem. Soc.* 124, 11737-11745.
- Eisenmann, E., Beuerle, J., Sulger, K., Kroneck, P.M.H., Schumacher, W. (1995) Lithotrophic growth of *Sulfurospirillum deleyianum* with sulfide as electron donor coupled to respiratory reduction of nitrate to ammonia. *Arch. Microbiol.* 164, 180-185.
- Eaves, D.J., Grove, J., Staudenmann, W., James, P., Poole, R.K., White, S.A., Griffiths, I., Cole, J.A. (1998) Involvement of products of the *nrfEFG* genes in the covalent attachment of haem *c* to a novel cysteine-lysine motif in the cytochrome *c*₅₅₂ nitrite reductase from *Escherichia coli*. *Mol. Microbiol.* 28, 205-216.
- Faller, P., Goussias, C., Rutherford, A.W., Un, S. (2003) Resolving intermediates in biological proton-coupled electron transfer: a tyrosyl radical prior to proton movement. *PNAS* 100, 8732-8735.
- Finnegan, M.G., Lappin, A.G., Scheidt, W.R. (1990) Instability of the nitrite/iron(III) porphyrinate system. *Inorg. Chem.* 29, 181-185.
- Ferrer, J.C., Guillemette, J.G., Bogumil, R., Inglis, S.C., Smith, M., Mauk, A.G. (1993) Identification of Lys79 as an iron ligand in one form of alkaline yeast iso-1-ferricytochrome *c*. *J. Am. Chem. Soc.* 115, 7507-7508.
- Elliott, S.J., Hoke, K.R., Heffron, K., Palak, M., Rothery, R.A., Weiner, J.H., Armstrong, F.A. (2004) Voltammetric studies of the catalytic mechanism of the respiratory nitrate reductase from *Escherichia coli*: how nitrate reduction and inhibition depend on the oxidation state of the active site. *Biochemistry* 43, 799-807.
- Ensign, S.A., Hyman, M.R., Arp, D.J. (1993) In vitro activation of ammonia monooxygenase from *Nitrosomonas europaea* by copper. *J. Bacteriol.* 175, 1971-1980.
- Esnouf, R.M. (1999) Further additions to MolScript version 1.4, including reading and contouring of electron-density maps. *Acta Crystall. D* 55, 938-940.
- Farver, O., Kroneck, P.M.H., Zumft, W.G., Pecht, I. (2002) Intramolecular electron transfer in cytochrome *cd*₁ nitrite reductase from *Pseudomonas stutzeri*; kinetics and thermodynamics. *Biophys. Chem.* 98, 27-34.

- Farver, O., Kroneck, P.M.H., Zumft, W.G., Pecht, I.** (2003) Allosteric control of internal electron transfer in cytochrome *cd₁* nitrite reductase. *Proc. Natl. Acad. Sci. (USA)* 100, 7622-7625.
- Ferguson, S.J.** (1998) Nitrogen cycle enzymology. *Curr. Opin. Chem. Biol.* 2, 182-193.
- Foster, J.F., Sterman, M.D.** (1956) Conformation changes in bovine plasma albumin associated with hydrogen ion and urea binding. II. Hydrogen ion titration curves. *J. Am. Chem. Soc.* 78, 3656-3660.
- Frijlink, M.J., Abee, T., Laanbroek, H.J., de Boer, W., Konings, W.N.** (1992) The bioenergetics of ammonia and hydroxylamine oxidation in *Nitrosomas europaea* at acid and alkaline pH. *Arch. Microbiol.* 157, 194-199.
- Fritz, G., Griesshaber, D., Seth, O., Kroneck, P.M.H.** (2001) Nonaheme cytochrome *c*, a new physiological electron acceptor for [Ni,Fe] hydrogenase in the sulfate-reducing bacterium *Desulfovibrio desulfuricans* Essex: primary sequence, molecular parameters, and redox properties. *Biochemistry* 40, 1317-1324.
- Fujita, T.** (1966) Studies on soluble cytochromes in *Enterobacteriaceae*. I. Detection, purification, and properties of cytochrome *c₅₅₂* in anaerobically grown cells. *J. Biochem. (Tokyo)* 60, 204-215.
- Fülöp, V., Moir, J.W.B., Ferguson, S.J., Hajdu, J.** (1995) The anatomy of a bifunctional enzyme: structural basis for reduction of oxygen to water and synthesis of nitric oxide by cytochrome *cd₁*. *Cell* 81, 369-377.
- Gordon, E.H.J., Sjögren, T., Löfqvist, M., Richter, C.D., Allen, J.W.A., Higham, C.W., Hajdu, J., Fülöp, V., Ferguson, S.J.** (2003) Structure and kinetic properties of *Paracoccus pantotrophus* cytochrome *cd₁* nitrite reductase with the *d₁* heme active site ligand tyrosine 25 replaced by serine. *J. Biol. Chem.* 278, 11773-11781.
- Gray, H.B., Malmström, B.G., Williams, R.J.P.** (2000) Copper coordination in blue proteins. *J. Biol. Inorg. Chem.* 5, 551-559.
- Guex, N., Peitsch, M.C.** (1997) Swiss-Model and the Swiss-Pdb-Viewer: An environment for comparative protein modeling. *Electrophoresis* 18, 2714-2723.
- Harborne, N.R., Griffiths, L., Busby, S.J., Cole, J.A.** (1992) Transcriptional control, translation and function of the products of the five open reading frames of the *Escherichia coli* nir operon. *Mol. Microbiol.* 6, 2805-2813.
- Hendrich, M.P., Logan, M., Andersson, K.K., Arciero, D.M., Lipscomb, J.D., Hooper, A.B.** (1994) The active site of hydroxylamine oxidoreductase from *Nitrosomonas*: evidence for a new metal cluster in enzymes. *J. Am. Chem. Soc.* 116, 11961-11968.
- Hendrich, M.P., Petasis, D., Arciero, D.M., Hooper, A.B.** (2001) Correlations of structure and electronic properties from EPR spectroscopy of hydroxylamine oxidoreductase. *J. Am. Chem. Soc.* 123, 2997-3005.

- Heukeshoven, J., Dernick, R.** (1985) Simplified method for silver staining of proteins in polyacrylamide gels and mechanism of silver staining. *Electrophoresis* 6, 103-112.
- Hole, U.** (1996) Biochemische und molekularbiologische Aspekte der Denitrifikation bei *Thiobacillus denitrificans*. PhD thesis, Universität Konstanz, Konstanz.
- Hooper, A.B., Logan, M., Arciero, D.M., McTavish, H.** (1991) C-cytochromes of the ammonia-oxidizing chemolithoautotrophic bacteria. *Biochim. Biophys. Acta* 1058, 13-16.
- Hooper, A.B., Vannelli, T., Bergmann, D.J., Arciero, D.M.** (1997) Enzymology of the oxidation of ammonia to nitrite by bacteria. *Antonie van Leeuwenhoek* 71, 59-67.
- Howes, B.D., Feis, A., Raimondi, L., Indiani, C., Smulevich, G.** (2001) The critical role of the proximal calcium ion in the structural properties of horseradish peroxidase. *J. Biol. Chem.* 276, 40704-40711.
- Hussain, H., Grove, J., Griffiths, L., Busby, S., Cole, J.A.** (1994) A seven-gene operon essential for formate-dependent nitrite reduction to ammonia by enteric bacteria. *Mol. Microbiol.* 12, 153-163.
- Igarashi, N., Moriyama, H., Fujiwara, T., Fukumori, Y., Tanaka, N.** (1997) The 2.8 Å structure of hydroxylamine oxidoreductase from a nitrifying chemoautotrophic bacterium, *Nitrosomonas europaea*. *Nat. Struct. Biol.* 4, 276-284.
- Jackson, R.H., Cornish-Bowden, A., Cole, J.A.** (1981) Prosthetic groups of the NADH-dependent nitrite reductase from *Escherichia coli* K12. *Biochem. J.* 193, 861-867.
- Jafferi, A., Allen, J.W.A., Ferguson, S.J., Fülöp, V.** (2000) X-ray crystallographic study of cyanide binding provides insights into the structure-function relationship for cytochrome *cd₁* nitrite reductase from *Paracoccus pantotrophus*. *J. Biol. Chem.* 275, 25089-25094.
- Jones, K.** (1973) Nitrogen. In *Comprehensive Inorganic Chemistry*. Edited by Bailar, J.C., Emeléus, H.J., Sir Nyholm, R., Trotman-Dickenson, A.F., Vol. 2, pp. 147-388. Pergamon Press, Oxford, New York, Toronto, Sydney, Braunschweig.
- Jones, T., Zou, J., Cowan, S., Kjeldgaard, M.** (1998) Improved methods for building protein models in electron-density maps and the location of errors in these models. *Acta Cryst.* A47, 110-119.
- Jormakka, M., Törnroth, S., Byrne, B., Iwata, S.** (2002) Molecular basis of proton motive force generation: structure of formate dehydrogenase-N. *Science* 295, 1863-1868.
- Jormakka, M., Byrne, B., Iwata, S.** (2003) Formate dehydrogenase - a versatile enzyme in changing environments. *Curr. Opin. Struct. Biol.* 13, 418-423.
- Jormakka, M., Richardson, D., Byrne, B., Iwata, S.** (2004) Architecture of NarGH reveals a structural classification of Mo-bisMGD enzymes. *Structure* 12, 95-104.
- Kabsch, W.** (1993) Automatic processing of rotation diffraction data from crystals of initially unknown symmetry and cell constants. *J. Appl. Cryst.* 26, 795-800.

- Kahn, O.** (1993) Molecular Magnetism. 1st Edition, VCH, Weinheim.
- Kaim, W., Schwederski, B.** (1995) Bioanorganische Chemie. 2nd Edition, B.G. Teubner Verlag, Stuttgart.
- Kim, Y.O., Goff, H.M.** (1990) Characterization of ammonia-ligated low-spin iron(III) porphyrin complexes. *Inorg. Chem.* 29, 3907-3908.
- Kim, K.R., Craig, H.** (1993) Nitrogen-15 and oxygen-18 characteristics of nitrous oxide: a global perspective. *Science* 262, 1855-1857.
- Kisker, C., Schindelin, H., Baas, D., Rétey, J., Meckenstock, R.U., Kroneck, P.M.H.** (1998) A structural comparison of molybdenum cofactor-containing enzymes. *FEMS Microbiol. Rev.* 22, 503-521.
- Kobayashi, K., Koppenhöfer, A., Ferguson, S.J., Tagawa, S.** (1997) Pulse radiolysis studies on cytochrome *cd₁* nitrite reductase from *Thiosphaera pantotropha*: evidence for a fast intramolecular electron transfer from *c*-heme to *d₁*-heme. *Biochemistry* 36, 13611-13616.
- Kroneck, P.M.H., Zumpft, W.G.** (1990) Bio-inorganic aspects of denitrification: structures and reactions of N_xO_y compounds and their interaction with iron and copper proteins. in *Denitrification in Soil and Sediment* (N.P. Revsbech and J Sørensen, eds.) Plenum Press, New York and London, 1-20.
- Kroneck, P.M.H., Beuerle, J., Schumacher, W.** (1992) Metal-dependent conversion of inorganic nitrogen and sulfur compounds. in *Metal Ions in Biological Systems* (H. Sigel and A. Sigel, eds.) M. Dekker Inc., New York, Basel, Hong Kong, Vol. 28, 455-505.
- Kroneck, P.M.H., Abt, D.J.** (2002) Molybdenum in nitrate reductase and nitrite oxidoreductase. in *Metal Ions in Biological Systems* (H. Sigel and A. Sigel, eds.) M. Dekker Inc., New York, Basel, Vol. 39, 369-403.
- LaCroix, L., Shadle, S.E., Wang, Y., Averill, B.A., Hedman, B., Hodgson, K.O. Solomon, E.I.** (1996) Electronic structure of the perturbed blue copper site in nitrite reductase: spectroscopic properties, bonding, and implications for the entatic/rack state. *J. Am. Chem. Soc.* 118, 7755-7768.
- Laemmli, U.K.** (1970) Cleavage of structural proteins during the assembly of the head of bacteriophage T4. *Nature* 227, 680-685.
- Lanzilotta, W., Schuller, D.J., Thorsteinsson, M.V., Kerby, R.L., Roberts, G.P., Poulos, T.L.** (2000) Structure of the CO sensing transcription activator CoxA. *Nature Struct. Biol.* 7, 876-880.
- Leslie, A.** (1991) in *Crystallographic computing V* (Moras, D., Podjarny, A.D., Thierry, J.C., eds.), Oxford University Press, Oxford, 27-38.
- Lindqvist-Reis, P., Lamble, K., Pattanaik, S., Persson, I., Sandström, M.** (2000) Hydration of the Y(III) ion in aqueous solution. An X-ray diffraction and XAFS structural study. *J. Phys. Chem. B* 104, 402-408.

- Liu, M.-C., Liu, M.-Y., Payne, W.J., Peck Jr., H.D., LeGall, J., DerVartanian, D.V.** (1987) Comparative EPR studies on the nitrite reductases from *Escherichia coli* and *Wolinella succinogenes*. *FEBS Lett.* 218, 227-230.
- Liu, M.C., Costa, C., Coutinho, I.B., Moura, J.J.G., Moura, I., Xavier, A.V., LeGall, J.** (1988) Cytochrome components of nitrate- and sulfate-respiring *Desulfovibrio desulfuricans* ATCC 27774. *J. Bacteriol.* 170, 5545-5551.
- Lin, J.T., Stewart, V.** (1998) Nitrate assimilation by bacteria. *Adv. Microb. Physiol.* 39, 1-30.
- Louro, R.O., deWaal, E.C., Ubbink, M., Turner, D.L.** (2002) Replacement of the methionine axial ligand in cytochrome *c*₅₅₀ by a lysine: effects on the haem electronic structure. *FEBS Letters* 510, 185-188.
- Makinen, M.W., Schichman, S.A., Hill, S.C., Gray, H.B.** (1983) Heme-heme orientation and electron transfer kinetic behavior of multisite oxidation-reduction enzymes. *Science* 222, 929-931.
- Margoliash, E., Frohwirt, N.** (1959) Spectrum of horse heart cytochrome *c*. *Biochem. J.* 71, 570-572.
- Martinez, S.E., Huang, D., Szczepaniak, A., Cramer, W.A., Smith, J.L.** (1994) Crystal structure of chloroplast cytochrome *f* reveals a novel cytochrome fold and unexpected heme ligation. *Structure* 2, 95-105.
- Massa, W.** (1994) Kristallstrukturbestimmung. Teubner Studienbücher: Chemie, Stuttgart.
- Massey, V., Hemmerich, P.** (1977) A photochemical procedure for reduction of oxidation-reduction proteins employing deazariboflavin as catalyst. *J. Biol. Chem.* 252, 5612-5614.
- Matias, P.M., Morias, J., Coelho, A.V., Meijers, R., Gonzales, A., Thompson, A.W., Sieker, L., Legall, J., Carrondo, M.A.** (1997) A preliminary analysis of the three-dimensional structure of dimeric di-haem split-Soret cytochrome *c* from *Desulfovibrio desulfuricans* ATCC 27774 at 2.5Å resolution using the MAD phasing method - a novel cytochrome fold with a stacked-haem arrangement. *J. Biol. Inorg. Chem.* 2, 507-514.
- Mayhew, S.G.** (1978) The redox potential of dithionite and SO₂⁻ from equilibrium reactions with flavodoxins, methyl viologen and hydrogen plus hydrogenase. *Eur. J. Biochem.* 85, 535-547.
- McPherson, A.** (1982) Preparation and analysis of protein crystals. Wiley & Sons Inc., New York.
- McRee, D.E.** (1993) Practical Protein Crystallography. Academic Press Inc., San Diego.
- Merritt, E.A., Bacon, D.J.** (1997) Raster3D: Photorealistic molecular graphics. *Meth. Enzymol.* 277, 505-524.
- Mitchell, G.J., Jones, J.G., Cole, J.A.** (1986) Distribution and regulation of nitrate and nitrite reduction by *Desulfovibrio* and *Desulfotomaculum* species *Arch. Microbiol.* 144, 35-40.

- Mitra, S.** (1983) Magnetic susceptibility of iron porphyrins. In *Iron porphyrins part two*. Edited by Lever, A.B.P., Gray, H.B., pp. 1-42. Addison-Wesley Publishing Company, London, Amsterdam, Don Mills/Ontario, Sydney, Tokio.
- Morel, F.M.M., Price, N.M.** (2003) The biogeochemical cycles of trace metals in the oceans. *Science* 300, 944-947.
- Moreno-Vivián, C., Cabello, P., Martínez-Luque, M., Blasco, R., Castello, F.** (1999) Prokaryotic nitrate reduction: molecular properties and functional distinction among bacterial nitrate reductases. *J. Bacteriol.* 181, 6573-6584.
- Moura, I., Bursakov, S., Costa, C., Moura, J.J.G.** (1997) Nitrate and nitrite utilization in sulfate-reducing bacteria. *Anaerobe* 3, 279-290.
- Moura, I., Moura, J.J.G.** (2001) Structural aspects of denitrifying enzymes. *Curr. Opin. in Chem. Biol.* 5, 168-175.
- Murphy, M.E.P., Lindley, P.F., Adman, E.T.** (1997) Structural comparison of cupredoxin domains: domain recycling to construct proteins with novel functions. *Prot. Sci.* 6, 761-770.
- Murphy, L.M., Dodd, F.E., Yousafzai, F.K., Eady, R.R., Hasnain, S.S.** (2002) Electron donation between copper containing nitrite reductases and cupredoxins: the nature of protein-protein interaction in complex formation. *J. Mol. Biol.* 315, 859-871.
- Naik, R.R., Murillo, F.M., Stolz, J.F.** (1993) Evidence for a novel nitrate reductase in the dissimilatory iron-reducing bacterium *Geobacter metallireducens*. *FEMS Microbiol. Lett.* 106, 53-58.
- Nath, U.** (1996) Spektroskopische (EPR) Untersuchungen an dem Tetrahämprotein Cytochrom *c* Nitritreduktase aus *Sulfurospirillum deleyianum*. Master thesis, Universität Konstanz, Konstanz.
- Neese, F.** (1995) The program EPR, Quantum Chemistry Program Exchange. Bulletin 15:5.
- Newman, D.K., Banfield, J.F.** (2002) Geomicrobiology: how molecular-scale interactions underpin biogeochemical systems. *Science* 296, 1071-1077.
- Nurizzo, D., Silvestrini, M.C., Mathieu, M., Cutruzzola, F., Bougeois, D., Fülöp, V., Hajdu, J., Brunori, M., Tegoni, M., Cambillau, C.** (1997) N-terminal arm exchange is observed in the 2.15 Å crystal structure of oxidized nitrite reductase from *Pseudomonas aeruginosa*. *Structure* 5, 1157-1171.
- Oganesyan, V.S., Butler, C.S., Watmough, N.J., Greenwood, C., Thomson, A.J., Cheesman, M.R.** (1998) Nature of the coupling between the high-spin Fe(III) heme and Cu_B(II) in the active site of terminal oxidases: dual-mode EPR spectra of fluoride cytochrome *bo*₃. *J. Am. Chem. Soc.* 120, 4232-4233.
- Ogura, H., Yatsunyk, L., Medforth, C.J., Smith, K.M., Barkigia, K.M., Renner, M.W., Melamed, D., Walker, F.A.** (2001) Molecular structures and magnetic resonance spectroscopic investigations of highly distorted six-coordinated low-spin iron(III) porphyrinate complexes. *J. Am. Chem. Soc.* 123, 6564-6578.

- Oremland, R.S., Stolz, J.F.** (2003) The ecology of arsenic. *Science* 300, 939-944.
- Palmer, G.** (1983) Electron paramagnetic resonance of hemoproteins. In *Iron prophyrins part two*. Edited by Lever, A.B.P., Gray, H.B., pp. 43-88. Addison-Wesley Publishing Company, London, Amsterdam, Don Mills/Ontario, Sydney, Tokio.
- Parkhill J., Wren, B.W., Mungall, K., Ketley, J.M., Churcher, C., Basham, D., Chillingworth, T., Davies, R.M., Feltwell, T., Holroyd, S., Jagels, K., Karlyshev, A.V., Moule, S., Pallen, M.J., Penn, C.W., Quail, M.A., Rajandream, M.A., Rutherford, K.M., van Vliet, A.H., Whitehead, S., Barrell, B.G.** (2000) The genome sequence of the food-borne pathogen *Campylobacter jejuni* reveals hypervariable sequences. *Nature* 403, 665-668.
- Parr, S.R., Barber, D., Greenwood, C., Brunori, M.** (1977) The electron-transfer reaction between azurin and the cytochrome *c* oxidase from *Pseudomonas aeruginosa*. *J. Biochem.* 167, 447-455.
- Peck Jr., H.D., Deacon, T.E., Davidson, J.T.** (1965) Studies on adenosine 5'-phosphosulfate reductase from *Desulfovibrio desulfuricans* and *Thiobacillus thioparus*. *Biochim. Biophys. Acta* 96, 429-446.
- Pereira, I.A.C., LeGall, J., Xavier, A.V., Teixeira, M.** (2000) Characterization of a heme *c* nitrite reductase from a non-ammonifying microorganism, *Desulfovibrio vulgaris* Hildenborough. *Biochim. Biophys. Acta* 1481, 119-130.
- Pettigrew, G.W., Moore, G.R.** (1987) Cytochromes *c*. Biological aspects. Springer-Verlag, Berlin, Heidelberg, New York, London, Paris, Tokyo.
- Pilbrow, J.R.** (1990) Transition ion electron paramagnetic resonance. Clarendon Press, Oxford.
- Pisa, R., Stein, T., Eichler, R., Gross, R., Simon, J.** (2002) The *nrfl* gene is essential for the attachment of the active site haem group of *Wolinella succinogenes* cytochrome *c* nitrite reductase. *Mol. Microbiol.* 43, 763-770.
- Pisa, R.** (2004) Untersuchungen zur Biogenese und zum Katalysemechanismus der Cytochrom *c*-Nitrit-Reduktase von *Wolinella succinogenes*. PhD thesis, Johann-Wolfgang-Goethe Universität, Frankfurt.
- Reysenbach, A.L., Shock, E.** (2002) Merging genomes with geochemistry in hydrothermal ecosystems. *Science* 296, 1077-1082.
- Ribeiro, J.M.C., Hazzard, J.M.H., Nussenzveig, R.H., Champagne, D.E., Walker, F.A.** (1993) Reversible binding of nitric oxide by a salivary heme protein from a bloodsucking insect. *Science* 260, 539-541.
- Richardson, D.J., Watmough, N.J.** (1999) Inorganic nitrogen metabolism in bacteria. *Curr. Opin. Chem. Biol.* 3, 207-219.
- Richardson, D.J.** (2000) Bacterial respiration: a flexible process for a changing environment. *Microbiol.* 146, 551-571.

- Richardson, D.J.** (2001) Introduction: nitrate reduction and the nitrogen cycle. *Cell. Mol. Life Sci.* 58, 163-164.
- Richardson, D.J., Berks, B.C., Russell, D.A., Spiro, S., Taylor, C.J.** (2001) Functional, biochemical and genetic diversity of prokaryotic nitrate reductases. *Cell. Mol. Life Sci.* 58, 165-178.
- Roberts, S.A., Weichsel, A., Qiu, Y., Shelnutt, J.A., Walker, F.A., Montfort, W.R.** (2001) Ligand-induced heme ruffling and bent no geometry in ultra-high-resolution structures of nitrophorin 4. *Biochemistry* 40, 11327-11337.
- Rossell, F.I., Ferrer, J.C., Mauk, A.G.** (1998) Proton-linked protein conformational switching: definition of the alkaline conformational transition of yeast iso-1-ferricytochrome *c*. *J. Am. Chem. Soc.* 120, 11234-11245.
- Rowlands, C.C., Murphy, D.M.** (1999) EPR spectroscopy, theory. Academic Press.
- Rudolf, M., Einsle, O., Neese, F., Kroneck, P.M.H.** (2002) Pentahaem cytochrome *c* nitrite reductase: reaction with hydroxylamine, a potential reaction intermediate and substrate. *Biochem. Soc. Trans.* 30, 649-653.
- Rudolf, M., Kroneck, P.M.H.** (2005) The nitrogen cycle. in *Metal Ions in Biological Systems* (H. Sigel and A. Sigel, eds.) M. Dekker Inc., New York, Basel, Hong Kong, Vol. 43.
- Sadana, J.C., Khan, B.M., Fry, I.V., Cammack, R.** (1986) Electron paramagnetic resonance studies of heme *c* and its nitrosyl derivative in *Vibrio (Achromobacter) fischeri* nitrite reductase. *Biochem. Cell. Biol.* 64, 394-399.
- Schichman, S.A., Gray H.B.** (1981) Kinetics of the anaerobic reduction of ferricytochrome *cd*₁ by Fe(EDTA)²⁻. Evidence for bimolecular and intramolecular electron transfer to the *d*₁ hemes. *J. Am. Chem. Soc.* 103, 7794-7795.
- Schumacher, W.** (1993) Dissimilatorische Reduktion von Nitrat zu Ammoniak. Ph.D. Thesis, Universität Konstanz, Konstanz.
- Schumacher, W., Neese, F., Hole, U., Kroneck, P.M.H.** (1997) Cytochrome *c* nitrite reductase and nitrous oxide reductase; two metalloenzymes of the nitrogen cycle with novel metal sites. in *Transition Metals in Microbial Metabolism* (G. Winkelmann and C.J. Carrano, eds.) Harwood Academic, Amsterdam, 329-356.
- Silvestrini, M.C., Tordi, M.G., Musci, G., Brunori, M.** (1990) The reaction of *Pseudomonas* nitrite reductase and nitrite. A stopped-flow and EPR study. *J. Biol. Chem* 265, 11783-11787.
- Simon, J., Gross, R., Einsle, O., Kroneck, P.M.H., Kröger, A., Klimmek O.** (2000) A NapC/NirT-type cytochrome *c* (NrfH) is the mediator between the quinone pool and the cytochrome *c* nitrite reductase of *Wolinella succinogenes*. *Mol. Microbiol.* 35, 686-696.
- Simon, J., Pisa, R., Stein, T., Eichler, R., Klimmek, O., Gross, R.** (2001) The tetraheme cytochrome *c* NrfH is required to anchor the cytochrome *c* nitrite reductase (NrfA) in the membrane of *Wolinella succinogenes*. *Eur. J. Biochem.* 268, 5776-5782.

- Simon, J.** (2002) Enzymology and bioenergetics of respiratory nitrite ammonification. *FEMS Microbiol. Rev.* 26, 285-309.
- Smil, V.** (1997) Cycles of life: civilization and the biosphere. Scientific American Library, W.H. Freeman and Company, New York.
- Smith, P.K., Krohn, R.I., Hermanson, G.T., Mallia, A.K., Gartner, F.H., Provenzano, M.D., Fujimoto, E.K., Goeke, N.M., Olson, B.J., Klenk, D.C.** (1985) Measurement of protein using bicinchoninic acid. *Anal. Biochem.* 150, 76-85.
- Sprent, J.I.** (1987) The ecology of the nitrogen cycle. Cambridge University Press, Cambridge.
- Stach, P., Einsle, O., Schumacher, W., Kurun, E., Kroneck, P.M.H.** (2000) Bacterial cytochrome *c* nitrite reductase: new structural and functional aspects. *J. Inorg. Biochem.* 79, 381-385.
- Stach, P.** (2001) Cytochrome *c* nitrite reductase: nature's machine for the six-electron reduction of nitrite to ammonia. PhD thesis, Universität Konstanz, Konstanz.
- Steinbach, A.K.** (2001) Kinetische Untersuchungen an der Nitritreduktase aus *Sulfurospirillum deleyianum*. Master thesis, Universität Konstanz, Konstanz.
- Sticht, H., Rösch, P.** (1998) The structure of iron-sulfur proteins. *Prog. Biophys. Mol. Biol.* 70, 95-136.
- Stolz, J.F., Basu P.** (2002) Evolution of nitrate reductase: molecular and structural variations on a common function. *ChemBiochem* 3, 198-206.
- Strous, M., Fuerst, J.A., Kramer, E.H., Logemann, S., Muyzer, G., van de Pas-Schoonen, K.T., Webb, R., Kuenen, J.G., Jetten, M.S.** (1999) Missing lithotroph identified as new planctomycete. *Nature* 400, 446-449.
- Stubbe, J., van der Donk, W.A.** (1998) Protein radicals in enzyme catalysis. *Chem. Rev.* 98, 705-762.
- Sundermeyer-Klinger, H., Meyer, W., Warninghoff, B., Bock, E.** (1984) Membrane-bound nitrite oxidoreductase of *Nitrobacter*: evidence for a nitrate reductase system. *Arch. Microbiol.* 149, 153-158.
- Suzuki, S., Kataoka, K., Yamaguchi, K.** (2000) Metal coordination and mechanism of multicopper nitrite reductase. *Acc. Chem. Res.* 33, 728-735.
- Swartz, H.M., Bolton, J.R., Borg, D.C.** (1972) Biological applications of electron spin resonance. Wiley & Sons Inc., New York, London, Sydney, Toronto.
- Thauer, R.K., Jungermann, K., Decker, K.** (1977) Energy conservation in chemotrophic anaerobic bacteria. *Bacteriol. Rev.* 41, 100-180.

- Ubbink, M., Beeumen, J.V., Canters, G.W.** (1992) Cytochrome c_{550} from *Thiobacillus versutus*: cloning, expression in *Escherichia coli*, and purification of the heterologous holoprotein. *J. Bacteriol.* 174, 3707-3714.
- Ubbink, M., Campos, A.P., Teixeira, M., Hunt, N.I., Hill, H.A.O., Canters, G.W.** (1994) Characterization of mutant Met100Lys of cytochrome c_{550} from *Thiobacillus versutus* with lysine-histidine heme ligation. *Biochemistry* 33, 10051-10059.
- Upadhyay, A.K., Petasis, D.T., Arciero, D.M., Hooper, A.B., Hendrich, M.P.** (2003) Spectroscopic characterization and assignment of reduction potentials in the tetraheme cytochrome c_{554} from *Nitrosomonas europaea*. *J. Am. Chem. Soc.* 125, 1738-1747.
- Walker, F.A.** (1999) Magnetic spectroscopy (EPR, ESEEM, Mössbauer, MCD and NMR) studies of low-spin ferriheme centers and their corresponding heme proteins. *Coord. Chem. Rev.* 185-186, 471-534.
- Walker, F.A.** (2004) Models of the bis-histidine-ligated electron-transferring cytochromes. Comparative geometric and electronic structure of low-spin ferro- and ferrihemes. *Chem Rev.* 104, 589-615.
- Weil, J.A., Bolton, J.R., Wertz, J.E.** (1994) Electron paramagnetic resonance: elementary theory and practical applications. Wiley & Sons Inc., New York, Chichester, Brisbane, Toronto, Singapore.
- Whittaker, M., Bergmann, D., Arciero, D.M., Hooper, A.B.** (2000) Electron transfer during the oxidation of ammonia by the chemolithotrophic bacterium *Nitrosomonas europaea*. *Biochim. Biophys. Acta* 1459, 346-355.
- Wieghardt, K.** (1984) Mechanistic studies involving hydroxylamine. *Adv. Inorg. Bioinorg. Mech.* 3, 213-274.
- Widdel, F.** (1986) Growth of methanogenic bacteria in pure culture with 2-propanol and other alcohols as hydrogen donor. *Appl. Environ. Microbiol.* 51, 1056-1062.
- Williams, P.A., Fülöp, V., Leung, Y.C., Chan, C., Moir, J.W.B., Howlett, G., Ferguson, S.J., Radford, S.E., Hajdu, J.** (1995) Pseudospecific docking surfaces on electron transfer proteins as illustrated by pseudoazurin, cytochrome c_{550} and cytochrome cd_1 nitrite reductase. *Nature Struct. Biol.* 2, 975-982.
- Williams, P.A., Fülöp, V., Garman, E.F., Saunders, N.F., Ferguson, S.J., Hajdu, J.** (1997) Haem-ligand switching during catalysis in crystals of a nitrogen-cycle enzyme. *Nature* 389, 406-412.
- Wood, P.M.** (1984) Bacterial proteins with CO-binding *b*- or *c*-type haem. Functions and absorption spectroscopy. *Biochim. Biophys. Acta* 768, 293-317.
- Yatsunyk, L.A., Carducci, M.D., Walker, F.A.** (2003) Low-spin ferriheme models of the cytochromes: correlation of molecular structure with EPR spectral type. *J. Am. Chem. Soc.* 125, 15986-16005.

- Ye, R.W., Thomas, S.M.** (2001) Microbial nitrogen cycles: physiology, genomics and applications. *Curr. Opin. Microbiol.* 4, 307-312.
- Zarowny, D.P., Sanwal, B.D.** (1963) Characterization of a nicotinamide adenine dinucleotide specific nitrite reductase from *Escherichia coli*, strain K12. *Can. J. Microbiol.* 9, 531-539.
- Zehnder, A.J.B., Wuhrmann, K.** (1976) Titanium(III) citrate as a nontoxic oxidation-reduction buffering system for the culture of obligate anaerobes. *Science* 194, 1165-1166.
- Zehr, B.D., Savin, T.J., Hall, R.E.** (1989) A one-step, low background Coomassie staining procedure for polyacrylamide gels. *Anal. Biochem.* 182, 157-159.
- Zumft, W.G.** (1997) Cell biology and molecular basis of denitrification. *Microbiol. Mol. Biol. Rev.* 61, 533-616.

6 Appendix

6.1 Abbreviations

Å	Ångström; $1 \text{ Å} = 10^{-10} \text{ m}$
Anammox	anaerobe ammonium oxidation
ATP	adenosine-5'-triphosphate
BCA	bicinchoninic acid
BSA	bovine serum albumin
ccNir	cytochrome <i>c</i> nitrite reductase
ccNirWT	cytochrome <i>c</i> nitrite reductase wild-type
ccNirK134H	cytochrome <i>c</i> nitrite reductase K134H variant
ccNirQ276E	cytochrome <i>c</i> nitrite reductase Q276E variant
ccNirY218F	cytochrome <i>c</i> nitrite reductase Y218F variant
ccNirStopI	cytochrome <i>c</i> nitrite reductase StopI variant
cd ₁ Nir	cytochrome <i>cd</i> ₁ nitrite reductase
Da	Dalton; $1 \text{ Da} = 1 \text{ g/mol}$
DMSO	dimethyl sulfoxide
DNase I	deoxyribonuclease I
EPR	electron paramagnetic resonance
HAO	hydroxylamine oxidoreductase
HEPES	N-(2-hydroxyethyl)piperazine-N'-(ethane sulfonic acid)
h.s.	high-spin
ICP-MS	inductively coupled plasma mass spectrometry
l.s.	low-spin
MGD	bismolybdopterin guanine dinucleotide
NADH	nicotinamide adenine dinucleotide
Nap	periplasmic dissimilatory nitrate reductase
Nar	membrane bound nitrate reductase

Nas	cytoplasmic assimilatory nitrate reductase
Nir	nitrite reductase
N-MHA	N-methylhydroxylamine
NMR	nuclear magnetic resonance
<i>nrf</i>	nitrite reduction with formate
NrfA	monomeric nitrite reductase
NrfA _S	monomeric nitrite reductase from soluble fraction
NrfA _M	monomeric nitrite reductase from membrane fraction
NrfHA	heterooligomeric nitrite reductase complex
OD	optical density
PAGE	polyacrylamide gel electrophoresis
PEG	polyethylene glycol
ppb	parts per billion
r.m.s.d.	root-mean-square deviation
SDS	sodium dodecylsulfate
SQUID	superconducting quantum interference device
TRIS	tris-(hydroxymethyl)-aminomethane
UV-Vis	ultraviolet-visible
v/v	volume per volume
w/v	weight per volume

6.2 Amino Acids

A	Ala	alanine	M	Met	methionine
B	Asx	Asn or Asp	N	Asn	asparagine
C	Cys	cysteine	P	Pro	proline
D	Asp	aspartic acid	Q	Gln	glutamine
E	Glu	glutamic acid	R	Arg	arginine
F	Phe	phenylalanine	S	Ser	serine
G	Gly	glycine	T	Thr	threonine
H	His	histidine	V	Val	valine
I	Ile	isoleucine	W	Trp	tryptophan
K	Lys	lysine	Y	Tyr	tyrosine
L	Leu	leucine	Z	Glx	Gln or Glu

6.3 Curriculum Vitae

Personal data

Name Marc Rudolf
born April 13th, 1977 in Jena, Germany

Education

1995 Abitur, Ernst Haeckel Gymnasium, Jena, Germany
1995-1996 Service at Deutsches Rotes Kreuz, Jena, Germany
1996-2000 Studies of chemistry/environmental chemistry, Universität Jena, Germany
2000-2001 Diploma thesis in chemistry, Universität Jena, Germany: “Dinukleare Eisen(II)-Komplexe dreizähliger Schiffischer Basen: Struktur, magnetisches Verhalten und Reaktivität”, supervisor Prof. E.G. Jäger
2001-2004 Ph.D. thesis, Universität Konstanz, Germany: “Cytochrome *c* nitrite reductase: further investigations of the multiheme enzyme by X-ray crystallography, site-directed mutagenesis, and EPR spectroscopy”, supervisor Prof. P.M.H. Kroneck

Courses and working experiences

1998-2000 Lab assistant at the Otto-Schott-Institut für Glaschemie, Universität Jena, Germany
2001-2001 Lab assistant at the Institut für Anorganische und Analytische Chemie, Universität Jena, Germany
 Tutoring of a chemistry lab course
2001 102nd BASF Summer Course, BASF, Ludwigshafen, Germany
2002 CW-EPR Training Course, Bruker, Rheinfelden, Germany
2002 Bioanalytic Workshop, Analytik Jena, Jena, Germany
2002 FEBS/EU Course, Université Catholique de Louvain, Louvain la Neuve, Belgium
2003 Protein purification workshop, Amersham Bioscience, Universität Konstanz, Germany

6.4 Publications

M. Rudolf (2001): Dinukleare Eisen(II)-Komplexe dreizähliger Schiffischer Basen: Struktur, magnetisches Verhalten und Reaktivität. Diplomarbeit, Universität Jena.

E.G. Jäger, G. Leibelng, M. Rudolf, H. Görls (2001): Bioinspired iron(II/III) complexes and molecule-based magnets. *Journal of Inorganic Biochemistry*, **86**, 277.

M. Rudolf, O. Einsle, F. Neese, P.M.H. Kroneck (2002): Pentahaem cytochrome *c* nitrite reductase: reaction with hydroxylamine, a potential intermediate and substrate. *Biochem. Soc. Trans.*, **30**, 649.

M. Rudolf, P.M.H. Kroneck (2005): The Nitrogen Cycle. Its Biology. (in *Metals Ions in Biological Systems, Vol. 43: Biogeochemical Cycles*, A. Sigel, H. Sigel, R.K.O. Sigel, Eds.), **submitted**.

M. Rudolf, G. Leibelng, H. Görls (2004): Iron(II) complexes of tridentate Schiff bases: synthesis, magnetic measurements and X-ray analysis. *Inorg. Chem.*, **in preparation**.

M. Rudolf, R. Pisa, A. Messerschmidt, J. Simon, P.M.H. Kroneck (2004): Probing the active site of cytochrome *c* nitrite reductase from *W. succinogenes* by mutagenesis, EPR spectroscopy and X-ray crystallography: properties of the K134H protein variant. *Biochem. Biophys. Res. Comm.*, **in preparation**.

M. Rudolf, R. Pisa, A. Messerschmidt, J. Simon, P.M.H. Kroneck (2004): Probing the active site of cytochrome *c* nitrite reductase from *W. succinogenes* by site directed mutagenesis, EPR spectroscopy and X-ray crystallography. *J. Biol. Chem.*, **in preparation**.

6.5 Conference Abstracts

- 2001 **E.G. Jäger, G. Leibel, M. Rudolf, H. Görls**: Bioinspired transition metal chelate complexes and molecule based magnets. 10th International Conference on Bioinorganic Chemistry (ICBIC 10), Firenze, Italy.
- 2002 **E.G. Jäger, G. Leibel, M. Rudolf, B. Weber**: Molecular magnets based on bioinspired transition metal chelate complexes. Colloquium 'Molecular Magnets', Eltville, Germany.
- 2002 **E.G. Jäger, G. Leibel, M. Rudolf, H. Görls**: Bioinspired metal complexes as catalysts and molecule based magnets. 2nd Symposium 'Metal Mediated Reaction after Nature', Jena, Germany.
- 2002 **M. Rudolf, O. Einsle, F. Neese, P.M.H. Kroneck**: Studies on the mechanism of cytochrome *c* nitrite reductase. VAAM Meeting, Göttingen, Germany.
- 2002 **M. Rudolf, P.M.H. Kroneck**: Novel aspects on cytochrome *c* nitrite reductase, interaction with hydroxylamine and magnetic properties. FEBS/EU Advanced Course 'Metals in Biological Systems', Louvain-la-Neuve, Belgium.
- 2003 **E.G. Jäger, C. Michael, M. Rudolf, A. Schütz, R. Wegner**: Oligonukleare Übergangsmetallkomplexe als bioanaloge Aktivzentren für Redoxreaktionen. Colloquium to Sonderforschungsbereich 436 (SFB 436), Jena, Germany.
- 2003 **M. Rudolf, R. Pisa, A. Messerschmidt, J. Simon, P.M.H. Kroneck**: Probing the active site of cytochrome *c* nitrite reductase by site directed mutagenesis, spectroscopy and X-ray crystallography. Colloquium 'Bioenergetics of Microorganisms', Oberreifenberg, Germany.
- 2003 **M. Rudolf, R. Pisa, A. Messerschmidt, J. Simon, P.M.H. Kroneck**: Probing the active site of cytochrome *c* nitrite reductase from *Wolinella succinogenes* by site directed mutagenesis, spectroscopy and X-ray crystallography. VAAM Meeting, Berlin, Germany.

- 2003 **M. Rudolf, R. Pisa, A. Messerschmidt, J. Simon, P.M.H. Kroneck:** Cytochrome *c* nitrite reductase: nature`s machine for the six-electron reduction of nitrite to ammonia. Symposium VW-Stiftung, Walberberg, Germany.
- 2004 **M. Rudolf, R. Pisa, A. Messerschmidt, J. Simon, P.M.H. Kroneck:** Probing the active site of cytochrome *c* nitrite reductase from *Wolinella succinogenes* by site directed mutagenesis, spectroscopy and X-ray crystallography. VAAM Meeting, Braunschweig, Germany.

7 Acknowledgment

Die vorliegende Arbeit entstand im Zeitraum von Oktober 2001 bis August 2004 in der Arbeitsgruppe für Bioanorganische Chemie an der Universität Konstanz.

Mein besonderer Dank geht an Prof. Dr. Peter M.H. Kroneck, Universität Konstanz, für die Aufnahme in seine Arbeitsgruppe und damit das Vertrauen in einen „fachfremden“ Mitarbeiter, die Betreuung und rege Unterstützung der vorliegenden Arbeit, für die umfangreiche Förderung der Zusammenarbeit mit anderen Labors und der Möglichkeit der Teilnahme an Tagungen und fortbildenden Seminaren.

Prof. Dr. Oliver Einsle, Universität Göttingen, danke ich zum einen für die Übernahme des Korreferats und zum anderen für die vielen hilfreichen Diskussionen.

Bei Prof. Dr. Albrecht Messerschmidt, MPI für Biochemie, Martinsried, bedanke ich mich herzlich für die ausgezeichnete Betreuung und Zusammenarbeit bei der Strukturlösung der Nitritreduktasevarianten.

PD Dr. Jörg Simon, Dr. Oliver Klimmek und Dr. René Pisa, Universität Frankfurt, danke ich für die freundliche Bereitstellung von Zellen der *Wolinella succinogenes* Mutanten und für experimentelle Anregungen und rege Diskussionen.

Desweiteren gilt mein Dank PD Dr. Frank Neese, MPI für Bioanorganische Chemie, Mülheim/Ruhr, für die anregenden Ideen und Diskussionen rund um die Nitritreduktase.

Für die Ermöglichung der Messungen am SQUID-Magnetometer danke ich Dr. Guido Leibeling, Universität Jena, recht herzlich.

Ein weiterer besonderer Dank geht an Klaus Sulger, Universität Konstanz. Ohne seine fachmännische Unterstützung, geduldige Art und immerwährende Hilfe bei Problemen wäre mir ein Einstieg in die „biologische“ Arbeitsweise sehr schwer gefallen.

Ebenso danke ich allen anderen und ehemaligen Mitgliedern der AG Kroneck für das gute Laborklima und ihre Hilfsbereitschaft, insbesondere Alma K. Steinbach, Grazyna Seiffert, Alexander Schiffer, Holger Niessen, Thorsten Ostendorp, Michael Koch und Günter Fritz.

Meinen Vertiefungskursstudenten Bao Trâm Nguyen und Dominik Gauss danke ich für die Hilfe und Mitarbeit bei zahlreichen Versuchen.

Nicht genug danken kann ich meinen Eltern und Schwestern für Rückhalt, Unterstützung, Geduld und einfach dafür, dass sie immer zu mir stehen.

Und meiner Frau Sonja und meinem Sohn Luca danke ich einfach dafür, dass es sie gibt. Was es für mich bedeutet zu ihnen zu gehören, kann man nicht in Worte fassen.